In Vitro Analysis of Boron-10 Uptake and Neutron Beam Design for Boron Neutron Capture Synovectomy

by

Emanuela Binello

S. B., Nuclear Engineering
Massachusetts Institute of Technology, 1995

Submitted to the Department of Nuclear Engineering in partial fulfillment of the requirements for the degree of

Master of Science

at the

MASSACHUSETTS INSTITUTE OF TECHNOLOGY

June 1996

Author .....
Nuclear Engineering Department
May 21, 1996

Certified by .....
Jacquelyn C. Yanch
Associate Professor of Nuclear Engineering
and Whitaker College of Health Sciences and Technology
Thesis Supervisor

Certified by .....
Sonya Shortkroff
Research Associate, Harvard Medical School
Orthopedic Research Laboratory, Brigham & Women's Hospital
Thesis Reader

Accepted by .....
Jeffrey P. Freidberg
Chairman, Nuclear Engineering Graduate Committee

In Vitro Analysis of Boron-10 Uptake and Neutron Beam Design for Boron Neutron Capture Synovectomy

by
Emanuela Binello

Submitted to the Department of Nuclear Engineering on May 21, 1996
in partial fulfillment of the requirements for the degree of Master of Science
at the Massachusetts Institute of Technology

Abstract

Boron Neutron Capture Synovectomy (BNCS) has been proposed as a novel application of the $^{10}B(n,\alpha)^{7}Li$ reaction for the treatment of Rheumatoid Arthritis (RA). RA is an autoimmune disease of the joints characterized by an inflammation of the synovium, the membrane lining the joint capsule. If drug regimes fail, treatment options are surgical synovectomy or radiation synovectomy. BNCS has advantages over these treatment approaches in that it is non-invasive and does not require the administration of radioactive substances. In BNCS, a ^{10}B labelled compound would be injected into the fluid space of the joint where it would be taken up by the synovium. The joint would then be irradiated with neutrons causing intense radiation damage to be delivered to the boron loaded cells. This thesis had two major goals. The first was to conduct an investigation of in vitro uptake of ^{10}B by human RA synovium and RA and osteoarthritic cartilage samples, thus allowing an estimate of levels potentially attained in vivo. The primary boron compound investigated was $K_2B_{12}H_{12}$, although some studies were also done with boric acid and boron particulate. Quantification of bulk uptake was performed using Prompt Gamma Neutron Activation Analysis. Cell kill as a result of the boron neutron capture reaction was verified by thermal neutron irradiation of boron-loaded tissue. An attempt was made to determine the spatial distribution of the boron compound using Neutron Induced Alpha Track Autoradiography. The second major aim of this thesis was to design an accelerator-based neutron beam for BNCS using the Monte Carlo for Neutron and Photon Transport code. A computational model of a knee joint was developed and the therapeutically useful neutron energy range was established by a series of ideal beam studies. A comparison was made between two neutron producing reactions for an accelerator source. Since neutrons coming from an accelerator source are very energetic and thus need moderation to the therapeutically useful neutron energy range, moderator/reflector configurations were examined. Materials for the moderator/reflector assembly were chosen and preliminary configurations were assessed in terms of their potential clinical usefulness in the joint phantom.

Thesis Supervisor: Jacquelyn C. Yanch
Title: Associate Professor of Nuclear Engineering and
Whitaker College of Health Sciences and Technology

Thesis Reader: Sonya Shortkroff
Title: Research Associate, Harvard Medical School
Orthopedic Research Laboratory, Brigham & Women's Hospital

Contents

1 Introduction

Boron Neutron Capture Synovectomy (BNCS) has been proposed as a novel application of the $^{10}B(n,\alpha)^{7}Li$ reaction for the treatment of Rheumatoid Arthritis (Johnson et al, 1994). Rheumatoid Arthritis is an autoimmune disease of synovial joints characterized by inflammation of the synovium, the membrane lining the joint. If left untreated, chronic synovial inflammation eventually leads to enzymatic destruction of the joint cartilage. Although the causes of cartilage destruction are not completely understood, it has been established that proliferation of the inflamed synovium plays an important role (Calabro, 1986).

The primary treatment for Rheumatoid Arthritis (RA) consists of the administration of drugs to reduce synovial inflammation. However, a single joint may remain unresponsive and thus require physical removal of the inflamed synovium (Mori, 1985). Removal of the inflamed synovium, termed synovectomy, has been shown to alleviate symptoms of RA for periods up to 5 years (Shortkroff et al, 1993). Currently existing options include surgical procedures and the injection of beta-particle emitters into the joint.

BNCS is a binary therapy approach. It has advantages over surgery and the injection of beta-particle emitters in that it is non-invasive and does not require the administration of radioactive materials. In BNCS, first a ^{10}B labelled compound would be injected into the fluid space of the joint where it would be taken up by the synovium. The joint would then be irradiated with neutrons causing intense radiation damage to be delivered to the boron loaded cells.

Preliminary work has demonstrated that very high ^{10}B concentrations can be obtained in the synovial lining in vitro (Johnson et al, 1994). In these preliminary studies, ^{10}B uptake concentrations by human RA synovium were measured using both a boron particulate and boric acid. With the boron particulate, ^{10}B uptake averaged 860 ± 250 ppm for a 1 hour incubation and 2300 ± 1600 ppm for a 24 hour incubation. The concentrations measured with the boric acid and same incubation times were 188 ± 28 ppm and 244 ± 37 ppm, respectively.

This thesis had two major goals. The first was to analyze in vitro uptake of ^{10}B by samples of human RA synovium and RA and osteoarthritic cartilage. This is important in order to get some idea of the levels potentially attained in vivo. The analysis performed included the determination of bulk tissue uptake and spatial distribution of the boron compound, $K_2B_{12}H_{12}$, as well as verification of cell kill following thermal neutron irradiation of boron-loaded tissue samples. Quantification of bulk tissue uptake of ^{10}B was performed using the Prompt Gamma Neutron Activation Analysis Facility at the MIT Research Reactor (Harling et al, 1993). In order to verify cell kill as a result of the boron neutron capture reaction, samples of synovium and cartilage were incubated in boron-containing medium, irradiated and histology was performed. The spatial distribution of boron uptake by RA synovium was investigated using Neutron Induced Alpha Track Autoradiography, a technique which has been used to obtain quantitative information (Liu, 1989) as well as information on spatial distribution (Abe et al, 1986).

The second aim of this thesis was to design an accelerator-based neutron beam for BNCS using the MCNP code (Monte Carlo for Neutron and Photon Transport) (Briesmeister, 1986). Although based on the same nuclear principles as Boron Neutron Capture Therapy, a very different neutron beam design was required for BNCS as a result of the fairly shallow depth of the synovial lining and the large concentrations of boron likely to be available in the synovium. The therapeutically useful neutron energy range for BNCS was determined through a series of ideal beam studies. Then, since neutrons coming from the accelerator will be very energetic and thus need moderation to the therapeutically useful neutron energy range, a moderator and reflector assembly was designed. The effects of different moderator/reflector dimensions were examined in a tissue-equivalent model of the knee joint and examples will presented. Also, a comparison was made between two neutron producing reactions.

The organization of this thesis is as follows. Chapter 2 will present an in-depth discussion of BNCS and RA. Chapters 3 and 4 will present the methods and results of the in vitro analysis of ^{10}B uptake, respectively. The details of the beam design will be presented in Chapters 5 and 6. Conclusions will be drawn at the end, in Chapter 7.

2 Boron Neutron Capture Synovectomy

In this chapter, the characteristics of Rheumatoid Arthritis and current treatment options are described. The details of BNCS will then be presented, including a discussion of the $^{10}B(n,\alpha)^{7}Li$ reaction, the cornerstone of the therapy. Finally, a comparison will be drawn between BNCS and BNCT.

2.1 Rheumatoid Arthritis

Rheumatoid Arthritis (RA) is a chronic autoimmune disease of the synovial joints which is characterized by an inflammation of the synovium. If left untreated, RA could lead to significant pain with joint deformation and disability. Approximately 1% of the US adult population is affected by RA (Harris, 1993). Women are affected about three times more often than men and roughly 80% of all RA patients develop the disease between the ages of 35 and 50 (Harris, 1993). The prevalence of RA in women compared to men diminishes as age increases, i.e. men and women become equally affected.

RA affects synovial joints by causing inflammation of the synovium. The synovium is among the principal structures found in a synovial joint. In a synovial joint the ends of two bones are covered with a thin layer of smooth and spongy articular cartilage which is the actual load bearing surface of the joint. Fluid space serves as a lubricant for the cartilage. This fluid is secreted and maintained by the synovium.

Among other functions, the synovium provides an unobtrusive, low-friction lining for the joint, and aids in joint stability. For the remainder of this thesis, the synovium will be described as having two components; the sub-synovium, a vascularized fibrous tissue composed of collagen and elastic fibers in a wide-meshed surface and the synovial lining (used interchangeably with the word synovium).

The precise cause of RA, or the trigger of the autoimmune response, is unknown. As the autoimmune response becomes more organized and the inflammation increases, new blood vessels develop in the synovium. These are essential to the progression of RA since

the blood vessels are the means whereby nutrients are delivered to the rapidly proliferating synovial lining cells. It has been well established that they play an important role in RA (Calabro, 1986).

As shown in Figure 2.1, chronic synovial inflammation eventually leads to enzymatic bone and cartilage destruction.

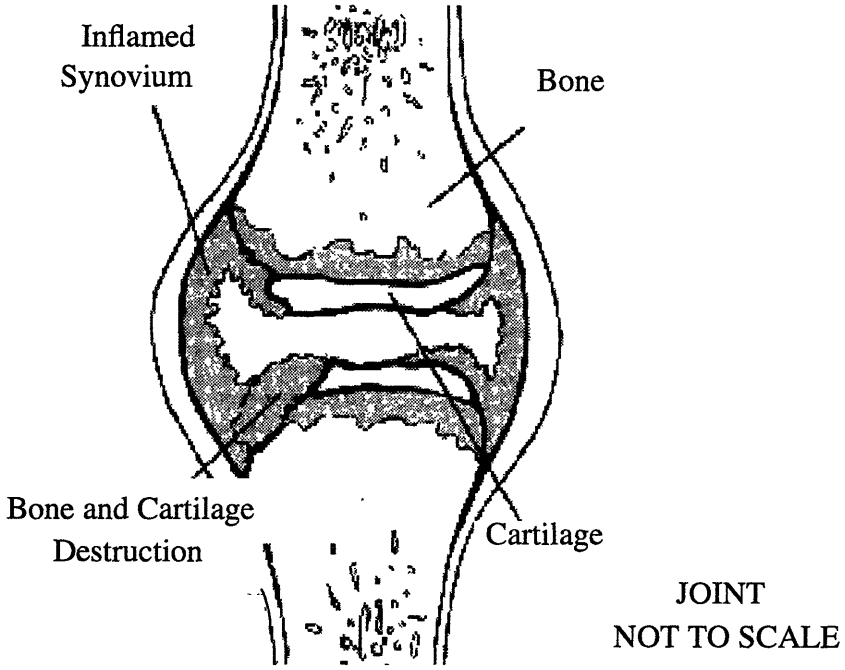

Figure 2.1: If left untreated, RA, characterized by inflammation of the synovium, can lead to bone and cartilage destruction and eventually to loss of joint function.

The majority of the destruction takes place when the proliferating synovium begins to invade the joint, i.e. there is an extravagant growth of the synovial lining cells. A tissue front develops and grows to form finger-like projections which then spread to cover the articular cartilage lining the joint.

Little cartilage destruction is necessary to weaken normal function of the synovial joint causing progressive and irreversible articular cartilage disintegration as a result of normal joint movement. Once destruction of articular cartilage is underway, attempts to protect the joint are considered to be futile (Lipsky, 1990).

The primary treatment for RA involves the administration of various drugs to reduce the synovial inflammation. These include aspirin, nonsteroidal anti-inflammatory agents, low doses of antimetabolites, steroids, remission inducing agent and intra-articular injections of corticosteroid. While for the majority of patients the symptoms of RA can be controlled satisfactorily with the variety of drug regimens currently available, a single joint may remain unresponsive thus requiring the physical removal of the synovium, a procedure termed synovectomy (Mori, 1985).

A current option for synovectomy is surgery. In this procedure the membrane is excised by either open or arthroscopic synovectomy. Surgical removal has been shown to provide relief of pain for 2 to 5 years (Shortkroff et al, 1993). However, several drawbacks to surgery exist. One is the technical difficulty involved in completely removing the synovium which is due to the complex geometry of the joint (Zuckerman & Sledge, 1985). Other drawbacks to surgery include inherent dangers in the procedure such as infection and anesthesia. Also, often hospitalization and prolonged rehabilitation are required.

The other existing option for synovectomy is the injection of beta-particle emitters into the joint, termed Radiation Synovectomy (Shortkroff et al, 1993). The injected radionuclide is incorporated into a large molecule such as a colloid which is then rapidly taken up by the synovial lining through phagocytosis and delivers approximately 10,000 rad (a dose empirically determined to provide symptomatic relief) to the synovium within a period of hours to weeks. Since the sub-synovium and synovium together have a thickness on the order of mm, the beta-emitters chosen are those which deposit the majority of their energy within 1 to 10 mm in tissue.

Radiation Synovectomy avoids the dangers of surgery and has reported success rates as high as 80% (Deutsch et al, 1993). However, its primary drawback is the delivery of dose to non-target organs. This is due to leakage of the radionuclide-containing compound from the joint cavity. Investigators have found leakage from a few percent to 60% of the injected dose resulting in unacceptable doses to the liver, spleen and lymphatic system (Shortkroff et al, 1993). Although Radiation Synovectomy is widely practiced in Austra-

lia, Canada and some parts of Europe, it has not gained acceptance in the US due to concern over the leakage of the beta-particle emitters from the joint to other organs (Shortkroff et al, 1993).

BNCS, which will be described below, has the potential of eliminating the drawbacks of surgical and radiation synovectomy. Unlike surgery it is non-invasive and unlike radiation synovectomy, it does not require the administration of radioactive compounds.

2.2 Principles of BNCS

The crux of BNCS lies in the $^{10}B(n,\alpha)^{7}Li$ reaction. A naturally occurring isotope of boron, ^{10}B has one of the highest thermal neutron capture cross sections of the non radioactive elements. Figure 2.2 illustrates the complete sequence of nuclear events in the $^{10}B(n,\alpha)^{7}Li$ reaction.

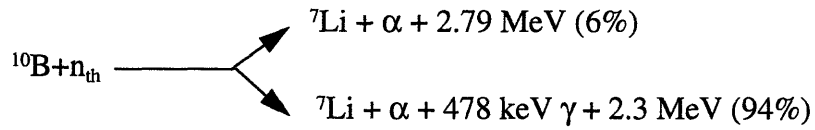

Figure 2.2: Sequence of nuclear events of the ^{10}B reaction with thermal neutrons

The capture cross section of ^{10}B is 3837 barns for neutrons with energies of approximately 0.025 eV. The total Q-value for the reactions is 2.79 MeV.

The particles released in this reaction are high "Linear Energy Transfer" (LET) which means that they give rise to closely spaced ionizations in sharp tracks; the particles have a range of less than 10 μm (on the order of the diameter of a cell). This theoretically limits the radiation effects to those cells previously loaded with boron (Barth et al, 1992) The released particles also have a high Relative Biological Effectiveness (RBE) which implies that they are more effective than x-rays at cell kill.

In order to minimize dose to non targeted cells and tissues, ^{10}B concentrations delivered to the target tissue should be as large as possible so that the neutron fluence can be kept as

small as possible. This is desired in order to maximize the dose delivered to the target cells via the $^{10}B(n,\alpha)^{7}Li$ reaction and minimize the dose to non-target tissue through such reactions as elastic scattering of fast neutrons and capture of thermal neutrons.

BNCS involves a two-part procedure. First a boron-labelled (non-radioactive) compound would be injected into the joint fluid space where it would be taken up by the synovium The joint would then be irradiated with neutrons, which must be thermal or near-thermal at the synovium to cause the $^{10}B(n,\alpha)^{7}Li$ reaction to occur. This process is schematically shown in Figure 2.3. The two high-LET, high-RBE particles released by the boron neutron capture reaction travel distances less than the diameter of a cell and thus deliver intense radiation damage to those cells previously loaded with boron (Barth et al, 1992). One major advantage of this type of system is that the two components can be manipulated independently.

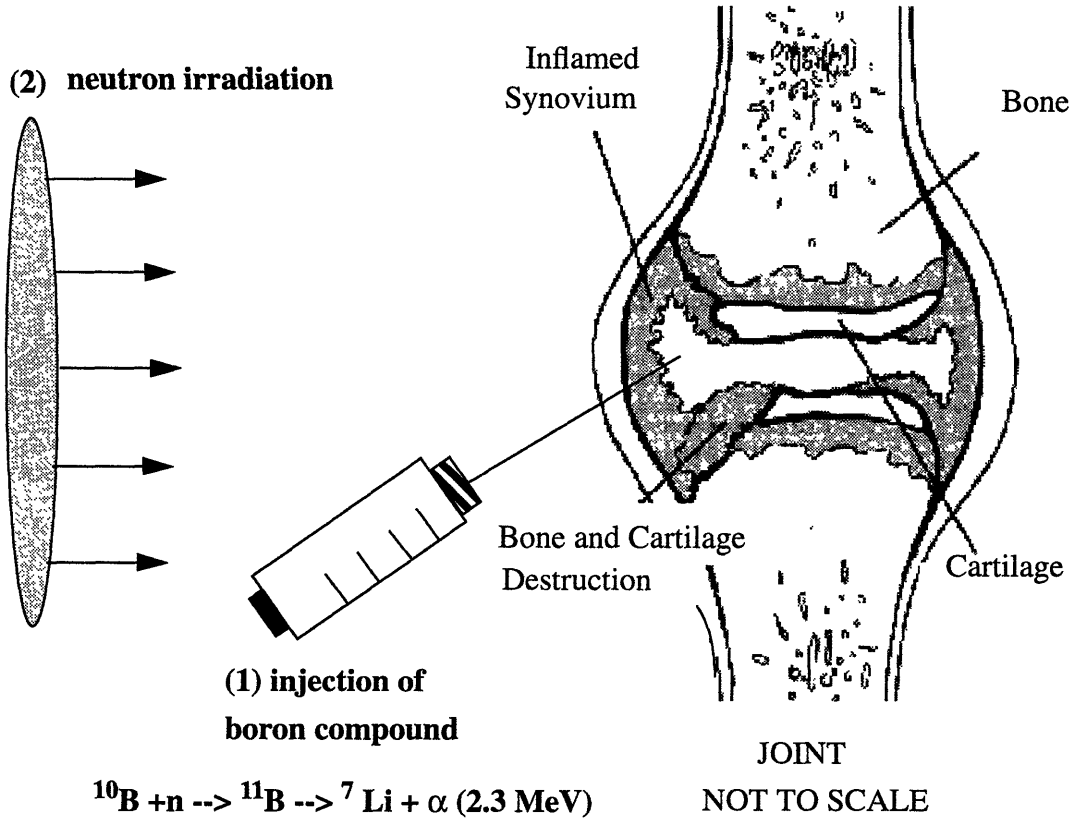

Figure 2.3 Schematic showing the binary nature of BNCS

Taken individually, the two steps in BNCS, i.e. the injection of a compound for the destruction of the synovium and the irradiation of a target area with neutrons, are not new ideas. The principle behind radiation synovectomy is to inject a substance, which happens to be radioactive, into the fluid space for the purpose of destroying the synovium. In BNCS, however, the compound that is injected into the joint is not radioactive and does not alone destroy the synovium. The concept of irradiating a target area previously loaded with ^{10}B is essentially the same as Boron Neutron Capture Therapy (BNCT) except that in BNCT tumors are generally the targets whereas the target in BNCS is the synovium. However, the combination of these two steps for the treatment of RA is novel and has never been tried before.

2.3 Comparison to BNCT

Although the physical principles of BNCT and BNCS are the same, the basic therapy parameters and requirements are significantly different as a result of the nature and depth of the target tissue. The target tissue in BNCT is tumor which typically lies several cm below the surface of the skin while in BNCS the target tissue is the synovium which lies from 1.3 to 1.5 cm below the surface of the skin.

The method of boron compound delivery to the target tissue differs between BNCT and BNCS. In BNCT, the boron-labelled pharmaceutical is administered intra-arterially or orally and must reach the tumor via the body's metabolic pathways. In BNCS, on the other hand, the method of delivery of the boron compound is by local injection, making it likely that relatively high concentrations can be achieved in target tissue. Preliminary work has shown that concentrations ranging from 10 to 100 times higher than those achieved in BNCT are readily achieved in vitro using a particulate (Johnson et al, 1994).

The above differences will have a profound effect on the required neutron beam energy range for BNCS. The rationale behind the design of epithermal beams for BNCT is that the neutrons in the beam need to be energetic enough so that by the time they reach the tumor they will have been moderated to thermal energies, i.e. energies at which the cross section for the $^{10}B(n,\alpha)^{7}Li$ reaction is highest. However, this rationale is not applicable to

BNCS due to the shallow depth of the synovium. A full investigation of the neutron beam energy requirements for BNCS is needed. This was performed as a preliminary step method in the neutron beam design process. Naturally, a different therapeutically useful neutron energy range will give rise to a different neutron beam design.

The difference in the size and location of the area to be irradiated will affect the neutron beam design. In BNCT the target is typically a brain tumor and current thinking says that it is best to irradiate the whole head in order to get any occult cells, thus implying that the neutron beam should be comparable to the head in size. In BNCS the target is a joint which can vary in size (although generally remains smaller than the head). Also, whereas in BNCT there are many radiosensitive organs near the irradiation area, the joints most commonly involved in RA are far away from the brain, chest and trunk, furthermore implying that the neutron beam design for BNCS will differ from that of BNCT.

Finally, unlike BNCT which, as previously mentioned, was designed for patients with malignant and terminal cancers, the patients in BNCS are otherwise healthy individuals. This implies that the limits on acceptable radiation dose to healthy tissue will be much more stringent for BNCS than they are for BNCT.

3 In Vitro Analysis of Boron-10 Uptake: Methods

This chapter will describe the methods used to perform in vitro analyses of ^{10}B uptake by both synovium and cartilage samples. Information on bulk tissue uptake was obtained via Prompt Gamma Neutron Activation Analysis (Harling et al, 1993). Cell kill via delivery of intense radiation dose to cells previously loaded with boron was verified by irradiating samples in the thermal beam port (2PH2) of the MIT Research Reactor. An attempt was made to obtain spatial information on boron uptake in tissue using Neutron Induced Alpha Track Autoradiography.

However, before embarking on a detailed description of the methods, attention will be drawn to the boron compound primarily used in this thesis, $K_2B_{12}H_{12}$. It is a salt form of the polyhedral closed form of the borane anion, $B_nH_n^{2-}$ which is among the best studied and most stable anion (Cotton & Wilkinson, 1985). It must also be noted that the boron in the compound was natural, i.e. unenriched in ^{10}B. Since natural boron only contains 20% ^{10}B, all incubation concentrations could be increased by a factor of five using a compound 100% enriched in ^{10}B.

Use of this compound was part of an effort to optimize the chemical form and conditions of boron delivery to the synovium. Eventually, BNCS will require a ^{10}B-labelled compound which is non-toxic, remains sufficiently long in the joint space and delivers large amounts of ^{10}B to the synovium. This thesis examined the delivery of ^{10}B to the synovium while future work will examine the toxicity of the compound and the length of its stay in the joint space.

3.1 Prompt Gamma Neutron Activation Analysis

Neutron Activation Analysis in general is aimed at quantifying the elemental composition of materials. Sample irradiation results in the production of gamma emitters whose gamma rays are used to identify the concentrations of the radionuclides. When sample irradiation and spectroscopic analysis are conducted simultaneously, the technique is

called Prompt Gamma Neutron Activation Analysis. Since determination of the activity is dependent on a wide variety of variables some of which fluctuate during the course of the measurement, standards must be used and a calibration curve constructed. Analysis of ^{10}B content by prompt gamma neutron activation analysis is dependent upon the detection of the 478 keV gamma-ray emitted from the excited state of ^{7}Li.

Prompt Gamma Neutron Activation Analysis has been used by investigators in BNCT for the determination of ^{10}B in animal tissue samples (Fairchild et al, 1983) and was in fact used for the BNCS preliminary in vitro studies (Johnson et al, 1994). Resolution for this technique is on the order of 1 ppm which is adequate for the concentrations achievable in BNCS. The technique was chosen particularly in light of the facility constructed at MIT (Harling et al, 1993) and the satisfaction of resolution and reliability requirements.

The Prompt Gamma Neutron Activation Analysis Facility at the MIT Research Reactor produces a diffracted neutron beam with reduced fast neutrons and core gamma-rays at the sample (Harling et al, 1993). A well moderated beam of thermal neutrons emerging from the reactor's reflector is incident on a multilayered graphite monochromator which diffracts the beam by 21°. A simplified schematic is shown in Figure 3.1. The neutron beam with an energy of 0.0143 eV is passed through a sapphire crystal which transmits 80% of the 0.0143 eV neutrons, less than 1% of the epithermal neutrons, 0.5% of the fast neutrons and 3 to 20% of the gamma rays in the energy range of 1 to 6 MeV. Collimators are used resulting in a beam of neutrons with an energy of 0.0143 eV, a flux of $6x10^{6}$ n/cm^{2}s and a diameter of 1 to 2 cm (Harling et al, 1993). A 122 cm^3 n-type solid state Germanium detector is positioned at 90° and its sides are lined with 7.5 cm of lead and 4 cm of lithium carbonate. The lead reduces the effects of stray neutrons and the background count of scattered gamma-rays. The end of the detector is shielded from stray neutrons by 1.25 cm lithium carbonate enriched in ^{6}Li. A Canberra Series 85 multichannel analyzer is used for spectroscopic analysis. (Harling et al, 1993)

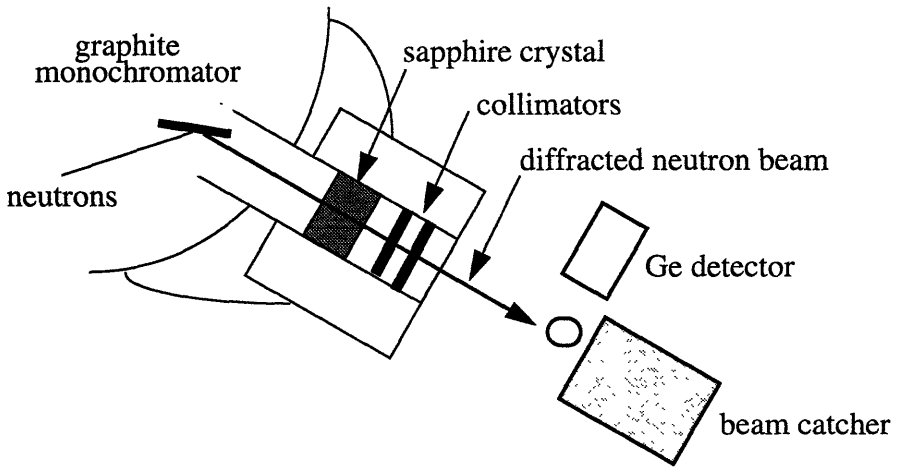

Figure 3.1 Schematic of the MIT Prompt Gamma Neutron Activation Analysis Facility (adapted from Harling et al, 1993).

3.1.1 General procedure

For each sample, the count rate of gamma-rays coming from both the hydrogen capture reaction (2.2 MeV) and the boron neutron capture reaction (478 keV) was determined by measuring the area under the appropriate gamma peak and dividing by the irradiation time. The background counts for the gamma-rays resulting from the hydrogen capture reaction were measured by counting an empty teflon vial while the background rate for the gamma-rays resulting from the boron neutron capture reaction was measured by counting a teflon vial filled with deionized water, under the assumption that the boron content of deionized water and soft tissue were similar.

The count rates for both the boron and hydrogen neutron capture reactions were obtained in order to calculate the $^{10}B/^{1}H$ ratio (B/H ratio) which was then used to calculate the ^{10}B concentration. Using this ratio reduces the effects of inconsistent sample positioning in the beam and variations in the thermal neutron flux during the measurement.

The calibration curve, relating B/H to boron concentration, was constructed each time Prompt Gamma Neutron Activation Analysis experiment was performed. Fresh standards were used each time although the actual standard preparation was only done once.

3.1.2 Preparation of standards for calibration

The preparation of the standards was divided in two parts; the preparation of the mother solution, 1500 ppm ^{10}B, and the daughter solutions, 750 ppm, 300 ppm, 150 ppm, and 30 ppm. The preparation of these standards, in that order, will be described below.

(a) Preparation of the mother solution

It has been determined that in order to produce a 100 ppm solution of ^{10}B solution 3.104165 g of boric acid standard must be added to 1000 ml solution of a mixture which is composed of one third saline and two thirds deionized water (Chabeuf, 1993). This was scaled in order to produce 10 ml of a 1500 ^{10}B ppm solution. Thus, it was necessary to add 4.6562 g of boric acid standard (Boric Acid 951 from the National Institute of Standards and Technology, Gatherburg, MD 20899).

In the first step, the mixture solution was created; 50 ml of saline and 150 ml of deionized water were combined. A light plastic boat was weighed and the 4.6562 $\pm$0.001 g of boric acid were added in order to produce a 1500 ppm solution of ^{10}B.

(b) Preparation of the daughter solutions

These were prepared by using the following formula:

$$K_1 V_1 = K_2 V_2 \qquad \text{(Eq. 3.1)}$$

where K_1 is the original concentration (ppm), V_1 is the unknown volume (ml), K_2 is the desired concentration (ppm) and V_2 is the desired volume (ml). For example: in order to obtain 10 ml of 750 ppm solution out of the 1500 ppm mother solution, the above equation becomes

$$1500 \cdot V_1 = 750 \cdot 10$$

which can be solved to yield

$$V_1 = 5ml$$

This means that 5 ml of the 1500 ppm solution must be added to the mixture of saline and

deionized water (more specifically composed of one third saline and two thirds deionized water). This yields 10 ml of 750 ppm solution.

The following table summarizes the preparations.

Table 3.1: Summary of daughter solution preparations

Conc. (ppm)	mother sol. (ml)	mix. sol. (ml)
750	5.0	5.0
300	2.0	8.0
150	1.0	9.0
30	0.2	9.8

3.1.3 Analysis

The B/H ratio was determined for all samples using the following equation

$$\frac{B_t}{H_t} = \frac{B_n - B_0}{H_n - H_0} \qquad \text{(Eq. 3.2)}$$

where B_n is the count rate of the gamma-rays from the boron neutron capture reaction, B_0 is the associated background count, H_n is the count rate of the gamma-rays from the hydrogen capture reaction and H_0 is its background.

The error in the B/H ratio was calculated in a series of steps. However, first, it must be noted that the error in the number of counts under the gamma peaks resulting from the boron and hydrogen neutron capture reactions was given by the multichannel analyzer which calculates the error assuming a Gaussian distribution. However, the "boron" peak, i.e. the peak resulting from the boron neutron capture reaction, is Doppler broadened which means that the multichannel analyzer overestimates the error.

The first step in the calculation of error was to determine the error in the count rates for each peak in each sample, i.e. the individual errors in B_n, B_0, H_n, H_0. This was done using the error calculation formula for "Multiplication or Division by a Constant" (Knoll, 1989).

The second step was to calculate the error in B_t and H_t, or the net boron and hydrogen count rates for each sample. This was done by directly applying the formula for the error in "Sums or Differences of Counts" (Knoll, 1989).

The third and last step was to determine the error in the B/H ratio given knowledge of the error in both the net boron and hydrogen count rates. This was calculated by applying the error propagation formula for "Multiplication or Division of Counts" (Knoll, 1989) to this particular problem, i.e.

$$\left(\frac{\Delta(B/H)}{B/H}\right)^2 = \left(\left(\frac{\Delta B_t}{B_t}\right)^2 + \left(\frac{\Delta H_t}{H_t}\right)^2\right) \qquad \text{(Eq. 3.3)}$$

This equation can be solved to yield the percent error in the B/H ratio which is the manner of error expression used in this thesis.

A calibration curve was constructed by plotting B/H ratio of the standards versus their ^{10}B concentration. The data were linearly fit with the origin of the line forced through (0,0). The error in the slope and the chi squared value were given as part of the line fit done with Mackintosh Kaleidagraph.

The next step in the analysis was to determine the ^{10}B concentration for the samples using the calibration curve. The B/H ratio of each sample was divided by the slope of the calibration curve since the expression of the slope was the increase in B/H ratio over the increase in concentration.

Again, error was calculated for the concentration by applying standard error propagation formula to this particular problem (Knoll, 1989), i.e.

$$\left(\frac{\Delta C}{C}\right)^2 = \left(\left(\frac{\Delta(B/H)}{B/H}\right)^2 + \left(\frac{\Delta m}{m}\right)^2\right) \qquad \text{(Eq. 3.4)}$$

where ΔC is the error in concentration, C is the concentration, Δm is the error in the slope of the calibration curve and m is the slope of the calibration curve.

Since for each set of conditions at least three samples were used, as a last step the average uptake and percent error were calculated. In addition, the uptake was plotted as a function of weight when there were three or more sets of samples for a given condition.

3.1.4 Specific experimental conditions

^{10}B Uptake was measured for freshly excised synovium and cartilage as a function of both incubation concentration and incubation time. The cartilage was either osteoarthritic (OA), i.e. from a joint not afflicted by RA, or rheumatoid arthritic (RA), i.e. from a joint afflicted with RA. These two forms of cartilage are expected to behave similarly. In one instance bovine cartilage was used as a substitute. Again, similar behavior was expected.

The boron compound used for these studies was $K_2B_{12}H_{12}$ unless otherwise specified. It was mixed with RPMI cell culture medium consisting of 1% penicillin streptomycin and 10% fetal bovine serum to yield boronated incubation medium of different concentrations, namely 100 ppm, 500 ppm and 1000 ppm.

Unless otherwise specified, tissue was obtained from an operating room of Brigham & Women's Hospital, cut into samples and incubated under the experimental conditions which will be described below. After incubation, the samples were thoroughly rinsed in saline.

Samples were stored at -70° until Prompt Gamma Neutron Activation Analysis at the MIT Research Reactor could be performed. Each teflon vial was measured with and without tissue in order to determine the weight of the tissue. The nine experimental conditions used will be described below.

(i) Uptake by RA synovium as a function of incubation concentration

RA synovium was incubated for 1 hour with nominal incubation media concentrations of 100, 500 and 1000 ppm ^{10}B. The actual media concentrations were measured during the Prompt Gamma Neutron Activation Analysis experiment.

(ii) Uptake by RA synovium as a function incubation time

RA synovium was incubated at a nominal concentration of 1000 ppm for varying time points, namely 15 minutes, 30 minutes and 1 hour. A sample was also incubated in 50 ppm ^{10}B boric acid solution for 1 hour.

(iii) Uptake by OA cartilage as a function of boron compound

OA cartilage was incubated for 1 hour at a nominal 100 ppm concentration of ^{10}B boric acid solution (unenriched in ^{10}B) and a nominal 1000 ppm concentration of $K_2B_{12}H_{12}$. The tissue was also sprinkled with about 10 mg. of boron particulate and incubated for 1 hour. The boron particulate was 99.9% boron metal, enriched in ^{10}B (94%), with particle sizes ranging from 5 to 40 μm in diameter and averaging about 15 μm.

(iv) Uptake by RA synovium and cartilage as a function of both incubation concentration and time

RA synovium was incubated for 1 hour with nominal incubation media concentrations of 100, 500 and 1000 ppm ^{10}B and for 24 hours with a nominal concentration of 1000 ppm. RA cartilage was incubated for 1 hour with nominal incubation concentrations of 500 and 1000 ppm.

(v) Uptake by RA synovium and cartilage as a function of both incubation concentration and time

Both RA synovium and cartilage were incubated in nominal concentrations of 100, 500 and 1000 ppm ^{10}B for 1 and 2 hours.

(vi) Uptake by RA cartilage as a function of incubation concentration and time

RA cartilage was incubated in nominal concentrations of 100 and 1000 ppm ^{10}B for 1 and 24 hours.

(vii) Uptake by RA synovium as a function of sample size

RA synovium samples were divided into three categories, small, medium and large, and incubated at nominal concentration of 1000 ppm for 1 hour.

(viii) Uptake by RA synovium as a function of sample size at a different time point
The same conditions as (vii) were used except that the incubation time was 24 hours.

(ix) Uptake by large pieces of bovine cartilage
A set of 4 samples of large bovine cartilage pieces were incubated for 1 hour at a nominal concentration of 1000 ppm.

The results of these experiments will be presented section 4.1.

3.2 Thermal Neutron Irradiation

In order to verify cell kill by the $^{10}B(n,\alpha)^{7}Li$ reaction, tissue previously incubated with the boron compound was irradiated with thermal neutrons in the thermal neutron beam port of the MIT Research Reactor. An identical set of samples was set aside, not to be irradiated, and was placed in incubators. The incubation specifications and dosimetry will be explained in the following section. After irradiation (or incubation for the same amount of time for the control samples), the tissue samples were fixed with formalin for histological analysis.

3.2.1 Incubation and dosimetry for RA synovium irradiation

A set of four samples of RA synovium was incubated for 1 hour at a nominal $K_2B_{12}H_{12}$ incubation medium concentration of 1000 ppm ^{10}B. After incubation samples were thoroughly rinsed in saline and placed into cryovials so that all four samples could fit into the holder to be used during thermal neutron beam irradiation. About 1 ml of fresh medium was placed in each cryovial. Two pieces of RA synovium tissue which were not incubated in ^{10}B were included as controls.

In light of the empirical finding that approximately 10,000 rad must be delivered to the synovium (Shortkroff et al, 1993), calculations were done in order to determine the time necessary to deliver 10,000 rad to the RA synovium samples using the 2PH2 port with a flux of $8x10^{11}$ n/cm^{2}s.

The first step in this calculation was to consider all the possible components of total dose to the sample, D_t, i.e. the dose due to fast neutrons, D_f, and slow neutrons, D_{th}, dose due to ^{10}B, D_{B10}, and gamma-rays, D_γ. The expression is

$$D_t = D_f + D_{th} + D_{B10} + D_\gamma \quad \text{(Eq. 3.5)}$$

where, in turn, D_γ, is equal to

$$D_\gamma = D_\gamma^{ind} + D_\gamma^{dir} + D_\gamma^{B10} \quad \text{(Eq. 3.6)}$$

or the dose due to induced gamma-rays, gamma-rays from the beam and gamma-rays from the boron neutron capture reaction.

These two equations can be simplified by using characteristics of the beam and the size of the sample. The fast neutron and gamma contamination in the thermal neutron beam at the 2PH2 port is negligible, thereby making the D_f and D_γ^{dir} zero. The dose due to the photons from the core, the induced photons and the photons from the D_γ^{B10}, can also be assumed negligible. Thus, the total dose delivered to the synovium has the following components

$$D_{tot} = D_{th} + D_{B10} \quad \text{(Eq. 3.7)}$$

(Solares, 1991). The dominant contributions to dose are made by the thermal neutrons and the dose delivered by the boron neutron capture reaction.

The dose delivered to the tissue by each component is a function of thermal neutron flux, time of irradiation, the appropriate KERMA values (to convert fluence to dose) and RBE values. The expression for the dose due to thermal neutrons is

$$D_{th} = \phi_{th} \cdot t_{ir} \cdot K_{th} \cdot RBE_{th} \quad \text{(Eq. 3.8)}$$

where ϕ_{th} is the thermal neutron fluence, t_{ir} is the irradiation time, K_{th} is the thermal neutron KERMA factor and RBE_{th} is the RBE value for thermal neutrons (Solares, 1991).

Similarly, for the dose delivered by the $^{10}B(n,\alpha)^7Li$ reaction

$$D_{B10} = \phi_{th} \cdot t_{ir} \cdot K_{th} \cdot RBE_{B10} \cdot C_{B10} \quad \text{(Eq. 3.9)}$$

where ϕ_{th} is the thermal neutron fluence, t_{ir} is the irradiation time, K_{th} is the thermal neu-

tron KERMA factor, RBE_{B10} is the RBE value for ^{10}B and C_{B10} is the ^{10}B concentration (Solares, 1991).

The above two equations, Eq. 3.8 and Eq. 3.9, can be combined yielding

$$D_{tot} = \phi_{th} \cdot t_{ir} (K_{th} \cdot RBE_{th} + K_{B10} \cdot RBE_{B10} \cdot C_{B10}) \qquad \text{(Eq. 3.10)}$$

which can be solved for t_{ir}, resulting in the following expression

$$t_{ir} = \frac{D_{tot}}{\phi_{th} (K_{th} \cdot RBE_{th} + K_{B10} \cdot RBE_{B10} \cdot C_{B10})} \qquad \text{(Eq. 3.11)}$$

The values for the calculation of t_{ir} are as follows:

D_{tot} = 10,000 cGy

$\phi_{th} = 8 \times 10^{11}$ n/cm^{2}s

$K_{th} = 1.5 \times 10^{-11}$ cGy/ (n/cm^2)

RBE_{th} = 3.2

$K_{B10} = 8.72 \times 10^{-12}$ cGy/ (n/cm^2)(ppm)

RBE_{B10} = 1.35

C_{B10} = 300 ppm

The RBE values are from Zamenhof et al (Zamenhof et al, 1989) and the KERMA values are from Caswell et al (Caswell et al, 1982). The boron concentration chosen was conservative, i.e. from the lower part of the uptake range, as will be shown in the next chapter.

Thus, the irradiation time required to deliver 10,000 rad of dose to the synovium was 3.49 seconds using the above parameters. However, for practical limitations, the sample was irradiated for 5 seconds. The dose delivered was approximately 14,300 rads. At this point in time it was discovered that the shutter in the reactor takes 8 seconds to open and to close. The sample holder is lowered manually into the beam and the time the shutter takes to open and close is a total of 16 seconds. The uncertainty in the exposure of the synovium sample to the thermal neutrons was 16 seconds due to the water shutter and 2 seconds due to the manual lowering of the sample, thus totalling 18 seconds. This was larger than the irradiation time, 5 seconds and, in turn, made the estimate of the error in the dose delivered on the order of 360%.

3.2.2 Incubation and dosimetry for bovine cartilage irradiation

The same general method was used for a set of samples of bovine cartilage except for a change in two parameters: total dose delivered to the cartilage, D_{tot}, was increased and concentration of ^{10}B likely to be in the tissue, C_{B10}, was decreased. These alterations were made so that the irradiation time could be increased to a level which would yield a large increase in accuracy in the dose delivered (corresponding to a decrease in error) and to absolutely ensure cell kill.

The sample was irradiated for 175 seconds, with an uncertainty of 18 seconds (16 seconds due to the shutter and 2 seconds due to manual operation error). The D_{tot} delivered was 56,160 rad $\pm$10% and the C_{B10} was 30 ppm.

3.3 Neutron Induced Alpha Track Autoradiography

The Neutron Induced Alpha Track Autoradiography technique was used in order to obtain spatial information on the ^{10}B uptake by RA synovium (Abe et al, 1986). Neutron Induced Alpha Track Autoradiography is based on the fact that the alpha particles from the boron neutron capture reaction are recorded in a track-etch detector (Thellier et al, 1991). Pits visible using an optical microscope are formed in the places where the alpha-particles have passed through the track-etch detector and created stress point tracks in it. In order to know the correspondence of the etched tracks to tissue slices, a superimposition of the etched tracks and stained tissue slices is performed (Amano et al, 1973). In this way, the spatial distribution of boron compounds can be obtained.

In addition to spatial information, quantitative information could be obtained by counting the number of tracks in a region of known area and comparing it with numbers obtained from standard specimens (Liu, 1986). The size of each pit depends on the amount of energy deposited by the alpha-particles and on the etching techniques that are used, e.g. time, temperature and etchant (Durani & Bull, 1987).

The track-etch detector chosen was polycarbonate CR 39 plates (allyl diglycol carbonate, American Acrylics and Plastic. CT). This track etch detector is insensitive to gamma-rays and beta-particles. However, it is sensitive to protons below 400 keV thus not completely eliminating the need to distinguish between tracks. CR 39 track etch detectors do have one advantage over the other type of track etch detector, cellulose nitrate LR 115 type films (Kodak), in that they do not have any nitrogen which would cause the release of protons as a result of the $^{14}N(n,p)^{14}C$ reaction and thus obscure the alpha particle tracks.

3.3.1 Sample preparation

Frozen samples mounted on a piece of cork were obtained from storage in the -70° freezer. The sample types will be described in the next section when their composition becomes relevant for determining experimental method.

First, the cork was removed from the samples and Optical Cutting Temperature (OCT) compound (Miles, Inc., Diagnostic Division, Elkhart, IN) was added to the sample. After the OCT froze, a square was cut with the sample in the center and then mounted on a cryostatic microtome (2800 Frigocut Donsanto). For each sample, a tissue slice was cut with a 5 μm thickness and mounted on polycarbonate CR 39 track etch detectors. The very next tissue slice was mounted on a glass slide to be stained for histological analysis. This was done to superimpose the etched tracks and the stained tissue slices in order to examine the spatial distribution of boron in the samples (Amano et al, 1973).

3.3.2 Neutron Irradiation

The samples were packed in dry ice and brought to the MIT Research Reactor port 2PH2 for neutron irradiation. However, first, the appropriate irradiation parameters had to be established in order to ensure the visibility of the tracks. Too much exposure would result in an oversaturation of tracks rendering the background too high to see the tracks left by the alpha particles. On the other hand, the power and or time had to be large enough to induce sufficient boron neutron capture reactions in the first place.

The irradiation parameters were determined using the following guideline for resolution:

15 minute irradiation of a 30 ppm sample at 100 kW (Solares, 1995). The time, sample concentration and reactor power all scale linearly.

Due to the significant time involved in manually lowering and raising the sample holder and in order to reduce the resulting experimental error, it was decided that the time should remain constant at 15 minutes and the reactor power would be adjusted. This implied that the samples had to be classified as "high" and "low" expected concentrations as based on previous results in order to scale the required reactor power accordingly. For example, the reactor power for the tissue incubated with the particulate or $K_2B_{12}H_{12}$ had to be a factor of ten lower than for the tissue incubated with boric acid.

Table 3.2 summarizes the type of sample used and the power required for each one, with the irradiation time fixed at 15 minutes. In the table below, surface refers to a slice that was taken from the surface of the tissue whereas inner refers to a slice taken 1 mm into the tissue.

Table 3.2: Autoradiography sample irradiation parameters

Sample	Power (kw)
^{10}B particulate: surface	3.3
^{10}B particulate: inner	3.3
$K_2B_{12}H_{12}$: 15 min.	3.3
$K_2B_{12}H_{12}$: 30 min.	3.3
Boric Acid: 1 hour	33
Standard: 11.63 ppm	33
Control: tissue in medium	33

3.3.3 Etching

A 6.5 N NaOH solution was made by dissolving 77.8 grams of solid NaOH (Molecular Weight of 40.00, lot 28F-0852, No. S-5881 Sigma Chemical Company, St. Louis, MO) in 300 ml of H_2O. This concentration was used because it has been empirically determined

that at this concentration of NaOH, tracks can be etched by soaking the CR 39 slides for 18 minutes in a 70° water bath (Solares, 1995). There are two factors affecting the rate at etching (Durani & Bull, 1987). The first is the temperature at which the etching takes place, i.e. the lower the temperature, the longer the time to etch. The other is the NaOH concentration, i.e. the lower the concentration, the longer the time to etch.

3.3.4 Staining

The tissue slices mounted on the glass slides were stained with hematoxylin-eosin stain according to the following protocol. First the slides were left in hematoxylin for 5 minutes and then rinsed in deionized water. Afterwards they were dipped in sodium borate solution (which was made by dissolving 64g of sodium borate powder, $Na_2B_4O_7$-$10H_2O$, in 100ml deionized water) and rinsed again in deionized water.

The next step in the procedure involved leaving the slides in Eosin for 5 minutes. The slides were soaked in 95% EtOH for 2 minutes and in 100% EtOH for 6 minutes. Finally, the slides were soaked in xylene for 4 minutes. Cover plates were mounted on the slides.

3.3.5 Analysis

The intended analysis was through the use of the superposition technique whose spatial resolution has been determined to be on the order of μm (Lui, 1989). In this technique micrographs of the etched detectors and glass stained slides are obtained and scanned into a computer. The digitized images are then superimposed to reveal the spatial distribution of ^{10}B in the samples. However, before embarking on this lengthy procedure, the etched detectors were carefully observed under a microscope.

This chapter has described the methods used in the in vitro analysis of ^{10}B uptake, namely Prompt Gamma Neutron Activation Analysis, Thermal Neutron Irradiation and Neutron Induced Alpha Track Autoradiography. Results of these experiments will be presented in the following chapter.

4 In Vitro Analysis of ^{10}B Uptake: Results

Complete results of the in vitro analysis of ^{10}B uptake will be presented in this chapter in the same order as the methods were described in the previous chapter, i.e. starting from the results of Prompt Gamma Neutron Activation Analysis, Thermal Neutron Irradiation and ending with Neutron Induced Alpha Track Autoradiography.

4.1 Prompt Gamma Neutron Activation Analysis

Results will be presented in the same order that the experimental conditions were presented in Section 3.1.3. Unless otherwise specified, the boron compound used was $K_2B_{12}H_{12}$. Before presenting the experimental results, it must be emphasized again that the boron compound was not enriched in ^{10}B. Since natural boron has only 20% ^{10}B, all the concentrations obtained could be increased by a factor of five if boron 100% enriched in ^{10}B were used.

(i) Uptake by RA synovium as a function of incubation concentration

RA synovium bulk uptake as a function of incubation concentration is shown in Table 4.1.

Table 4.1: Uptake by RA synovium as a function of incubation concentration

Incubation	Weight (g)	Uptake (ppm)	Error (%)	Ave. Uptake (ppm)	Ave. Error (%)
100 ppm	0.13	41.1	10.7	39	14
	0.10	45.2	14.9		
	0.14	31.5	16.6		
500 ppm	0.18	513.4	9.4	322	9
	0.18	227.9	8.8		
	0.13	224.8	9.5		
1000 ppm	0.20	539.2	8.7	497	10
	0.18	406.2	9.0		
	0.15	545.3	10.7		
Control	0.08	0	0	0	0

For this experiment, the concentrations of the media were measured. The nominal 100 ppm solution was actually measured to contain 110 ppm, the 500 ppm solution 570 ppm and the 1000 ppm solution 1050 ppm. This shows that there is good agreement between the intended concentration and the actual one. In general, they are within 10% of each other. This is important because the concentrations of the media were not measured in all experiments.

As can be seen from Table 4.1, average ^{10}B concentrations achievable in RA synovium range from approximately 40 ppm to 500 ppm with the incubation medium concentration ranging from 100 ppm to 1000 ppm. The uptake by RA synovium does not increase in a linear fashion. The data do not immediately suggest a saturation mechanism in that the average concentration achieved with a 1000 ppm incubation, 497 ppm, should be lower if a saturation mechanism were in effect. However, this does not exclude that the uptake could be approaching saturation, a process which could be affected differences in tissue.

(ii) Uptake by RA synovium as a function of incubation time

Uptake by RA synovium as a function of incubation time is shown in Table 4.2(a). The incubation concentration was constant at a measured concentration of 1146±7.5%ppm.

Table 4.2 (a): Uptake by RA synovium as a function of incubation time

Incubation Time	Weight (g)	Uptake (ppm)	Error (%)	Ave. Uptake (ppm)	Ave. Error (%)
15 min.	0.24	189.6	8.8	197	9
	0.26	239.1	8.2		
	0.14	161.7	10.3		
30 min.	0.20	297.7	8.3	297	8
	0.21	312.0	7.1		
	0.12	282.5	9.1		
1 hr.	0.18	474.5	9.3	381	9
	0.11	344.4	10.0		
	0.25	324.9	8.4		

Table 4.2 (a): Uptake by RA synovium as a function of incubation time

Incubation Time	Weight (g)	Uptake (ppm)	Error (%)	Ave. Uptake (ppm)	Ave. Error (%)
control	0.09	0	0	0	0

These results indicate that the rate of uptake is not constant. The fastest rate of uptake occurs in the first fifteen minutes with one half to one third of the uptake taking place. For an increase in time by a factor of 4 (from 15 minutes to 1 hour), the concentration less than doubled, going from an average of 197 ppm to an average of 381 ppm.

In addition, a set of samples was incubated in a boric acid (BA) solution measured to be 50 ppm ±7.8% and the results are presented in Table 4.2(b). The average uptake was 15 ppm, less than half the concentration in the medium. This uptake is consistent with the uptake reported in preliminary work with boric acid which showed that about 40 ppm was taken up after incubation for 1 hour at a nominal incubation concentration of 90 ppm of unenriched boric acid (Johnson et al, 1994).

Table 4.2 (b): Uptake of Boric Acid by RA synovium

Incubation	Weight (g)	Uptake (ppm)	Error (%)	Ave. Uptake (ppm)	Ave. Error (%)
BA: 1 hr	0.14	16.7	9.2	15	17
	0.13	10.3	31.0		
	0.18	17.4	11.4		

It must be noted that there are no controls included in Table 4.2(b) because this experiment was done at the same time as the experiment whose results are presented in Table 4.2(a) and only one control was done for the whole experiment.

(iii) Uptake by OA cartilage as a function of boron compound type

The uptake in OA cartilage as a function of boron compound was measured using the three different compounds described in section 3.1.4. In Table 4.3, which presents the results of this experiment, the following notation will be used. The boron particulate will be denoted by BP. The unenriched boric acid solution at the nominal concentration of 100 ppm will be denoted as BA and the boron compound, $K_2B_{12}H_{12}$, unenriched in ^{10}B at a

nominal concentration of 1000 ppm, will be noted by KBH. The incubation time for all compounds was constant at 1 hour. The concentrations of the media were not measured. However, as can be seen from the experimental results presented in (i) of this section, the media should equal the nominal concentrations to within 10%.

Table 4.3: Uptake of OA cartilage as a function of boron compound

Incubation	Weight (g)	Uptake (ppm)	Error (%)	Ave. Uptake (ppm)	Ave. Error (%)
BP	0.02	39.1	7.0	56	7
	0.01	24.5	7.2		
	0.01	68.9	6.9		
	0.04	92.0	6.9		
BA	0.07	4.84	8.4	2.6	12
	0.02	---	---		
	0.03	0.45	14.7		
	0.02	---	---		
KBH	0.03	31.2	7.1	30	7
	0.01	29.9	7.3		
	0.05	35.6	7.1		
	0.02	24.3	7.6		
Control	0.02	0	0	0	0

Those entries marked with (---) correspond to samples for which no reasonable result could be obtained, i.e. the concentration was negative. Possible reasons for this include the weight of the sample relative to the error in the vial weight. This will be discussed in detail in the final chapter of this thesis. Table 4.3 shows that the highest uptake of OA cartilage is with the boron particulate averaging 56 ppm. The lowest is the boric acid solution which averages 2.6 ppm. The uptake of $K_2B_{12}H_{12}$, averaging 30 ppm, is comparable to the fraction uptake of the boric acid solution.

(iv) Uptake by RA synovium and RA cartilage as a function of incubation concentration and incubation time

The results of this set of experimental conditions, as described in 3.1.4, are shown in the following table, Table 4.4.

Table 4.4: Uptake by RA synovium and RA cartilage as a function of concentration and incubation time

Incubation	Weight (g)	Uptake (ppm)	Error (%)	Ave. Uptake (ppm)	Ave. Error (%)
sy:100 ppm:1 hr	0.60	16.8	8.7	19	9
	0.35	18.7	9.0		
	0.93	22.1	8.6		
	0.57	16.6	8.8		
sy:500 ppm:1 hr	0.54	63.4	8.5	79	8
	0.40	105.2	8.1		
	0.36	82.1	8.4		
	0.47	64.4	8.2		
sy:1000 ppm:1 hr	0.62	124.9	8.1	190	8
	0.80	145.2	7.4		
	0.64	217.5	7.8		
	0.30	270.8	8.0		
sy:1000 ppm:2 hr	0.45	190.8	8.1	198	10
	0.41	250.2	7.4		
	0.73	158.9	7.8		
	0.50	191.7	8.0		
sy: 1000 ppm:24 hr	0.37	49.6	6.9	44	7
	0.56	35.9	6.9		
	0.50	45.5	6.8		
	0.62	44.4	6.8		
sy: controls	0.61	0	0	0	0

Table 4.4: Uptake by RA synovium and RA cartilage as a function of concentration and incubation time

Incubation	Weight (g)	Uptake (ppm)	Error (%)	Ave. Uptake (ppm)	Ave. Error (%)
	1.00	0	0		
	0.77	0	0		
	0.44	0	0		
ct:500 ppm:1 hr	0.04	45.1	7.0	30	8
	0.02	15.3	9.1		
	0.03	30.5	7.5		
ct: 1000 ppm: 1 hr	0.07	84.9	6.9	107	7
	0.05	128.6	6.9		
ct: controls	0.03	0	0	0	0
	0.05	0	0		
	0.03	0	0		

The average concentrations achieved in the synovium samples at the same incubation solutions and times are significantly lower than those presented in Table 4.1, i.e. the average concentration for a 1 hour 100 ppm incubation was 19 ppm, for 500 ppm was 79 ppm and for 1000 ppm was 190 ppm compared to the averages 39 ppm, 322 ppm and 497 ppm, respectively, from Table 4.1.

The weights of the samples in this experiment, however, were higher than the weights in experiment (i). The ranges for the 1 hour incubations at nominal concentrations of 100, 500 and 1000 ppm were 0.35-0.93g, 0.36-0.54g, 0.30-0.64g in this experiment while in experiment (i) the ranges were 0.10-0.14g, 0.13-0.18g and 0.15-0.20g, respectively. The dependence of measured uptake on sample size will be specifically tested in experimental conditions (viii) and (ix).

The synovium samples incubated for 24 hours in the 1000 ppm seem to be inconsistent with the rest of the experiment; their average uptake was 44 ppm while the average uptake

of the samples incubated for 1 hour was 107 ppm. The average uptake for 24 hour should have been greater than for 1 hour if the uptake were to keep increasing with time.

The uptake of cartilage when incubated in a 500 ppm solution for 1 hour was less than half of the uptake of synovium. The magnitude of this differential was not maintained when samples were incubated in a 1000 ppm solution. The average cartilage uptake increased to 107 ppm, more than half of the synovium uptake at that concentration, 190 ppm.

(v) Uptake by RA synovium and RA cartilage as a function of incubation concentration and time

Results of this experiment are presented in Table 4.5. Essentially, the same type of experiment was performed as (iv) except that the comparison is more complete. The nominal incubation medium concentration for 100 ppm corresponded to a measured value of 97±7.6% ppm, for 500 ppm to 490±7.2% and then for 1000 ppm to 1025±7.5%. Again, the measured concentrations are within 10%. In the table, the nominal concentrations are listed rather than the measured ones.

Table 4.5: Uptake by RA synovium and cartilage as a function of incubation concentration and incubation time

Incubation	Weight (g)	Uptake (ppm)	Error (%)	Ave. Uptake (ppm)	Ave. Error (%)
sy:100 ppm: 1hr	0.23	33.2	7.1	42	7
	0.23	46.1	7.1		
	0.20	42.2	7.0		
	0.25	44.7	7.1		
sy:100 ppm:2 hr	0.37	49.8	8.8	57	9
	0.33	48.4	8.5		
	0.20	70.4	8.9		
	0.36	58.7	9.0		
sy:500 ppm: 1 hr	0.24	185.5	8.1	166	8

Table 4.5: Uptake by RA synovium and cartilage as a function of incubation concentration and incubation time

Incubation	Weight (g)	Uptake (ppm)	Error (%)	Ave. Uptake (ppm)	Ave. Error (%)
	0.43	150.4	7.6		
	0.37	203.8	7.8		
	0.37	126.0	7.6		
sy:500 ppm:2 hr	0.40	189.5	7.4	241	7
	0.42	227.1	7.3		
	0.28	269.5	7.7		
	0.27	277.6	7.4		
sy:1000 ppm: 1 hr	0.26	228.5	7.8	289	7
	0.25	314.3	7.5		
	0.27	280.2	7.6		
	0.26	331.1	7.6		
sy:1000 ppm: 2 hr	0.35	468.3	7.4	428	7
	0.25	473.2	7.9		
	0.32	369.7	7.3		
	0.41	401.3	7.3		
sy: control	0.43	0	0	0	0
	0.41	0	0		
	0.28	0	0		
	0.28	0	0		
ct:100 ppm: 1 hr	0.02	54.6	8.2	58	8
	0.04	87.3	7.9		
	0.02	34.4	7.4		
ct:100 ppm: 2 hr	0.03	----	----	----	----
	0.06	----	----		
	0.03	----	----		
ct: 500 ppm: 1 hr	0.02	----	---	186	9

Table 4.5: Uptake by RA synovium and cartilage as a function of incubation concentration and incubation time

Incubation	Weight (g)	Uptake (ppm)	Error (%)	Ave. Uptake (ppm)	Ave. Error (%)
	0.02	---	---		
	0.02	186	9		
ct: 500 ppm: 2 hr	0.03	-----	----	----	----
	0.02	----	----		
	0.03	----	----		
ct: 1000 ppm: 1 hr	0.01	----	----	----	----
	0.03	----	----		
	0.01	----	----		
ct: 1000 ppm: 2 hr	0.01	----	----	----	----
	0.04	----	----		
	0.03	----	----		
ct: control	0.03	0	0	0	0
	0.01	0	0		
	0.01	0	0		

The average uptake of the synovium at the incubation time of 1 hour and concentration of 100 ppm was 42 ppm, comparable to the 39 ppm of experiment (i). As indicated in the above table, the average synovium uptake at the incubation concentrations of 500 ppm and 1000 ppm were 166 ppm and 289 ppm, lower than the uptake at the corresponding concentrations in experiment (i), i.e. 322 ppm and 497 ppm. It must be noted that the average weights of the samples was greater in this experiment than in experiment (i).

Within this experiment, the two hour incubation caused increased uptake which as before was not linear with increased incubation time. However, this time, the concentration did not overestimate a linear increase, i.e. the uptake more than doubled with the doubling of the time, but rather underestimated it, i.e. the uptake was less than double with the doubling of time. This suggests the beginning of a saturation point in the uptake.

The cartilage samples in this experiment did not give satisfactory results. The few results which were obtained did not indicate a differential with synovium uptake, i.e. the uptakes of cartilage and synovium were comparable.

(vi) Uptake by RA cartilage as a function of incubation concentration and time

Results for examples at this set of experimental parameters is shown in Table 4.6.

Table 4.6: Uptake by RA cartilage as a function of incubation concentration and time

Incubation	Weight (g)	Uptake (ppm)	Error (%)	Ave. Uptake (ppm)	Ave. Error (ppm)
100 ppm: 1 hr	0.01	3.45	15.6	4	14
	0.03	4.99	12.9		
	0.05	3.78	14.7		
100 ppm:24 hr	0.01	1.32	23.0	2	12
	0.03	2.37	17.4		
	0.03	3.31	15.6		
1000 ppm:1 hr	0.04	17.8	7.62	42	7
	0.04	60.6	6.93		
	0.02	47.6	7.05		
1000 ppm:24 hr	0.01	29.9	7.48	28	7
	0.04	25.2	7.48		
	0.04	---	---		
controls	0.01	0	0	0	0
	0.01	0	0		
	0.02	0	0		

As can be seen in the Table 4.6, the uptake of cartilage is an average of 4 ppm as a result of incubation with a nominal solution concentration of 100 ppm and an average of 42 ppm for incubation with a nominal solution concentration of 1000 ppm. The increase in uptake

as a function of incubation concentration appears to be linear. This uptake is about ten times less than the uptake observed in synovium which is on the order of 40 ppm for incubation with 100 ppm and on the order of 400 for incubation with 1000 ppm. This would mean that there is a differential of 10:1 between synovium and cartilage uptake.

However, the data suggest that after a point uptake may be inversely proportional to the incubation time. The average uptake for incubation with a nominal concentration of 100 ppm is halved when the average uptake for incubation with a nominal concentration of 1000 ppm decreases by one quarter. From these two observations, it can be said at 24 hours the average uptake decreases with increasing incubation concentrations.

(vii) Uptake by RA synovium as a function of sample size

For this experiment, the nominal incubation concentration was set at 1000 ppm and the time of incubation set to 1 hour. Results of the uptake as a function of sample size are shown in Table 4.7.

Table 4.7: Uptake by RA synovium as a function of sample size

Size	Weight (g)	Uptake (ppm)	Error (%)	Ave. Uptake (ppm)	Ave. Error (%)
large	0.26	228.5	7.8	289	8
	0.25	314.3	7.5		
	0.27	280.2	7.6		
	0.26	331.1	7.6		
control	0.24	0	0	0	0
	0.23	0	0		
medium	0.21	321.7	8.4	320	8
	0.16	332.4	8.7		
	0.20	275.4	8.4		
	0.17	350.9	8.2		
control	0.09	0	0	0	0
	0.06	0	0		

Table 4.7: Uptake by RA synovium as a function of sample size

Size	Weight (g)	Uptake (ppm)	Error (%)	Ave. Uptake (ppm)	Ave. Error (%)
small	0.08	340.4	9.6	344	9
	0.09	300.4	9.1		
	0.08	355.7	9.8		
	0.10	380.3	9.2		
control	0.03	0	0	0	0
	0.03	0	0		

The difference in average uptake between the "large" and "medium" pieces is not very large. In fact, taking into account the magnitude of the errors, there is overlap between the ranges. For example, taking the higher possible value for the average uptake of the large pieces, i.e. 289 + 8% of 289 ppm, yields 312 ppm. This is higher than taking the lowest value for the medium size uptake, i.e. 320 - 8% of 320 ppm which yields 294 ppm. The average weight of the large pieces is 0.26 g while of the medium pieces of 0.19 g and of the small pieces of 0.09 g with no overlapping sizes.

(viii) Uptake by RA synovium as a function of sample size at a different time point

This experiment is essentially the same as (vii) except that time of incubation was increased to 24 hours. Results are shown in Table 4.8 below.

Table 4.8: Uptake by RA synovium as a function of sample size at a different time point

Size	Weight (g)	Uptake (ppm)	Error (%)	Ave. Uptake (ppm)	Ave. Error (%)
large	0.18	410.6	7.2	426	8
	0.18	458.3	8.7		
	0.19	417.1	8.7		
	0.20	419.2	8.6		
control	0.11	0	0	0	0
	0.12	0	0		

Table 4.8: Uptake by RA synovium as a function of sample size at a different time point

Size	Weight (g)	Uptake (ppm)	Error (%)	Ave. Uptake (ppm)	Ave. Error (%)
medium	0.05	462.6	8.2	526	9
	0.07	551.4	8.8		
	0.09	551.5	8.7		
	0.08	537.8	8.9		
control	0.04	0	0	0	0
	0.07	0	0		
small	0.03	1144.2	8.6	1080	10
	0.04	1252.4	10.9		
	0.03	1069.0	10.4		
	0.02	854.0	10.9		
control	0.04	0	0	0	0
	0.04	0	0		

The difference between average sample uptake of the three different sizes is significant. In other words, taking the highest possible value in the average uptake of the large samples (426 + 0.08*426) yields 460 ppm which is lower than 573 ppm, the lowest value using the averages and errors for the medium samples listed above (526+0.09*526). The average weights in this experiment were, 0.19 g for the large pieces, 0.75 g for the medium pieces and 0.03 g for the small ones.

(ix) Uptake by large pieces of bovine cartilage

Bulk tissue uptake was measured for large pieces of bovine cartilage and Table 4.9, below, shows the results.

Table 4.9: Uptake by large pieces of bovine cartilage

Size	Weight (g)	Uptake (ppm)	Error (%)	Ave. Uptake (ppm)	Ave. Error (%)
large	0.36	436.4	7.2	617	8.7

Table 4.9: Uptake by large pieces of bovine cartilage

Size	Weight (g)	Uptake (ppm)	Error (%)	Ave. Uptake (ppm)	Ave. Error (%)
	0.11	644.1	8.7		
	0.13	803.1	8.7		
	0.21	585.2	10.2		
control	0.22	0	0	0	0
	0.18	0	0		
	0.21	0	0		
	0.13	0	0		

In this set of samples the uptake by cartilage was large, an average of 617 ppm comparable to synovium. This is in direct conflict with other experimental data presented previously.

In an attempt to understand the relationship between uptake and sample size, a plot was made of uptake versus sample size, using only those experiments with three or more sets of samples. All the data in the previous tables were combined and shown in Figure 4.1.

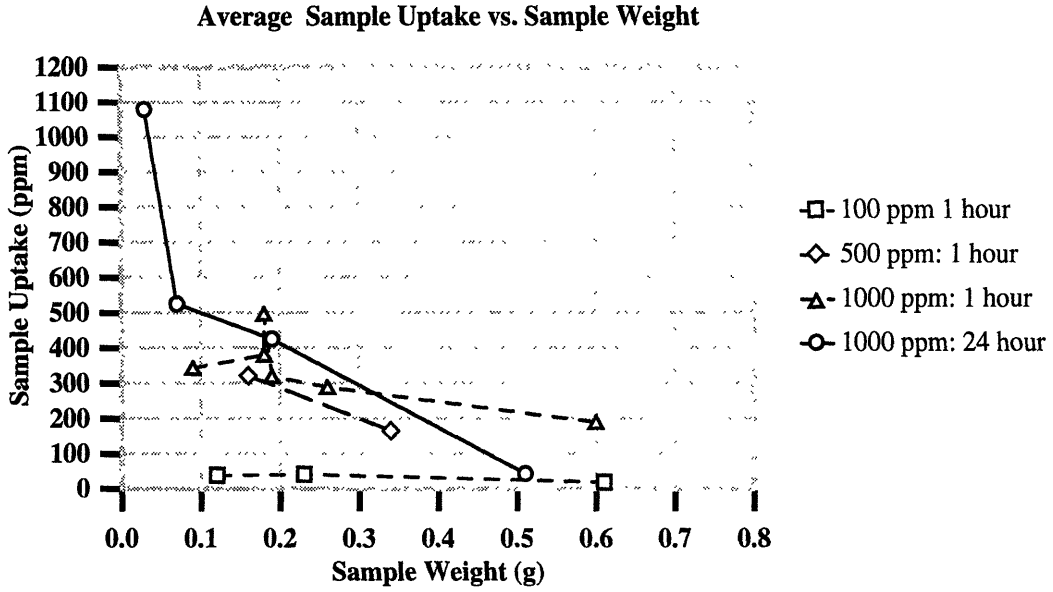

Figure 4.1 Average Sample Uptake vs. Weight for sets with three or more experiments.

As seen in Figure 4.1, the uptake for the 24 hour incubation at a nominal concentration of 1000 ppm yielded uptake that was greater than 1000 ppm. For the 1 hour incubation at 1000 ppm, the decrease in uptake versus sample size is not smooth but shows an increase around 0.2 g. The average uptake for the samples incubated for 1 hour at 100 ppm remained relatively constant as the weight of the sample changed.

A possible explanation for Figure 4.1 could be related to a limited diffusion distance of the boron compound inside the tissue. When boron uptake is determined via Prompt Gamma Neutron Activation Analysis, the B/H ratio is used in order to correct the effects of improper sample positioning in the beam and reduce variations in thermal neutron flux. However, if the boron compound were only able to diffuse a certain distance into the tissue and the sample size were big, then the ratio which is inversely proportional to the size of the tissue, or the hydrogen content would decrease.

4.2 Thermal Neutron Irradiation

In light of the unacceptably large error in the dose delivered to the RA synovium samples, those results are not hereby included. The results of the thermal neutron irradiation of the cartilage samples were equivocal. There did not appear to be any difference between the boronated and nonboronated irradiated cells, or between the irradiated and nonirradiated sets of samples. A wash out of proteoglycans was observed in all samples, suggesting that the wash out could be due to in vitro cell culture rather than irradiation. In fact, a problem with in vitro work is that tissue is slowly undergoing autolysis, i.e. breaking down, making it difficult to attribute cell kill to irradiation rather than normal autolysis.

Results of this experiment with RA cartilage are shown in the following figures. More specifically, Figure 4.2 shows the results of thermal neutron irradiation of both boronated and nonboronated cells. Figure 4.3 shows the control set of samples, i.e. the boronated and nonboronated samples that were placed in incubators rather than irradiated. In all pictures, the washout of the proteoglycans is indicated by gradual discoloring towards the bottom of each picture.

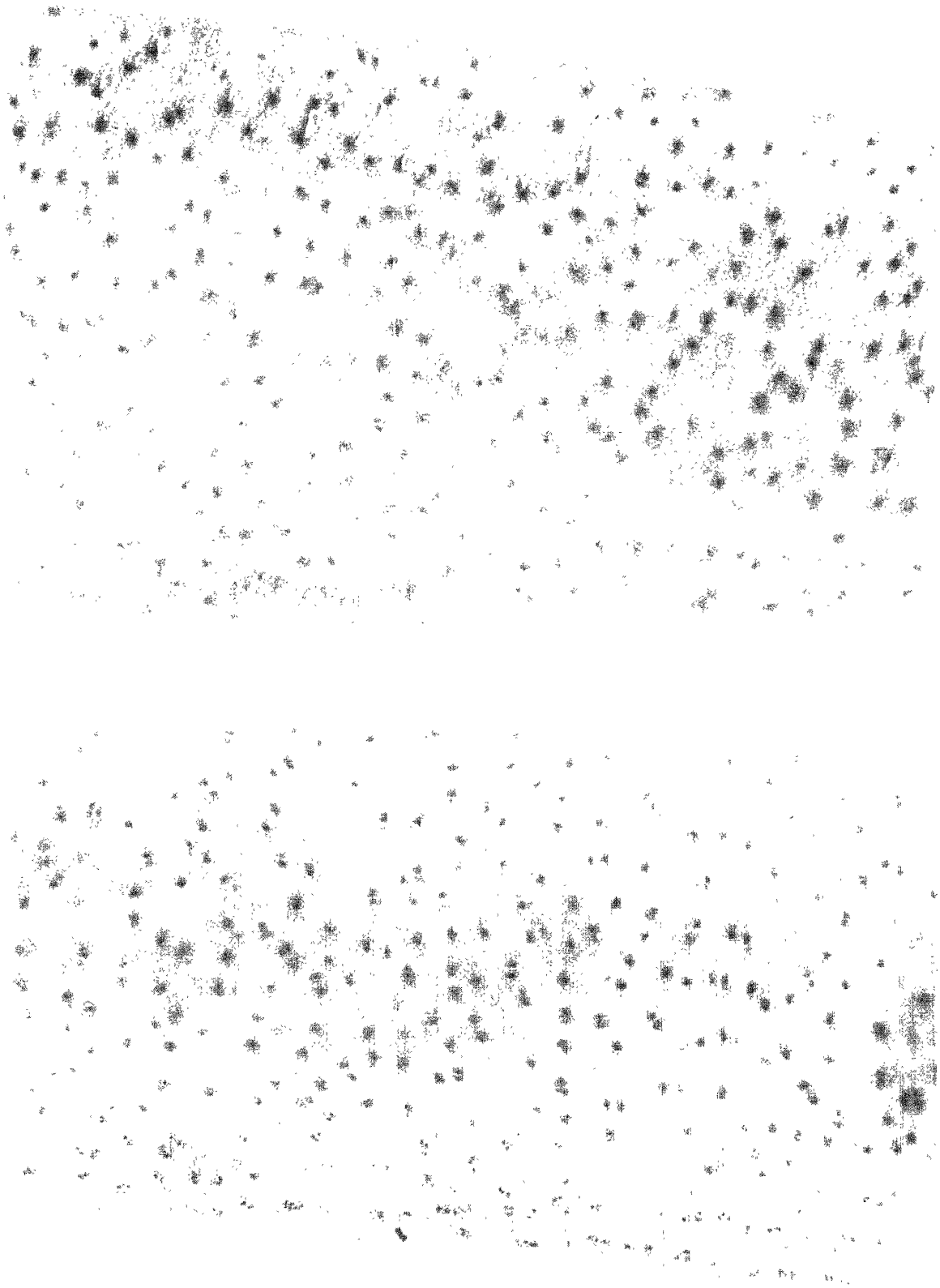

Figure 4.2 Results of thermal neutron irradiation on (a) boronated and (b) nonboronated samples of osteoarthritic cartilage

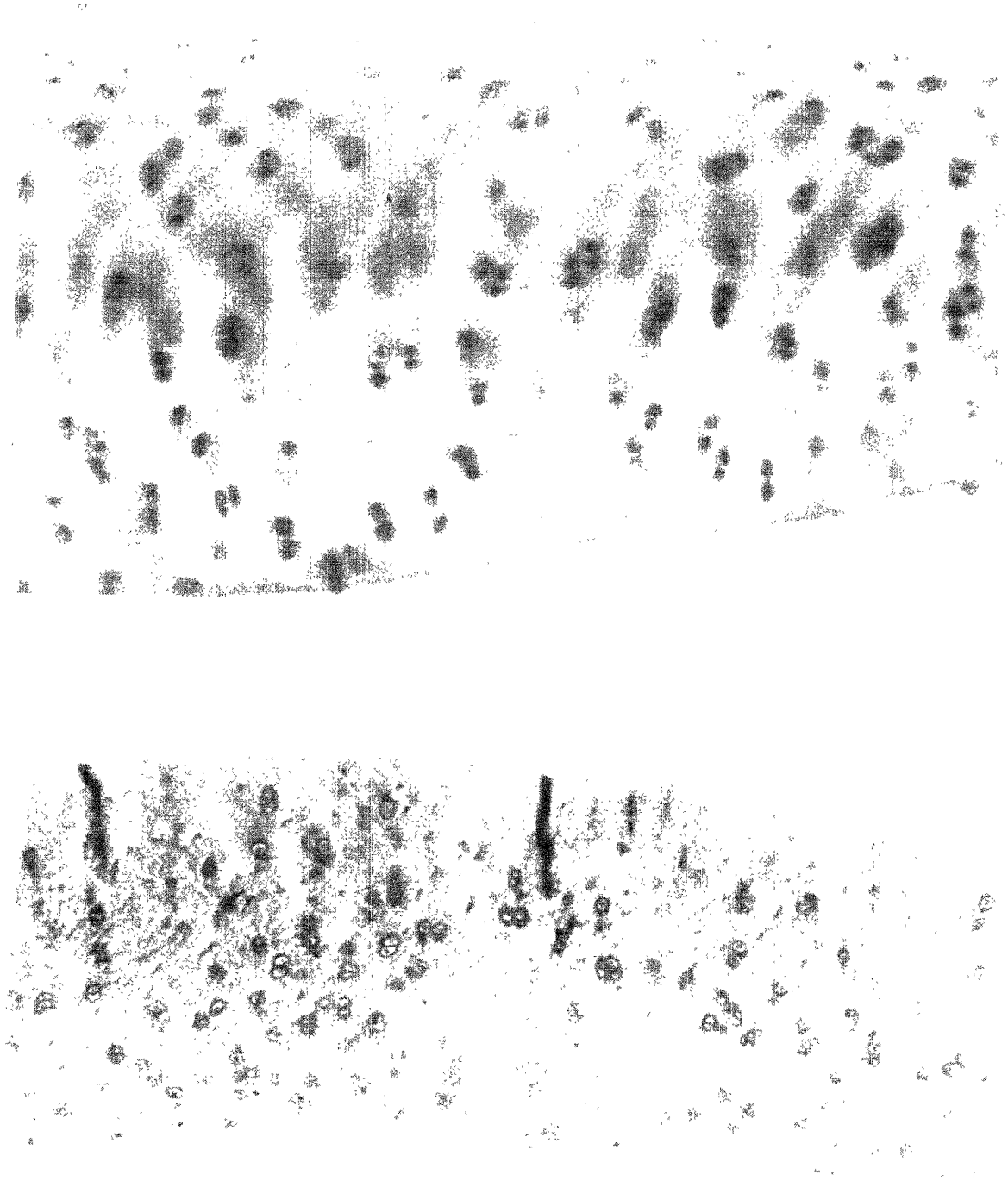

Figure 4.3 Illustration of the (a) boronated and (b) nonboronated samples of osteoarthritic cartilage which were incubated rather than irradiated.

4.3 Neutron Induced Alpha Track Autoradiography

Of all the track etch detectors used and samples tried, only one of the sample which had been incubated in a boron particulate gave an indication of alpha particle tracks. However, the corresponding section of tissue was not available and hence the superimposition of the track etch detector with the glass slide could not be done to yield significant information on the boron distribution. The rest of the slides showed either undersaturation, i.e. the boron neutron capture reaction was not induced, or oversaturation, i.e. the track etch detector was exposed for too long and the background from the protons was so strong that it overpowered the alpha particle tracks. During the experiment, a problem occurred with the shutter of the reactor and the reactor power was only known with an uncertainty of approximately 50%. Since Neutron Induced Alpha Track Autoradiography is sensitive to reactor power, this uncertainty caused the lack of useful results.

5 Neutron Beam Design: Methods

This chapter will present the method used to design an accelerator-based neutron beam for BNCS. The first step in the design was to determine the neutron beam energy range required for BNCS. This was done by studying the dosimetric properties of "ideal", monoenergetic, photon-free neutron beams ranging in energy from 0.025 eV to 10 keV in a phantom model of a knee. Both monodirectional and isotropic ideal neutron beams were studied representing the two extremes of angular distribution of neutrons emerging from a moderator/reflector assembly. The methodology used will be described in section 5.1

Having determined the therapeutically useful neutron energy range for BNCS, attention was then turned to the design of a moderator/reflector assembly which would be able to moderate the energetic neutrons coming from the accelerator source to the therapeutically useful neutron energy range determined in the first step. In order to evaluate the assembly in air rather than in a phantom, thereby reducing the computation time required, a Figure of Merit was formulated and tested by comparison of the results with those obtained in a phantom, as discussed in section 5.2.

The next step was to evaluate which of two neutron producing reactions, $^{7}Li(p,n)^{7}Be$ or $^{9}Be(p,n)^{9}Be$, would be most appropriate for BNCS. The material, such as lithium and beryllium, which when irradiated with protons produces neutrons is referred to as target material. The process of target selection will be discussed in section 5.3.

Finally, materials for the moderator/reflector assembly were selected. This selection was done by modifying work done by Yanch et al for an accelerator based epithermal neutron beam design for BNCT (Yanch et al, 1992) to fit the requirements of BNCS. The dose and flux dependence on both the length and diameter of both the moderator and reflector was investigated. This part of the neutron beam design process will be described in section 5.4.

The computational method used for the entire beam design was Monte Carlo for Neutron and Photon Transport Code (MCNP) version 4A (Breismeister, 1986) which is installed on Sun Sparc Stations at the Whitaker College Biomedical Imaging and Computational

Laboratory at MIT. Advantages of this code which has been used extensively for many years include the use of point-wise continuous energy cross-section data from a number of sources, complete three-dimensional freedom in designing any configuration of materials and a sophisticated built-in geometry package to aid in debugging.

5.1 Determination of Optimal Neutron Energy Range

5.1.1 Monodirectional Ideal Beams

The geometry used for the monodirectional ideal beam studies is shown in Figure 5.1. The phantom model consists of a series of concentric cylinders representing the different tissue layers found in the arthritic joint. The knee was chosen as the model because it is the joint on which synovectomy is most commonly performed (Fleming et al, 1976). The tissue thicknesses of the knee phantom were obtained from Magnetic Resonance Images of human arthritic knees. A 10 cm diameter monoenergetic neutron beam was placed 1.65 cm away from the phantom surface. Absorbed doses were tallied in a cross-section of a cylinder, with width of 2.5 cm, as shown in Figure 5.1, and height of 6 cm, in the plane perpendicular to the beam.

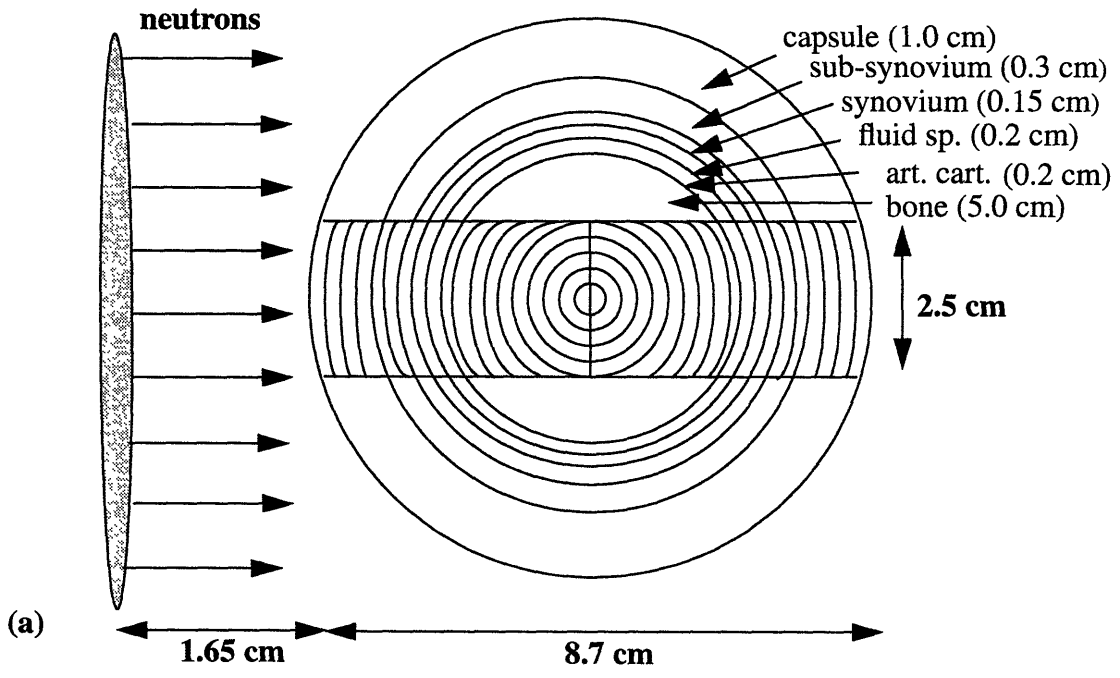

Figure 5.1 Ideal beam study geometry of cylindrical joint phantom using a monodirectional source of neutrons.

Several assumptions were made in the calculation of dose per depth in the joint phantom. The first one was that the synovium contained 400 ppm of ^{10}B, a conservative estimate of the concentrations readily achieved in vitro as seen in chapter 4. The second assumption was that $3.6x10^{12}$ n/s were being emitted from the source. This number was derived from the total neutron yield expected from the $^{7}Li(p,n)^{7}Be$ reaction using a proton current of 4 mA, the maximum current expected from the tandem electrostatic accelerator constructed by Newton Scientific Inc., for the MIT Laboratory for Accelerator Beam Applications (LABA). Lastly, no RBE values were applied to the calculation of dose.

Fifteen beam energies were simulated ranging from 0.025 eV to 10 keV. Particle flux was determined as a function of depth for all components: thermal neutrons (neutrons with a cutoff energy of 0.36 eV), nonthermal neutrons (neutrons with energies above 0.36 eV) and induced photons, including the 478 keV prompt photon emitted in the $^{10}B(n,\alpha)^{7}Li$ reaction. In order to obtain dose rates, both the neutron and photon fluxes were modified by the fluence-to-kerma conversion factors of Caswell et al (Caswell et al, 1982) and Zamenhof et al (Zamenhof et al, 1975).

To estimate the $^{10}B(n,\alpha)^{7}Li$ contribution to dose in the synovial lining, the thermal neutron flux was modified by the ^{10}B fluence-to-kerma conversion factors provided by Zamenhof et. al (Zamenhof et al, 1975) and multiplied by 400. A similar procedure was followed for the boron dose contribution to healthy tissue which was assumed to contain 1 ppm of ^{10}B.

Individual dose components were plotted as a function of depth in the joint model for each energy. Figure 5.2 shows the dose components for beams of energy 0.025 eV and 0.1 eV, both thermal, according to our definition. Note that two peaks appear in the plots as a result of calculating synovial dose at both the "front" and "back" of the knee model. For the 0.025 eV beam, the percent of the gamma dose increases from about 44% of the total dose at the surface of the phantom to 78% at the midpoint of the bone with the exception of the synovial lining where the gamma contribution is less than 1% and the boron contribution is approximately 98% of the total dose. The neutron dose decreases from 35% at

the surface of the phantom to approximately 13% at the midpoint of the phantom. As is clearly seen in Figure 5.2, the boron dose contribution in non-target tissue is the lowest. The fractional dose contributions for the 0.1 eV are very similar to the 0.025 eV except that the gamma dose contribution is slightly greater at the surface of the phantom than the 0.025 eV case. The neutron and boron dose contributions, except at the synovium of course, are slightly lower than the 0.025eV case.

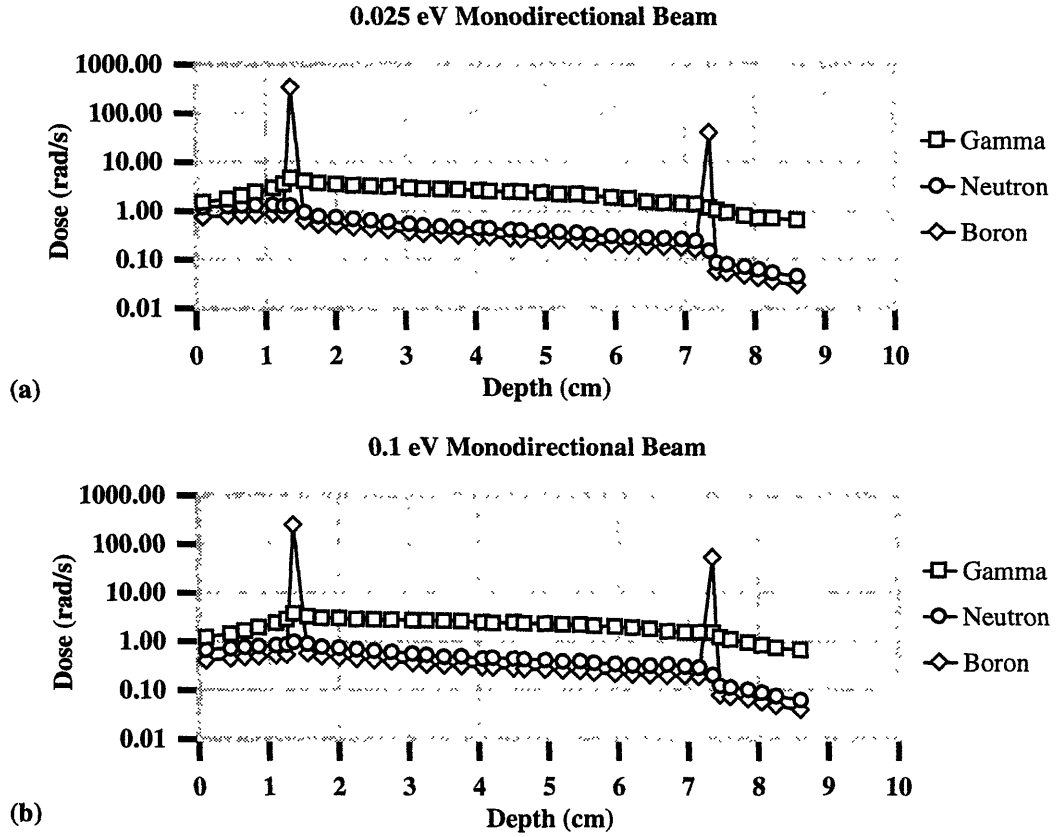

Figure 5.2 Dose per depth in phantom for ideal monodirectional beams energies of (a) 0.025 eV and (b) 0.1 eV.

In the next group of beam energies, i.e. 1 eV, 5 eV and 10 eV, shown in Figure 5.3, the neutron beam energy is increased over the threshold delineating thermal and nonthermal neutrons and thus there is the appearance of the nonthermal neutron component to dose. It is interesting to note that in the 1 eV beam, the fractional gamma dose contribution at the phantom surface is 61% of the total dose, higher than the contribution see from lower energies even though there is the addition of the nonthermal component to dose. It is also

interesting to note that the fractional gamma dose increases to approximately the same value at the midpoint of the bone as the lower energies. For all three beam energies shown in Figure 5.3, the fast neutron dose is comparable to the thermal and boron doses ranging from about 10% to 15%. The gamma dose typically ranges from composing 60% of the total dose at the phantom surface to approximately 80% of the dose at the midpoint of the bone.

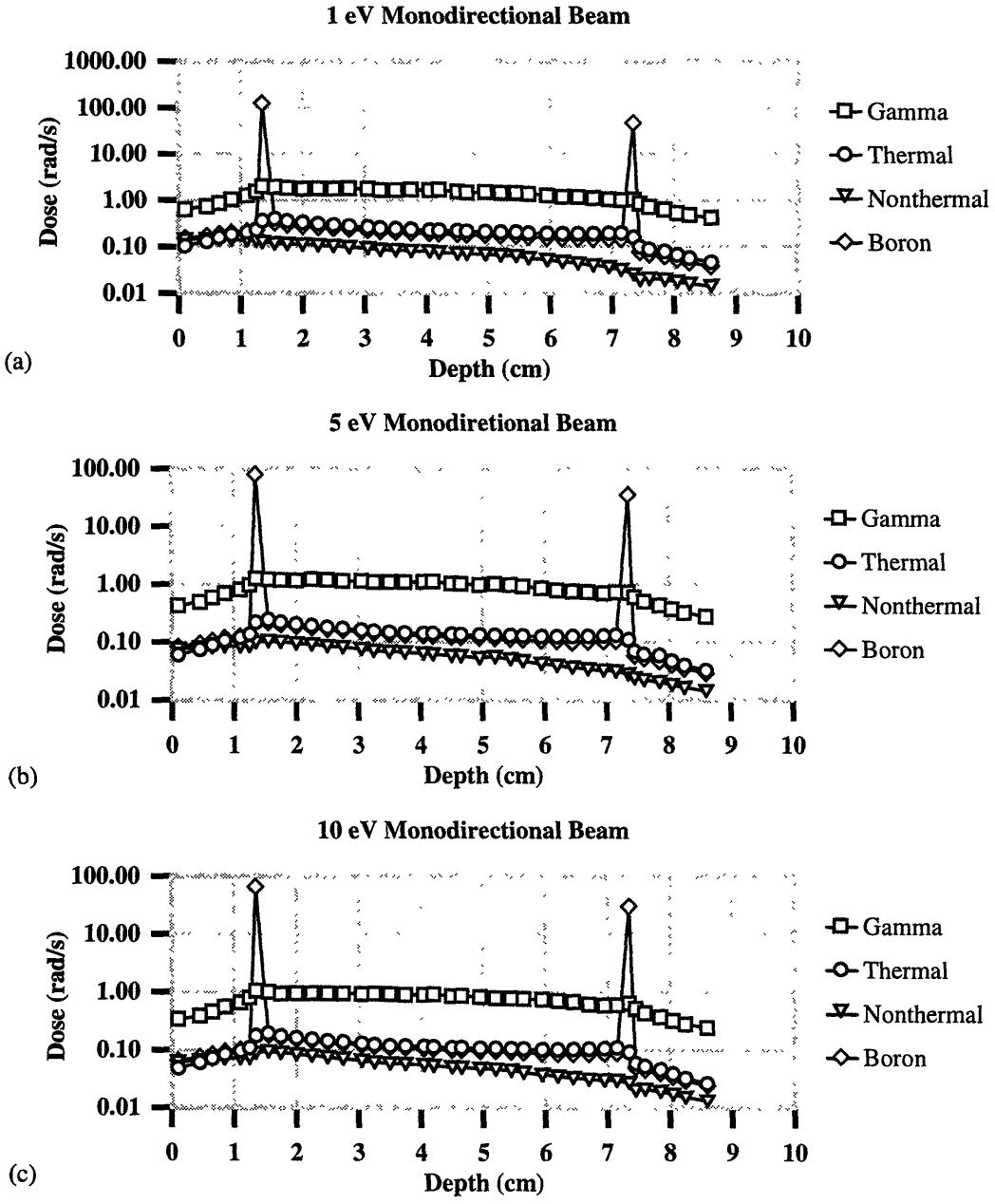

Figure 5.3 Dose per depth in phantom for ideal monodirectional beams energies of (a) 1 eV, (b) 5 eV and (c) 10 eV.

In the next set of three energies, shown in Figure 5.4, the nonthermal neutron dose component rises, reaching the thermal component at 25 eV, coming closer at 50 eV until at 75 eV the fraction of dose due to the nonthermal neutrons is higher than that due to the thermal neutrons at the skin (though still lower than the gamma dose) and equivalent to both the boron and the thermal doses by 75 eV. The gamma dose remains relatively constant throughout these three dose profiles.

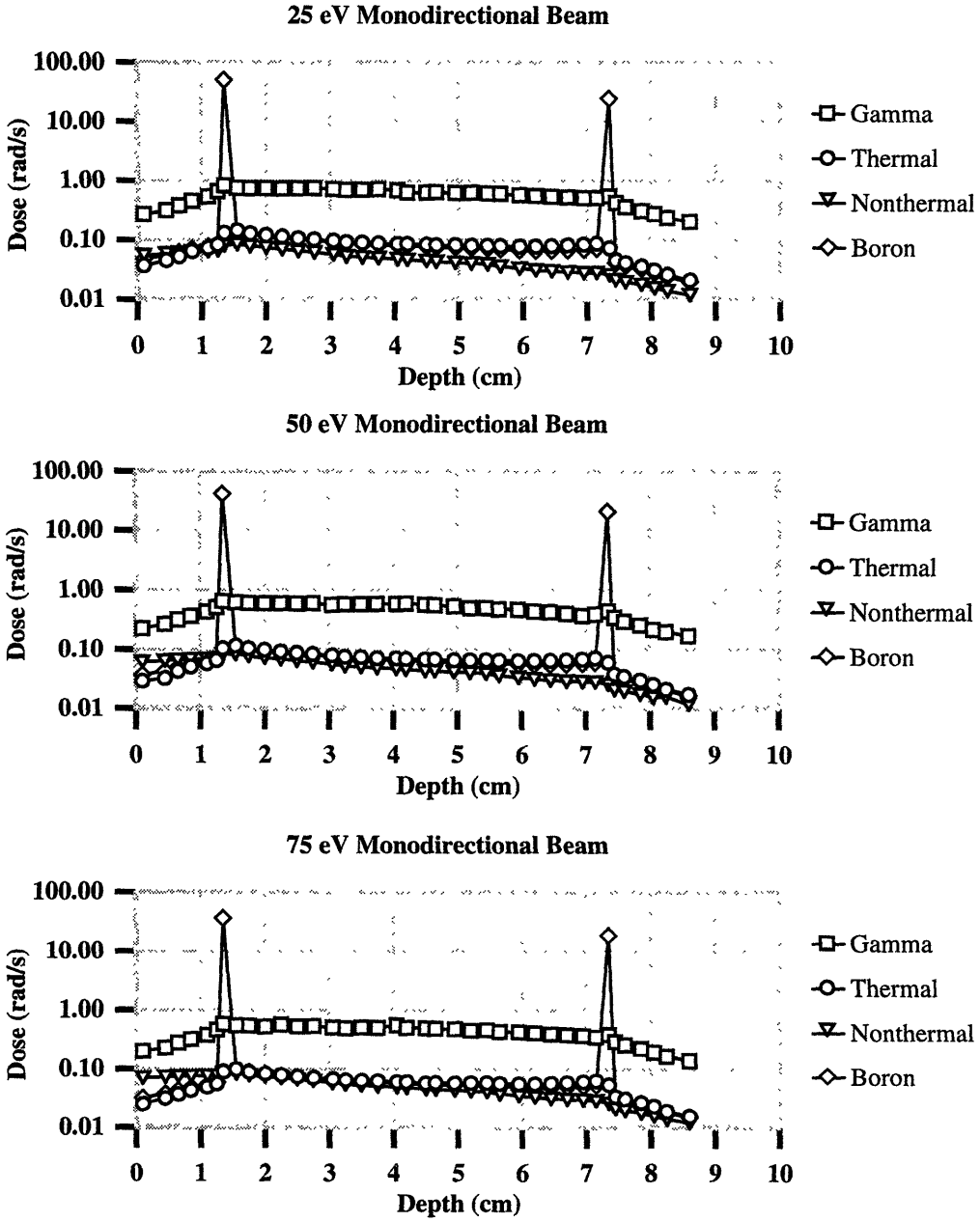

Figure 5.4 Dose per depth in phantom for ideal monodirectional beams energies of (a) 25 eV, (b) 50 eV and (c) 75 eV.

Between the next two energies tested and shown in Figure 5.5, the nonthermal neutron dose increases such that it is comparable to the gamma dose at 125 eV and begins to be higher than the thermal and boron doses. This hasn't affected the percent contribution of the boron to the synovium which is still around 98%.

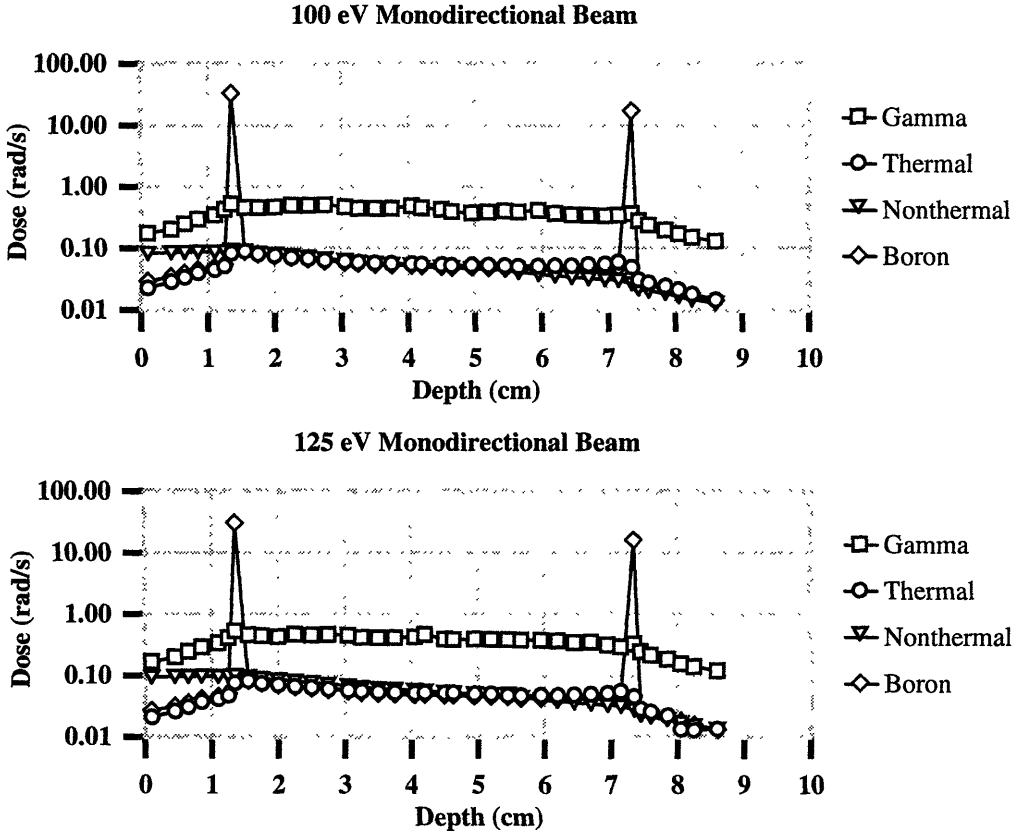

Figure 5.5 Dose per depth in phantom for ideal monodirectional beams energies of (a) 100 eV and (b) 125 eV.

By 250 eV, as shown in Figure 5.6, the fast neutron dose is exactly equal to the gamma dose, both contributing about 45% to the total dose. The boron and thermal contributions for the 250 eV beam are about 5% each. The fast neutron dose remains consistently higher than both the thermal and nonthermal for the entire phantom depth. In fact by 500 eV, the nonthermal neutron dose to the skin is higher than the gamma dose, and the nonthermal neutron dose is approaching the gamma dose though it is still less. Finally, by 750 eV the nonthermal dose not only surpasses the gamma dose at the surface but is approximately equal to the gamma dose until a depth of about 6 cm. At this energy, the fraction of gamma dose to total dose at the surface of the skin is 20% while the nonthermal dose contribution

is greater by a factor of three, in fact, around 76%. The boron contribution, except at the synovium where it is around 97%, remains less than 7% throughout the entire depth of the phantom. The dose contribution of thermal neutrons ranges from 2% at the surface of the phantom to 6% at the midpoint of the bone. The features described in the above paragraphs can be seen in Figure 5.6 below.

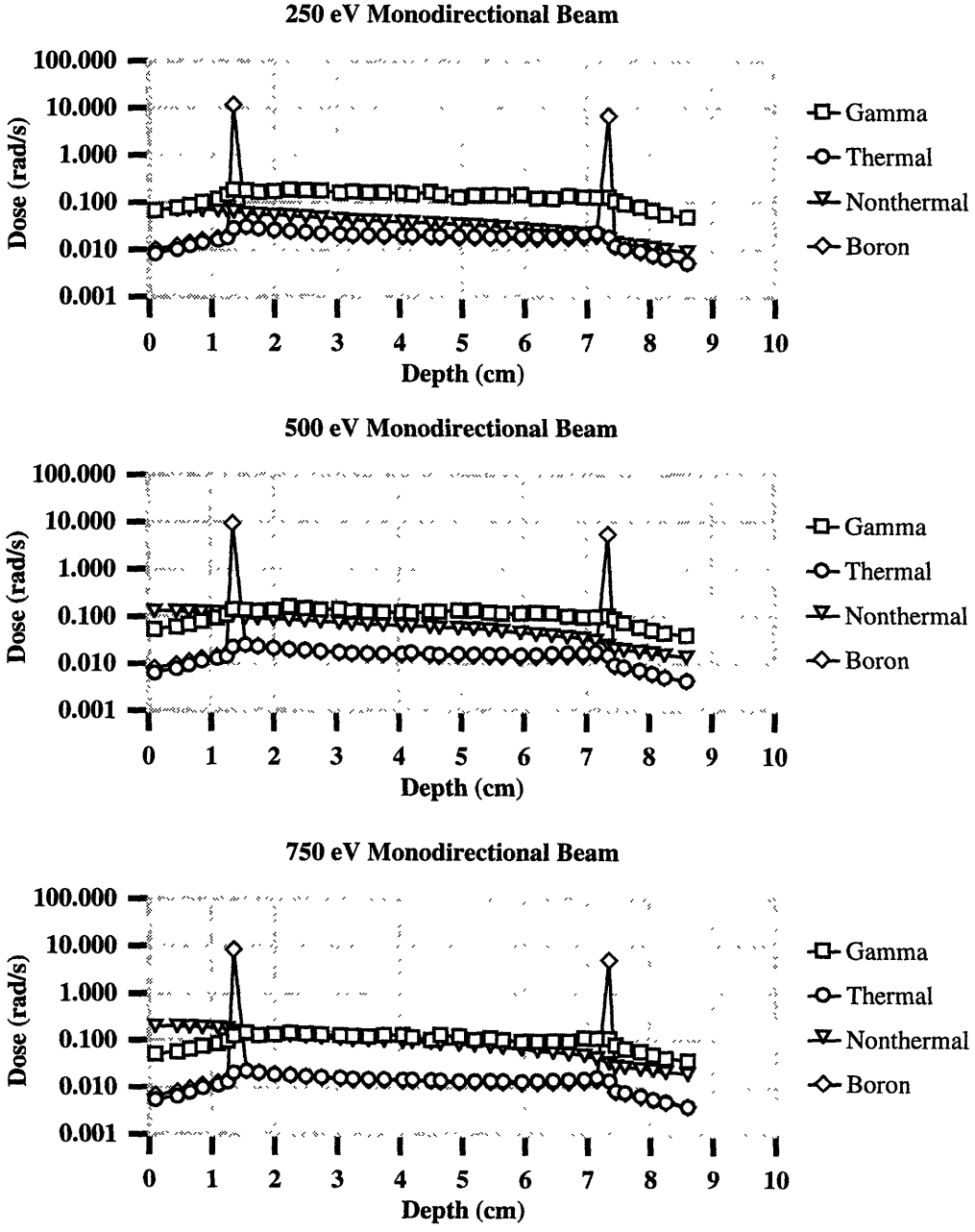

Figure 5.6 Dose per depth in phantom for ideal monodirectional beams energies of (a) 250 eV, (b) 500 eV and (c) 750 eV.

The most striking increase in nonthermal neutron dose is seen in the 10 keV beam, Figure 5.7(b). At 10 keV the nonthermal neutron dose is comparable to the boron dose at the synovium which, as been pointed out before, was around 98%. In fact, the nonthermal neutron dose at the surface of the phantom in the 10 keV was calculated to be 98% of the total dose, with the other components contributing negligible amounts of dose. The nonthermal neutron dose has far outstripped the other dose components throughout the joint phantom.

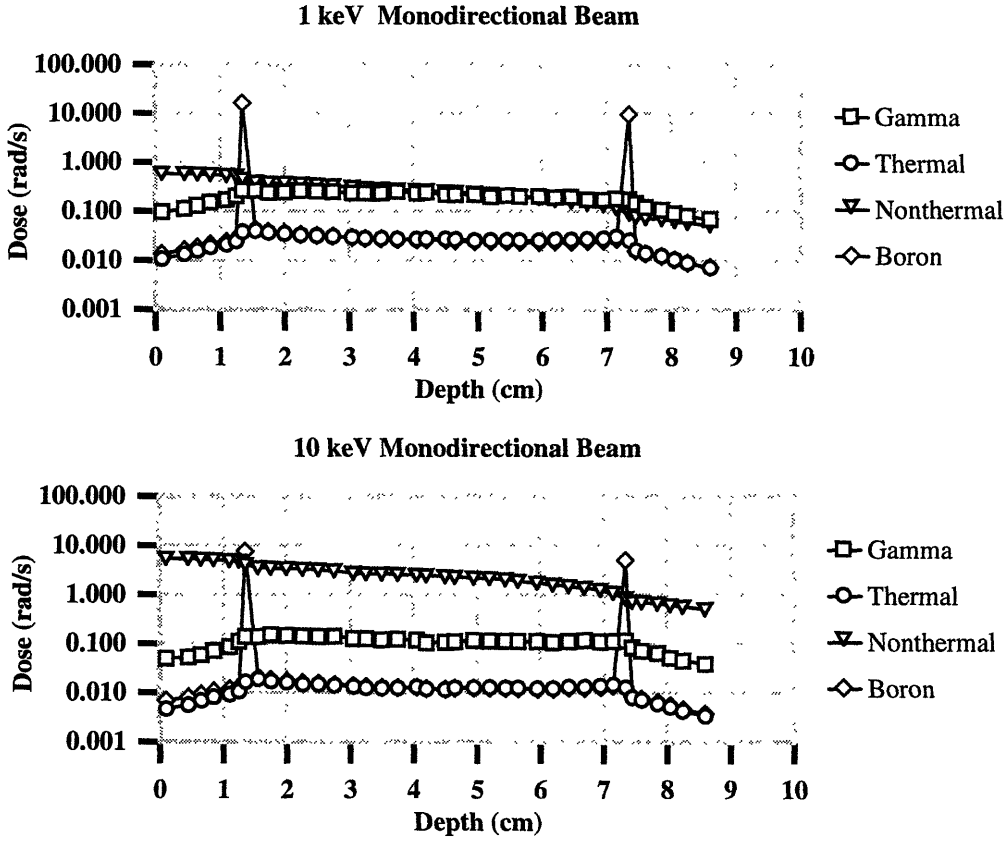

Figure 5.7 Dose per depth in phantom for ideal monodirectional beams energies of (a) 1 keV and (b) 10 keV.

5.1.2 Isotropic Ideal Beams

The study conducted in section 5.1.1 was repeated using isotropic ideal beams rather than monodirectional. This was done to approximate the angular characteristics of the beam following moderation with a large mass of low-Z material. The results will be divided into the same sets as the monodirectional studies and comparisons will be made between the two where possible.

The geometry for the study is shown in Figure 5.8 and is essentially the same as that used in the monodirectional studies except for the angular distribution of neutrons emitted from the source. The calculation of dose per depth in the joint phantom is also the same as in the monodirectional studies.

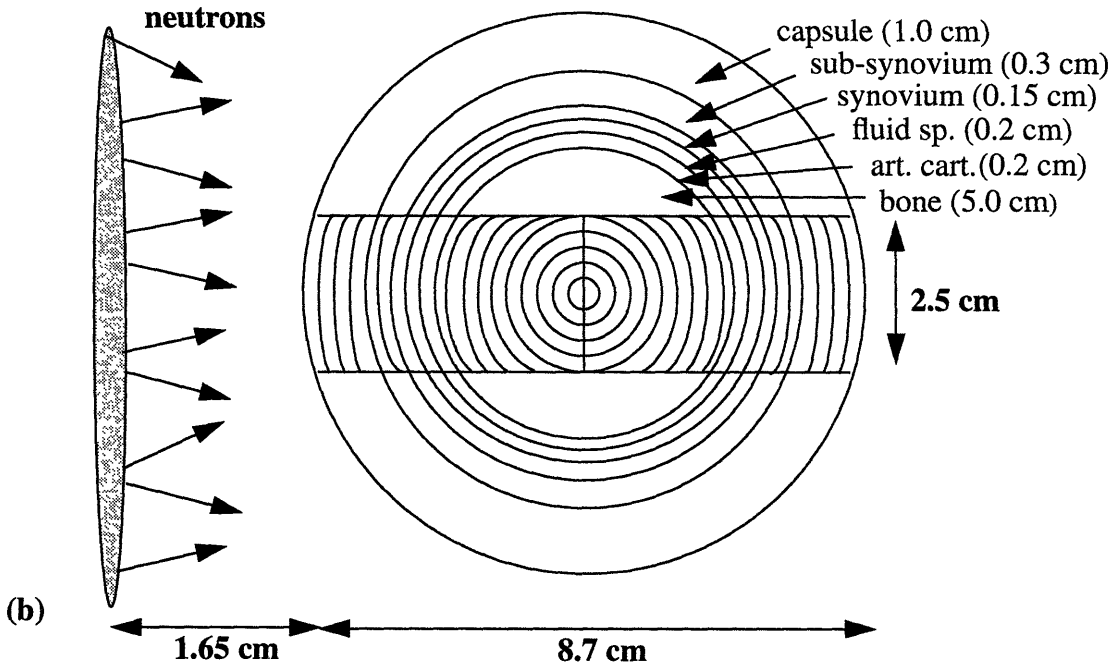

Figure 5.8 Ideal beam study geometry of cylindrical joint phantom using an isotropic source of neutrons.

Figure 5.9, on the following page, shows the dose per depth profiles in a phantom for the beam energies of 0.025 eV and 0.1 eV, both of which are considered thermal according to the previous definition. One immediate difference between the isotropic and monodirectional studies is the difference in dose rate. In the isotropic studies, the dose rate for all components of the 0.025 eV isotropic beam are around $1x10^{-3}$ rad/s whereas in the monodirectional study the dose rate was approximately three orders of magnitude higher. The percent contribution at the surface is about 50% for the gamma rays, 30% for the neutrons (only thermal exist in this beam) and 20% for the boron. Halfway into the phantom, in the middle of the bone, these ratios change to 85% for the gammas, 10% for the neutrons and 5% for the boron. The gamma dose rate remains relatively constant throughout the depth of the phantom while the thermal neutron and boron dose contributions decrease. The 0.1 eV beam has similar dose fraction contributions. Again, as before, the dose at the two

peaks, representing the front and the back synovium layer, is primarily due to boron., i.e. approximately 98%.

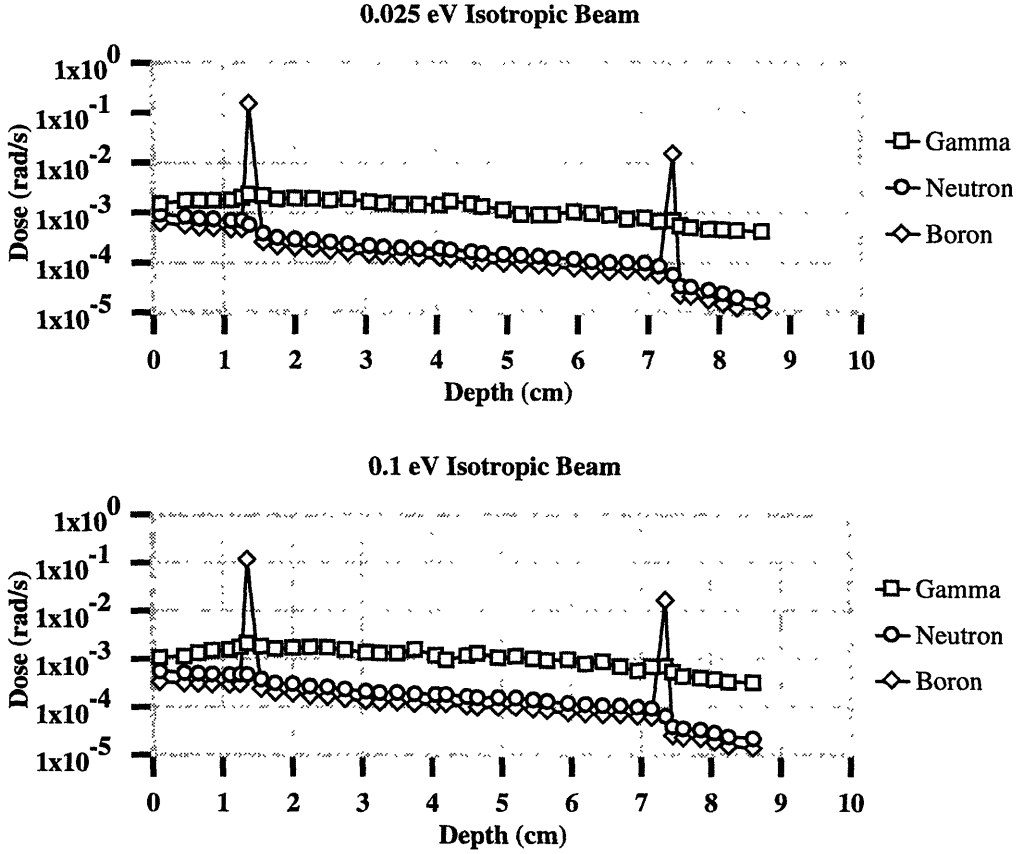

Figure 5.9 Dose per depth in phantom for ideal isotropic beams energies of (a) 0.025 eV and (b) 0.1 eV.

Similarly to the monodirectional beams, as neutron energy increases above the 0.36 eV threshold a nonthermal component to the dose appears, as seen in Figure 5.10 below. Although the nonthermal component is stronger than both the thermal neutron and boron dose components at the surface of the skin, it is still the lowest component in the rest of the phantom. As in almost all of the dose profiles, the gamma dose stays fairly constant throughout the depth of the phantom. The fluctuations in the gamma dose component, most prominent in Figure 5.10(c), are due to poor statistics. The uncertainty in the gamma dose was approximately 20% at the surface of the phantom. It then increased in the middle of the phantom to about 40%, only to decrease towards the end of the phantom to between 20 and 30%. Uncertainty in the boron, thermal and nonthermal neutrons remained below

10%.

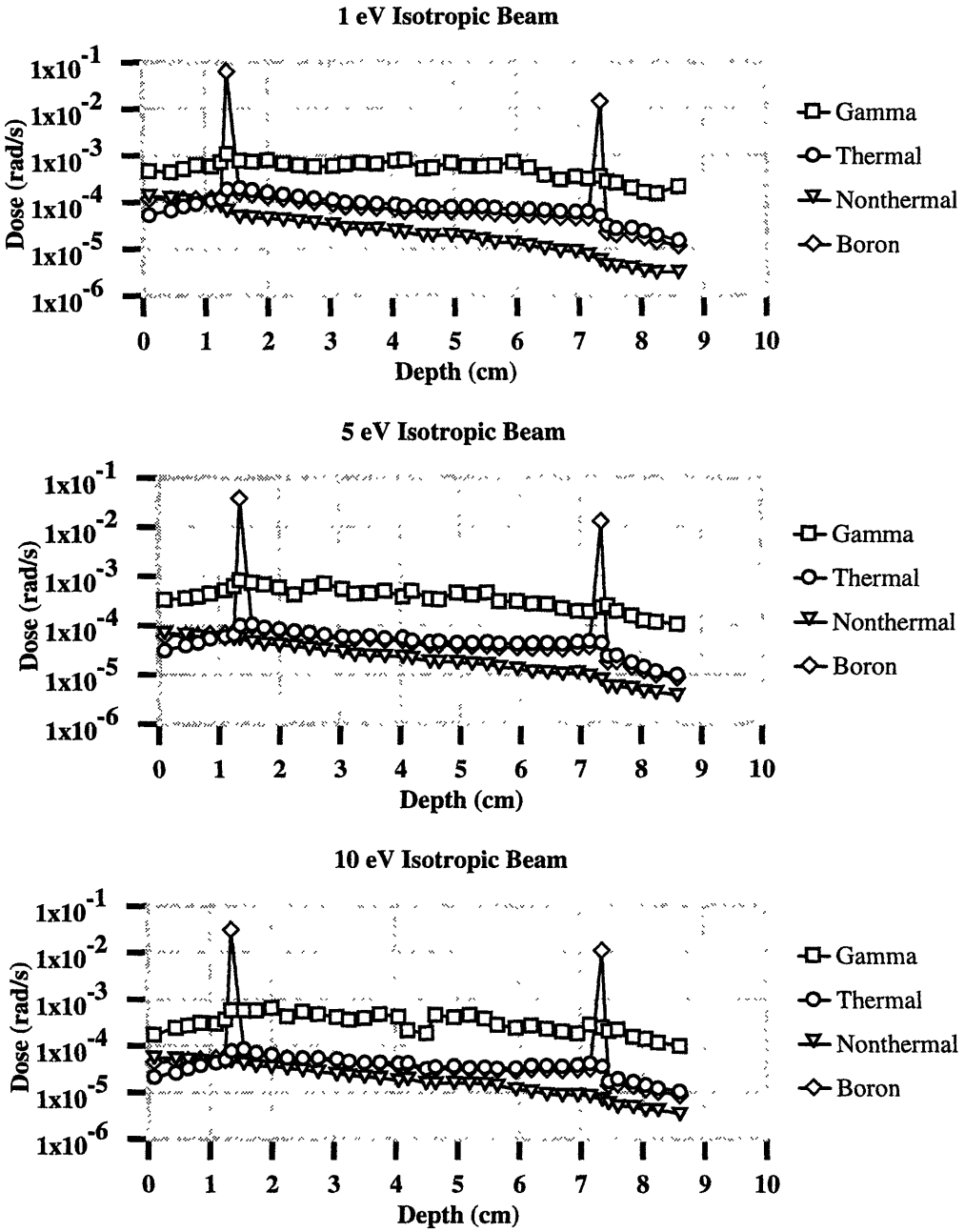

Figure 5.10 Dose per depth in phantom for ideal isotropic beams energies of (a) 1 eV, (b) 5 eV and (c) 10 eV.

As expected, the nonthermal neutron contribution becomes stronger with increasing neutron beam energy such that at 75 eV, the nonthermal neutron dose is close to the gamma dose and in the phantom it is comparable to the thermal and boron doses (Figure 5.11). This behavior is similar to that seen with monodirectional beams. Again, the fluctuations

in the gamma dose are due to poor statistics since few but very energetic capture gammas are generated in the phantom.

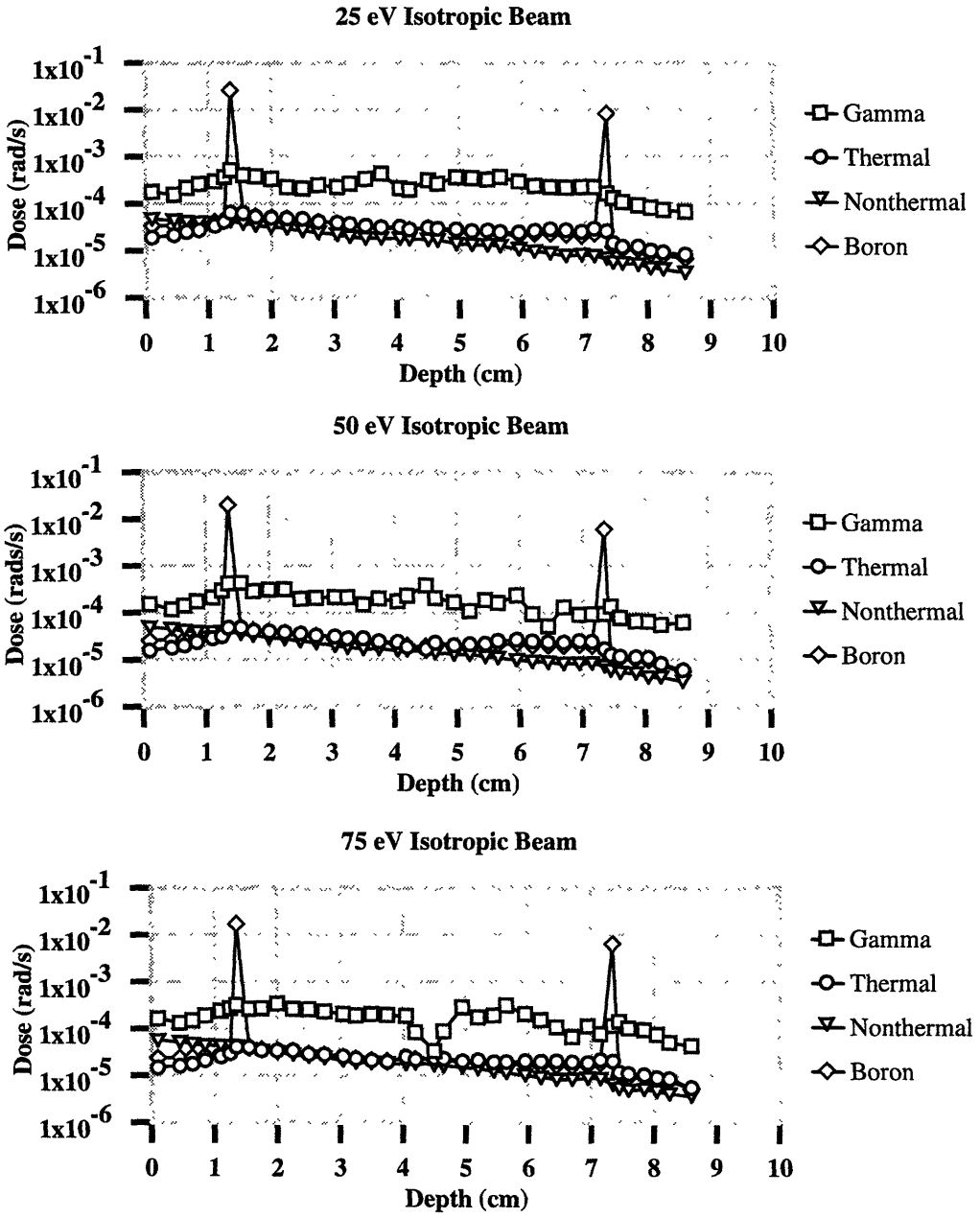

Figure 5.11 Dose per depth in phantom for ideal isotropic beams energies of (a) 25 eV, (b) 50 eV and (c) 75 eV.

Poor statistics in the gamma dose is a common feature of all the plots, despite the fact that 40 million particle histories were run, compared with 1 million particle histories with the monodirectional source. The reason that so many more are required in the isotropic beam

studies is that many of the particles don't even enter the phantom since they are emitted at all angles from the plane of the source.

Figure 5.12 shows the dose per depth in a phantom for ideal isotropic beam energies of 100 eV and 125 eV. Again, similar to the monodirectional beams at these energies, the nonthermal dose component has increased and is comparable to the gamma-ray dose at the phantom surface.

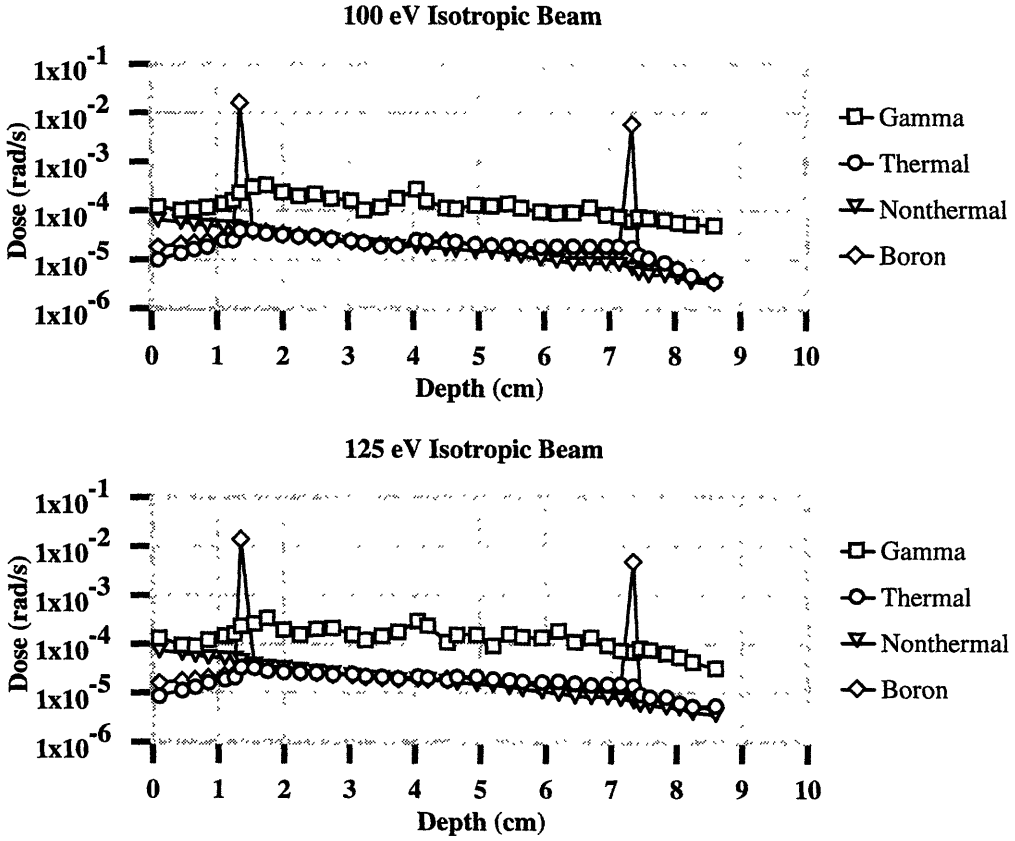

Figure 5.12 Dose per depth in phantom for ideal isotropic beams energies of (a) 100 eV and (b) 125 eV.

In the next set of figures, Figure 5.13 (a) (b) and (c), the point at which the nonthermal neutron dose becomes larger than the gamma, thermal or neutron doses at the surface of the phantom is identified. At 250 eV, the nonthermal neutron dose is equal to the gamma dose at the surface of the phantom and is slightly higher than the thermal neutron dose in the phantom itself. At 500 eV, however, the nonthermal neutron dose has surpassed the gamma dose to the surface of the phantom, Figure 5.13(b), and is equal to the gamma dose

at the synovium. In the phantom, the nonthermal dose is approaching the level of the gamma component which shows the highest dose rate.

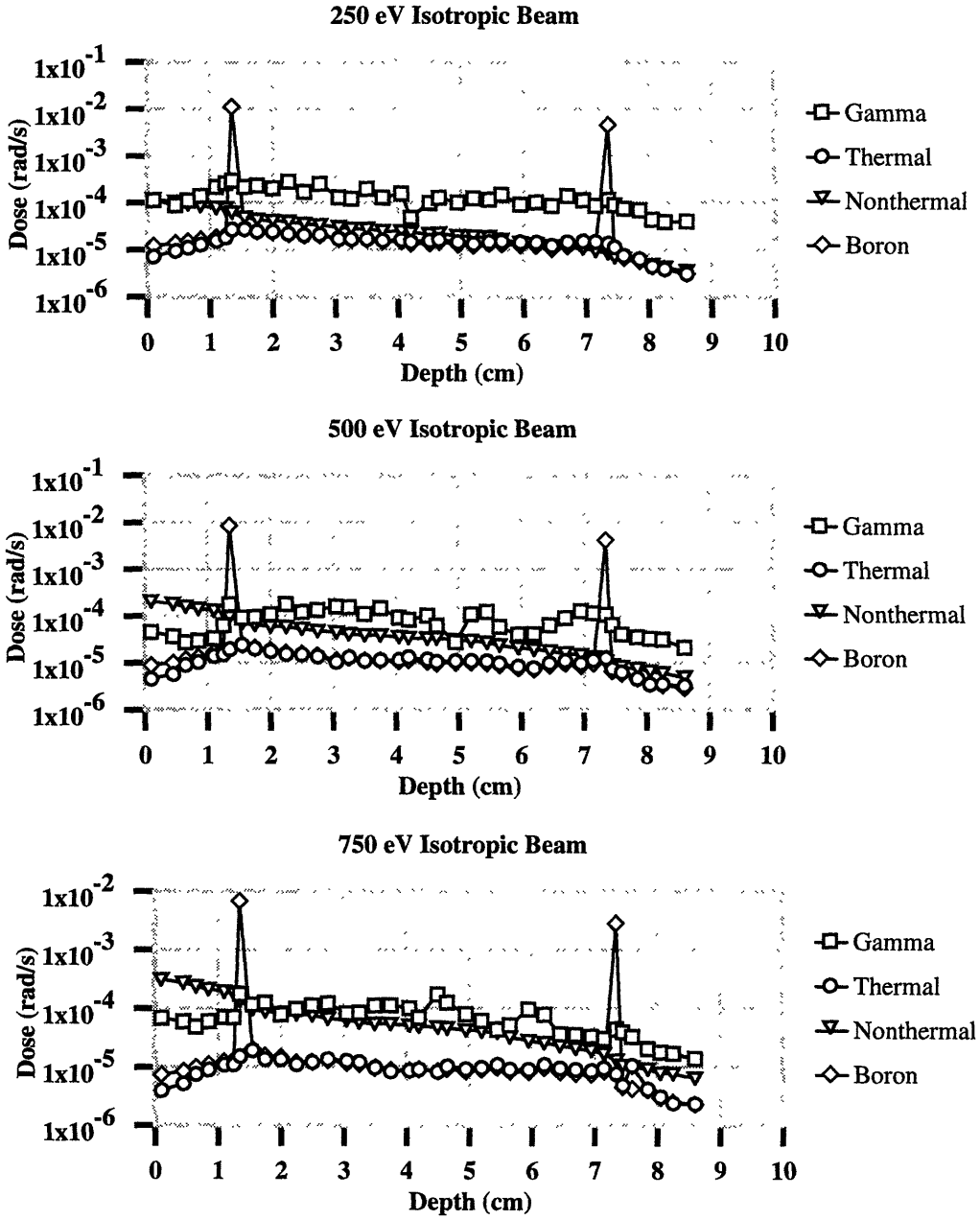

Figure 5.13 Dose per depth in phantom for ideal monodirectional beams energies of (a) 250 eV, (b) 500 eV and (c) 750 eV.

In the final two energies tested, 1 keV and 10 keV, shown in Figure 5.14, the nonthermal dose component grew such that by 10 keV, the nonthermal dose was comparable to the boron dose to the synovium which was loaded with 400 ppm of ^{10}B. For 10 keV, the num-

ber of particle histories was increased from 40 million (used for the entire study) to 100 million in order to decrease the fluctuations the gamma dose. The graph in Figure 5.14(b) is the result using 100 million particle histories.

The average gamma contribution to the capsule, i.e. from the surface of the phantom to a depth of 1.1 cm, was 1% while the thermal and boron dose contributions were approximately 0.1% and the nonthermal dose contribution comprised the rest. The average contributions of the different components to the bone (only considering the "front half", from a depth of 2.0 cm to 4.5 cm) were approximately 6% for the gamma, 0.6% for the thermal neutrons, 0.6% for the boron and 93%(rounding off) for the nonthermal neutrons.

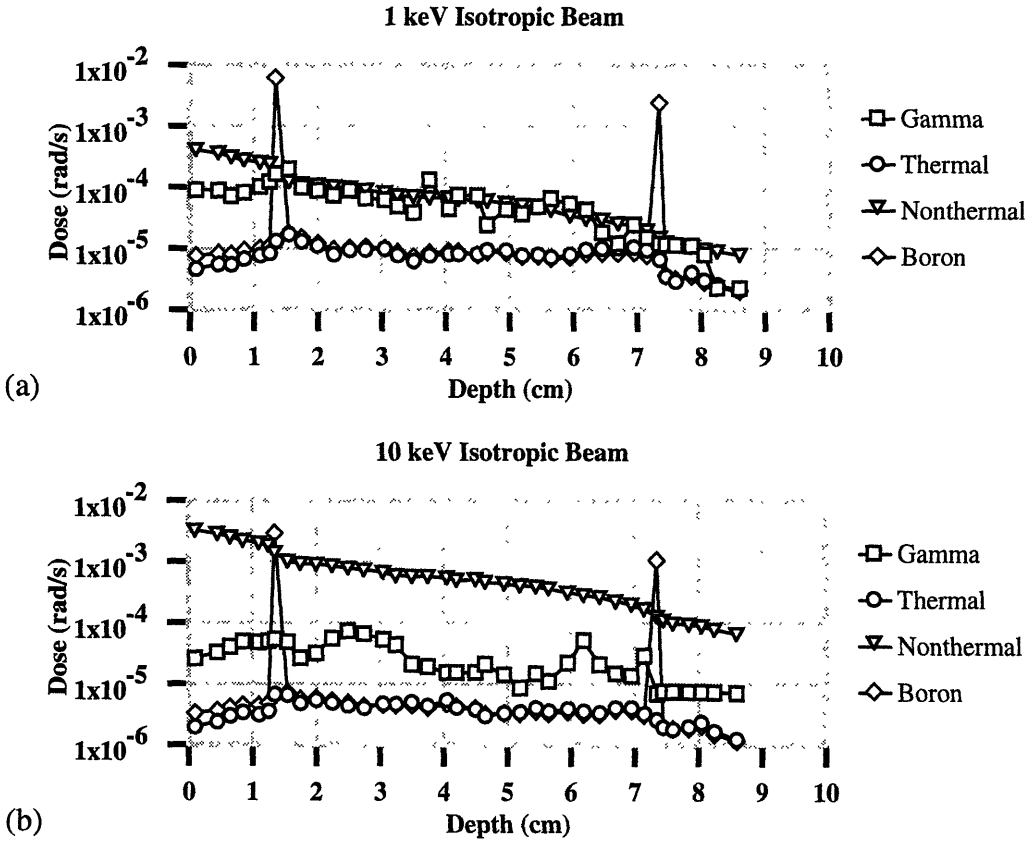

Figure 5.14 Dose per depth in phantom for ideal monodirectional beams energies of (a) 1 keV and (b) 10 keV.

5.1.3 Therapeutic Usefulness Ratios

Determination of the therapeutic usefulness of the monoenergetic beams was carried out by examining the ratio of synovium dose to healthy tissue dose for all the tissues in the

phantom. First, total dose was determined by summing all the dose components. The ratio of the total synovial lining dose to the healthy tissue dose was then calculated for all tissue layers and for all beam energies.

Table 5.1 shows the ratios of the synovium dose to capsule dose for the monodirectional and isotropic sources. The range of values is derived from the existence of 4 tally regions contributing to the capsule in the computational model.

Table 5.1: Ratio of Synovium Dose to Capsule Dose

	Monodirectional		Isotropic	
Energy (eV)	Average	Range	Average	Range
0.025	88	75 - 101	52	50 - 53
0.1	94	78 - 112	58	53 - 62
1	101	81 - 122	79	70 - 87
5	102	81 - 125	72	64 - 79
10	106	83 - 129	82	70 - 106
25	102	79 - 125	86	72 - 103
50	97	78 - 119	87	77 - 98
75	93	75 - 112	70	62 - 78
100	90	72 - 110	80	77 - 84
125	84	68 - 101	70	62 - 79
250	66	59 - 75	48	45 - 52
500	45	42 - 49	39	33 - 45
750	32	34 - 31	21	18 - 24
1,000	23	23 - 24	15	13 - 17
10,000	2	2 - 2	2	1 - 2

The values show a similar pattern of increasing to a plateau around 1 eV, with a slight peak around 10 eV, and decreasing sharply after 100 eV, as seen more clearly when plotted in

Figure 5.15. In this figure, the average value is plotted and the ranges are indicated by the vertical bars (i.e. these are not "error bars").

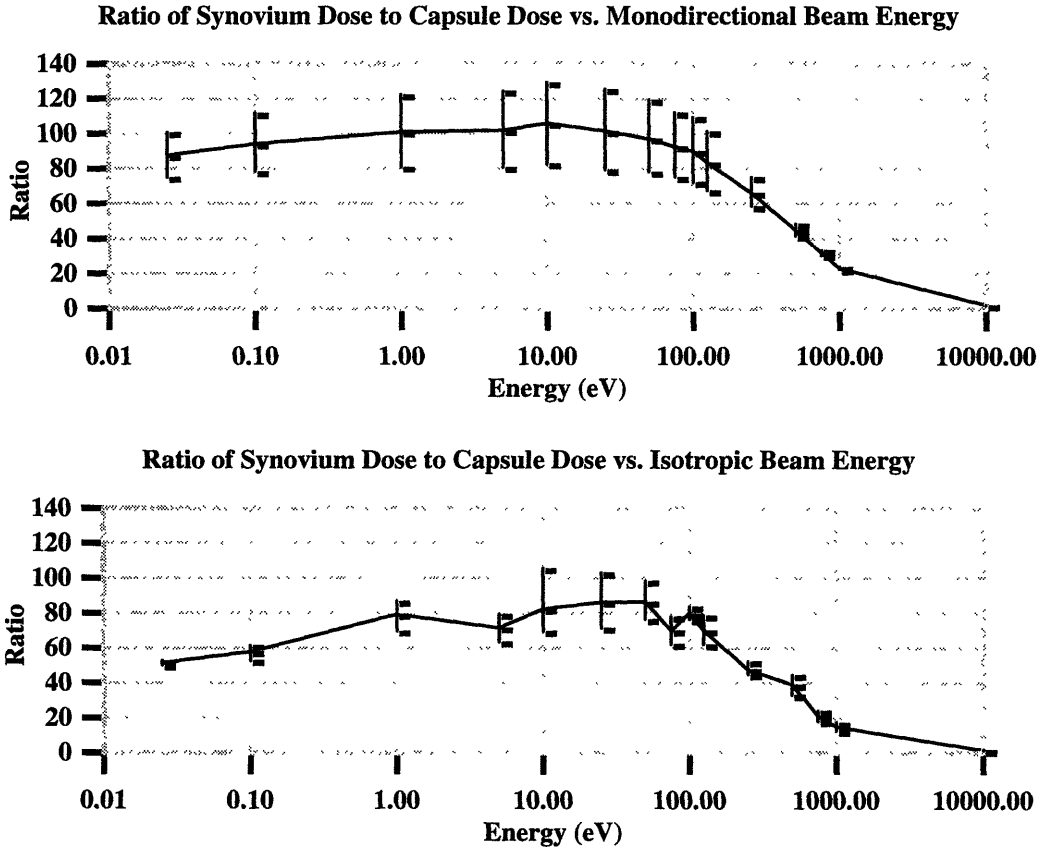

Figure 5.15 Ratio of Synovium Dose to Capsule Dose for different beam energies using both (a) monodirectional and (b) isotropic beams.

The values for the isotropic beam study are considerably lower than the monodirectional beam study until the 1 keV and 10 keV energies where the values are almost the same. The shape of the curve for the isotropic beam study is not as smooth as for the monodirectional study, as can be seen particularly in the plateau regions of the curves shown in Figure 5.15. This is probably due to statistical fluctuations.

The ratio of synovium dose to subsynovium dose using both monodirectional and isotropic beams is shown in Table 5.2. Again there is a range of values because the subsynovium had more than one tally region. The subsynovium, 0.3 cm thick, was divided into two tally regions 0.15 cm each.

Table 5.2: Ratio of Synovium Dose to Subsynovium Dose

	Monodirectional		Isotropic	
Energy (eV)	Average	Range	Average	Range
0.025	64	61 - 68	51	50 - 53
0.1	64	60 - 69	49	47 - 52
1	65	60 - 70	67	62 - 72
5	66	61 - 71	52	48 - 56
10	67	61 - 72	65	60 - 71
25	63	58 - 68	58	53 - 64
50	63	59 - 68	57	51 - 66
75	61	56 - 66	49	47 - 52
100	59	54 - 64	65	62 - 68
125	56	52 - 60	57	55 - 59
250	50	47 - 54	32	30 - 35
500	38	37 - 40	42	40 - 45
750	30	29 - 30	25	25 - 26
1,000	22	22 - 22	17	17 - 17
10,000	2	2 - 2	2	2 - 2

As in the ratio of synovium dose to capsule dose, the values from the isotropic beams are lower than the values of the monodirectional beams. The average value of the ratio has decreased from the corresponding values in the previous table which listed the synovium dose to capsule dose for all energies. The decrease applies to all neutron energies except the monodirectional and isotropic energies of 10 keV where the value remained the same.

The values in Table 5.2 are shown in figure 5.16. Again, the average value is plotted and the vertical bars indicate the higher and lower value (since the subsynovium is only divided into two tally regions).

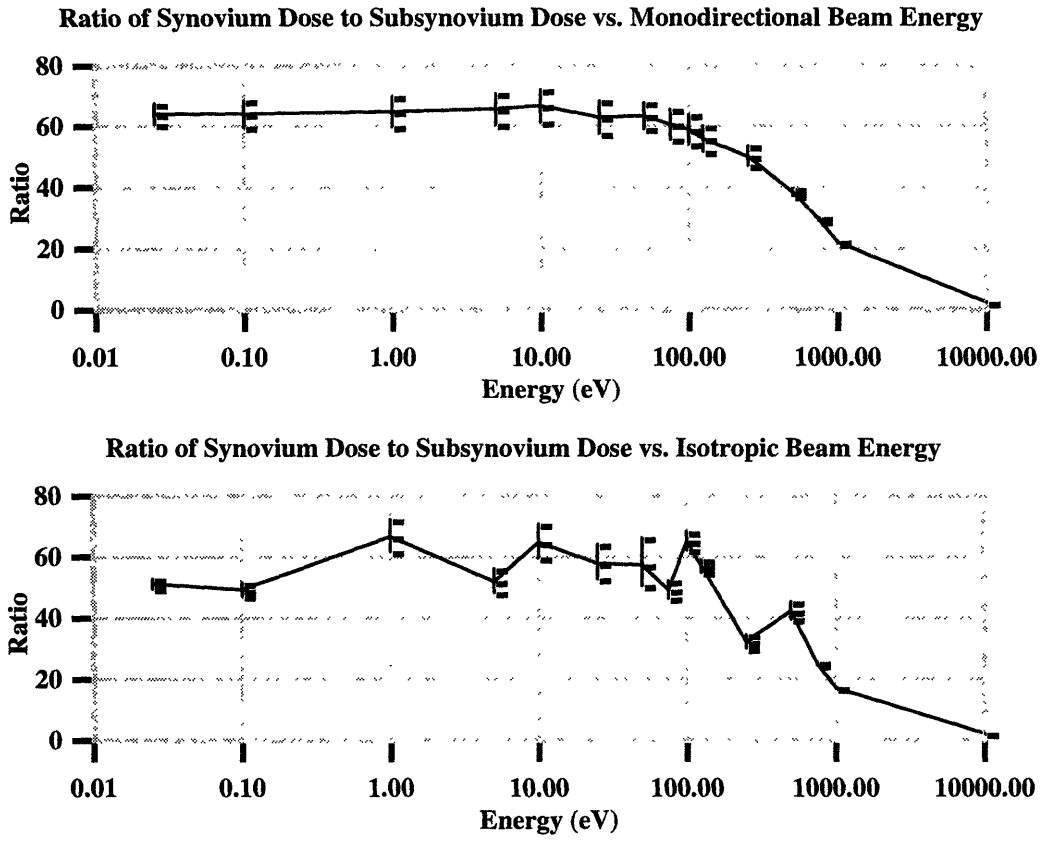

Figure 5.16 Ratio of Synovium Dose to Subsynovium Dose for different beam energies using both (a) monodirectional and (b) isotropic beams.

In the monodirectional beam case, the average value remains fairly constant between 0.025 eV and 10 eV, although the range of values increases. The ratio then begins to decrease with the sharpest decrease beginning at 100 eV. In the isotropic beam case, the average ratio oscillates between 50 and 65 (approximately) between 0.025 and 100 eV, after which it suffers a sharp decrease with the exception of the small increases at the 750 eV energy. The sharp decrease begins at 100 eV for both monodirectional and isotropic beams. The ratio is reduced to the same value for both beam types by 10 keV.

The next table, Table 5.3, shows the average values for the synovium dose to fluid space dose. Here there is no range because the fluid space, 0.2 cm thick, was tallied in one region only.

Table 5.3: Ratio of Synovium Dose to Fluid Space Dose

Energy (eV)	Monodirectional	Isotropic
0.025	62	55
0.1	54	49
1	46	55
5	45	40
10	45	40
25	46	46
50	45	36
75	44	46
100	46	39
125	44	38
250	39	35
500	34	42
750	27	28
1,000	23	18
10,000	3	4

The values of the synovium dose to fluid space dose for the monodirectional and isotropic beams are closer than the ratios for previous tissues, capsule and subsynovium. There is a small increase between the synovium to subsynovium ratio and the synovium to fluid space at for the 1 keV and 10 keV energies of both monodirectional and isotropic beam energies.

The results from Table 5.2 are plotted in Figure 5.17. A different type of behavior emerges in the plot of the monodirectional beam case. The ratio begins at a high of approximately 60 and then decreases to a plateau between 1 and 100 eV, after which it begins to decrease. The ratios for the isotropic beam case, on the other hand, exhibit the same behavior as the ratio of synovium dose to subsynovium dose. It should be emphasized that in both the

monodirectional and isotropic beam cases, the sharp decrease in synovium dose to fluid space dose, as in the other ratios plotted thus far, begins after 100 eV.

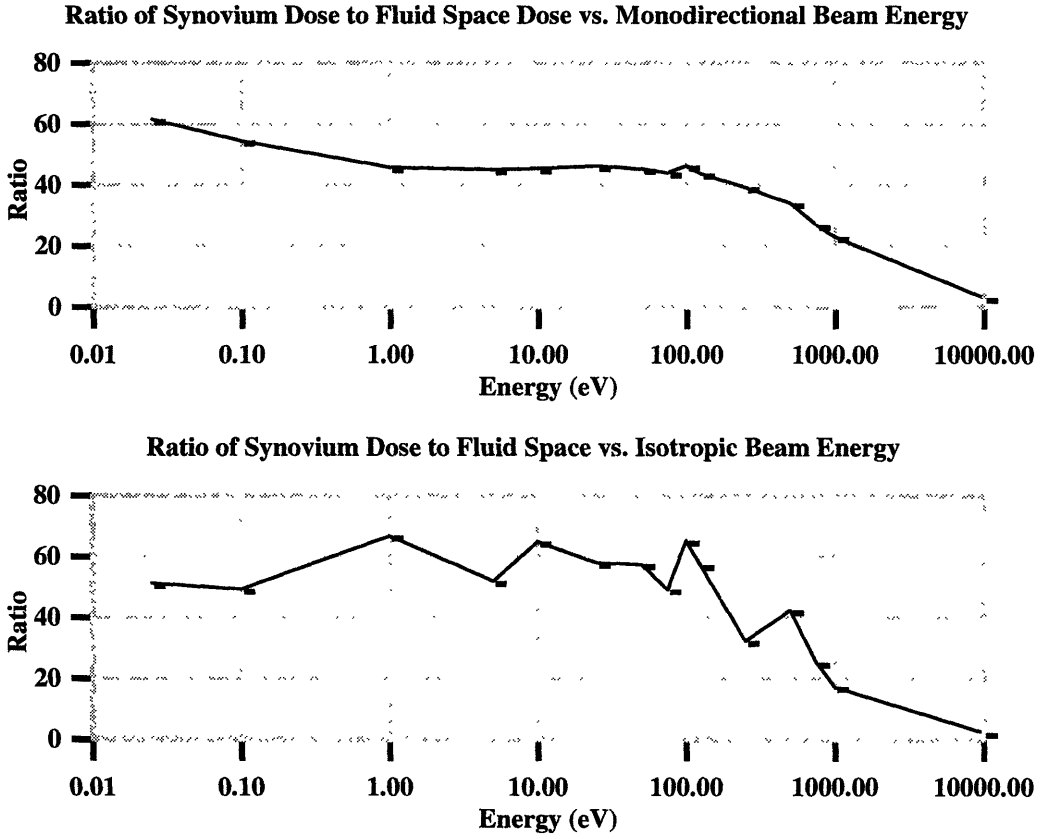

Figure 5.17 Ratio of Synovium Dose to Fluid Space Dose for different beam energies using both (a) monodirectional and (b) isotropic beams.

As before, the ratio of synovium dose to fluid space dose is smooth with monodirectional beams whereas it oscillates with the isotropic beams, a phenomenon most likely due to statistical fluctuations.

Following the tissue layers in the cylindrical joint phantom, the next (and second to last) ratio to be considered is the ratio of synovium dose to articular cartilage dose. Attention needs to be paid to this ratio particularly in light of the fact that, as was mentioned in the introduction, very little articular cartilage destruction is necessary to weaken normal joint function causing progressive and irreversible articular cartilage disintegration. In fact, one of the motivations behind removing the synovium (besides the fact that its increased size

causes a painful increase in joint pressure), is to stop its destruction of articular cartilage by preventing the secretion of particular cytokines and enzymes. Table 5.4 lists the values of the ratio of synovium dose to articular cartilage dose. Again, as in the subsynovium, there is no range because the articular cartilage (0.2cm thick) was tallied in one region only.

Table 5.4: Ratio of Synovium Dose to Articular Cartilage Dose

Energy (eV)	Monodirectional	Isotropic
0.025	69	65
0.1	59	56
1	49	59
5	48	44
10	49	42
25	48	51
50	48	51
75	46	47
100	48	37
125	46	33
250	42	35
500	36	44
750	29	29
1,000	24	27
10,000	3	5

The trends in this ratio, which are more easily seen when plotted (see Figure 5.18), differ from the previous ratio. In the monodirectional beam case, the ratio of synovium dose to articular cartilage dose follows the same trend as for the fluid space, i.e. it starts at a relatively high value and then decreases to a plateau between 1 an 100 eV, after which it suffers a sharp decrease. The first two ratios in the isotropic beam case are similar to the

monodirectional case. However, it remains at approximately the same value for 1 eV and then slopes up and down before a clear cut decrease after 1 keV. Since there is only one tally region and cell, relatively small in size, a large uncertainty in the gamma component, which as shown before, is dominant until approximately 500 eV could have a large effect on the ratio.

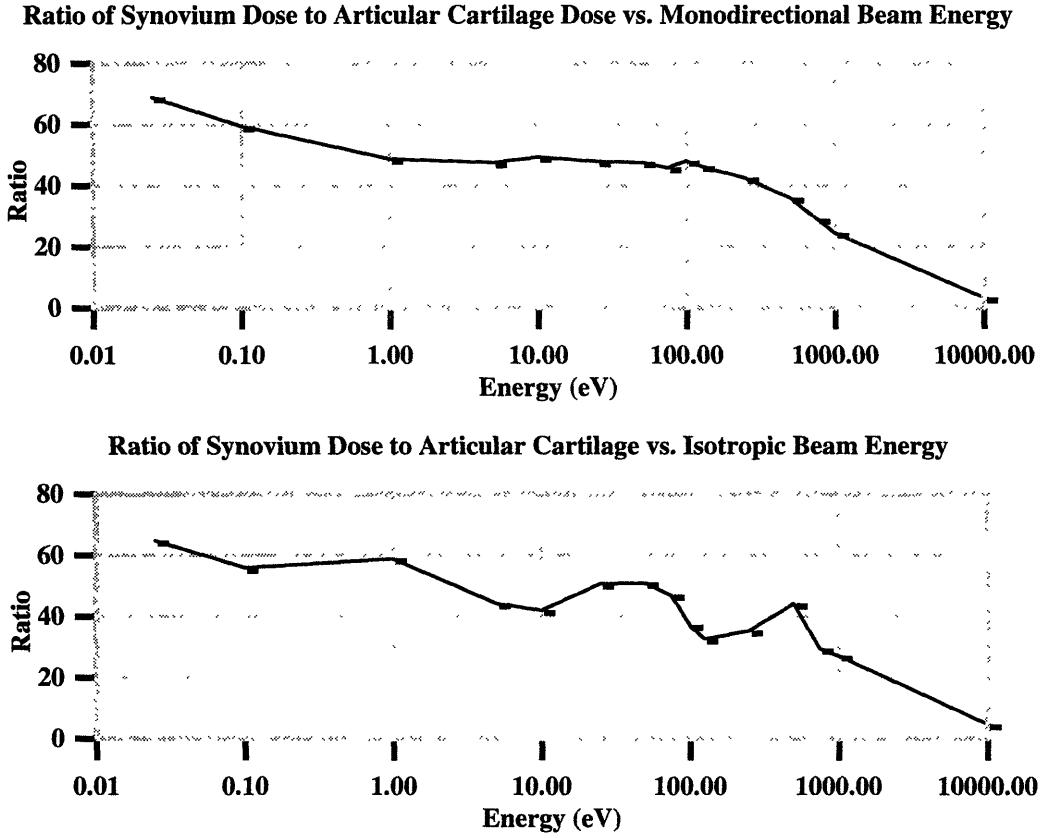

Figure 5.18 Ratio of Synovium Dose to Articular Cartilage Dose for different beam energies using both (a) monodirectional and (b) isotropic beams.

The final healthy tissue to be considered is the bone. The synovium dose to bone dose ratios are listed in Table 5.5. Special attention also needs to be paid to the bone since the bone surface has been identified by the International Commission on Radiation Protection Report 26 (ICRP, 1977) as a principal radiosensitive target to be protected in procedures involving bone irradiation. Again, since the bone was divided into ten tally regions, in order to obtain detailed dose profiles in the phantom, both the range and average values are given for each energy.

It must be noted that the size of the range could be related to the size of the last tally region of the bone which is very small. This small size results in larger uncertainty, particularly in the isotropic beam case, which can cause fluctuations in the value found in that specific tally region and thus increase the value of the upper region.

Table 5.5: Ratio of Synovium Dose to Bone Dose

	Monodirectional		Isotropic	
Energy (eV)	Average	Range	Average	Range
0.025	90	73 - 106	76	64 - 91
0.1	71	61 - 83	64	55 - 97
1	55	51 - 58	71	58 - 78
5	53	48 - 56	58	51 - 100
10	54	50 - 57	54	38 - 99
25	54	49 - 61	70	51 - 96
50	53	49 - 55	67	49 - 92
75	51	46 - 56	57	40 - 119
100	52	48 - 56	65	49 - 97
125	51	46 - 55	57	39 - 68
250	45	41 - 52	46	31 - 115
500	38	33 - 44	42	33 - 62
750	32	29 - 37	38	33 - 51
1,000	28	25 - 31	38	30 - 51
10,000	4	3 - 5	6	5 - 9

The highest average value of the synovium dose to bone dose ratio for both the monodirectional and isotropic beam energies occurs at 0.025 eV. As Figure 5.19 indicates, the average value of the ratio increases in the monodirectional case as energy decreases and reaches a plateau at 1 eV until approximately 100 eV where the ratio begins to drop

sharply. In the isotropic beam energy case the average of the ratio oscillates (again due to statistical fluctuations) between approximately 75 and a low of approximately 54 before it begins a course of sharp decrease after 100 eV.

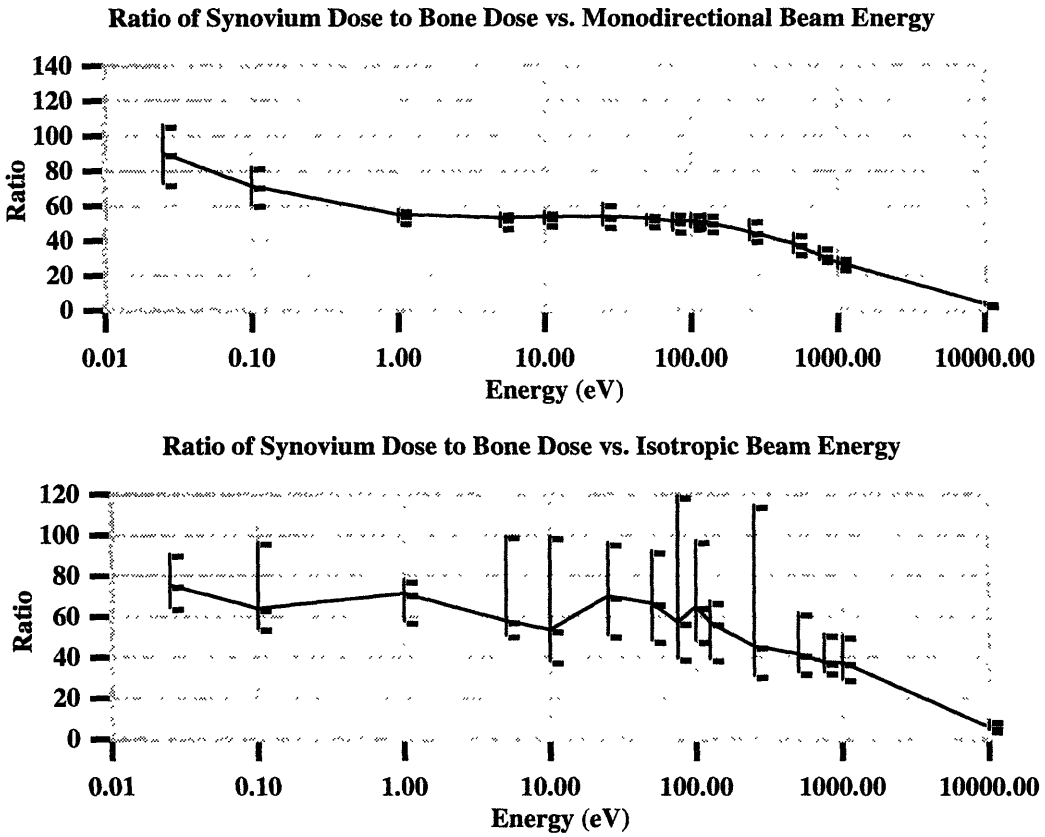

Figure 5.19 Ratio of Synovium Dose to Bone Dose for different beam energies using both (a) monodirectional and (b) isotropic beams.

Ideal neutron beam studies have demonstrated that low energy neutrons, roughly in the range from thermal energies to 100 eV, will provide the highest therapeutic ratio in BNCS. This energy range, therefore, will represent a design goal in studies aimed at modelling a useful therapy beam for a practical neutron source. Also, before turning to another topic, it must be noted that the magnitude of these ratios are high compared to conventional BNCT where concentrations of the boron compound achieved in the tumor are only about ten times higher than those in healthy tissue resulting in therapeutic ratios ranging from about 2 to 10 as reported in the ideal beam study to determine the optimal neutron energy range for BNCT (Yanch et al, 1991).

5.2 Figure of Merit

The formulation of the Figure of Merit was prompted by a desire to evaluate possible assemblies in air rather than in a phantom thereby reducing the required computation time. As part of the process in developing the Figure of Merit, a preliminary moderator/reflector configuration was established. The geometry was chosen based on a previous finding that the optimal moderator and reflector geometry is cylindrical and that the insertion of the target a few centimeters into the moderator greatly increases the available neutron flux (Yanch et al, 1992). The rationale behind the material selection and the dimensions will be discussed in sections 5.3.1 and 5.3.2. The focus of this section will be the development and test of the Figure of Merit and its test by comparison of the results with those obtained in a phantom.

5.2.1 Formulation

The geometry used is shown in Figure 5.20. An extra surface was placed 1 cm away from the moderator end in order to simulate the relative position of a joint phantom.

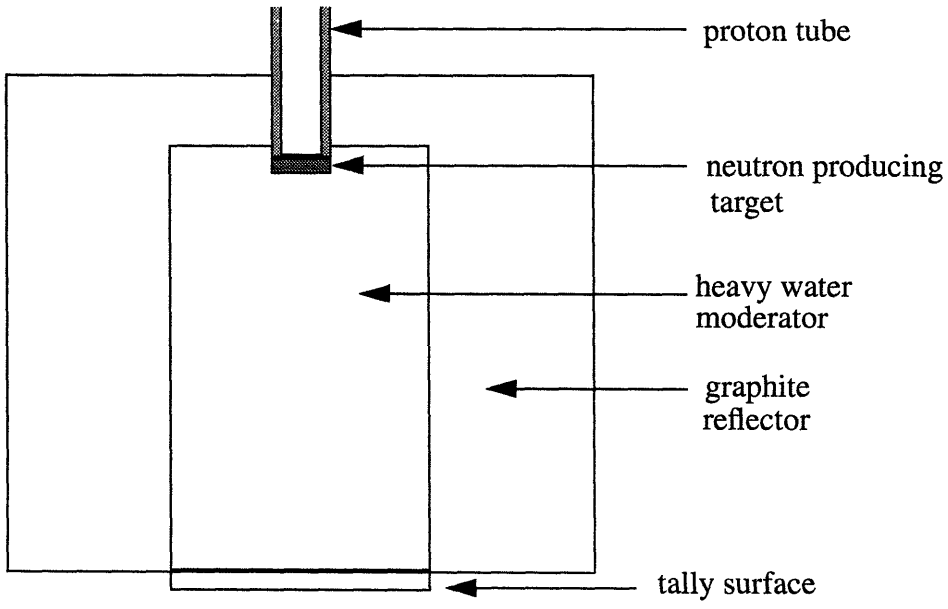

Figure 5.20 Moderator/Reflector configuration with an extra tally surface added during the evaluation of the configuration using the developed figure of merit.

The flux was divided into bins representing the energies tested in the ideal beam studies.

The flux in each bin was weighted by the average ratio of synovium to capsule dose and then normalized by the total neutron flux over the entire extra surface. Weighting was also done using the synovium to bone dose. The difference by the weightings of the different ratios and different neutron source distributions were examined.

Two moderator/reflector configurations were tried. The first configuration which will be denoted by M/R #1 had the following dimensions: moderator diameter 24 cm and length of 21 cm; reflector thickness of 18 cm and length 26 cm. The second configuration which will be denoted by M/R #2 had the following dimensions: moderator diameter 15 cm and length 50 cm; reflector thickness 18 cm and thickness 55 cm. Both configurations used the spectrum for 2.5 MeV protons on a lithium target. In both cases, the moderator material was heavy water and the reflector material was graphite. Results are shown in Table 5.6.

.

Table 5.6: Evaluation using Figures of Merit

Ideal Beam Study	Ratio used for Figure of Merit	M/R #1	M/R #2
Monodirectional	Syn/Capsule	53	91
	Syn/Bone	73	78
Isotropic	Syn/Capsule	51	56
	Syn/Bone	53	69

As expected, the Figures of Merit using the monodirectional weightings were higher than those using the isotropic weighting. The difference in the M/R #1 using the synovium dose to capsule dose weighting (Syn/Capsule) is similar for the monodirectional and isotropic cases, giving 53 and 51 as Figures of Merit, respectively. A greater discrepancy exists in using the synovium dose to bone dose weighting (Syn/Bone), yielding Figures of Merit of 91 versus 56. The situation is reversed for the M/R #2 where the greater discrepancy occurs between the Syn/Capsule of the beams, i.e. Figures of Merit of 91 versus 56 for the monodirectional and isotropic, respectively, rather than the Syn/Bone, i.e. Figures of Merit of 78 versus 69 for monodirectional and isotropic, respectively.

5.2.2 Evaluation in Phantom

The validity of the figure of merit described above was tested in the phantom model described in the ideal beam studies. The cylindrical joint phantom was simply inserted into the moderator/reflector geometry with the tally region oriented towards the moderator end, as shown in Figure 5.21. The dose per depth in the phantom and ratio of synovium dose to healthy tissue dose was determined in the same way as was outlined in section 5.1 and compared to the Figure of Merit developed in section 5.2.1.

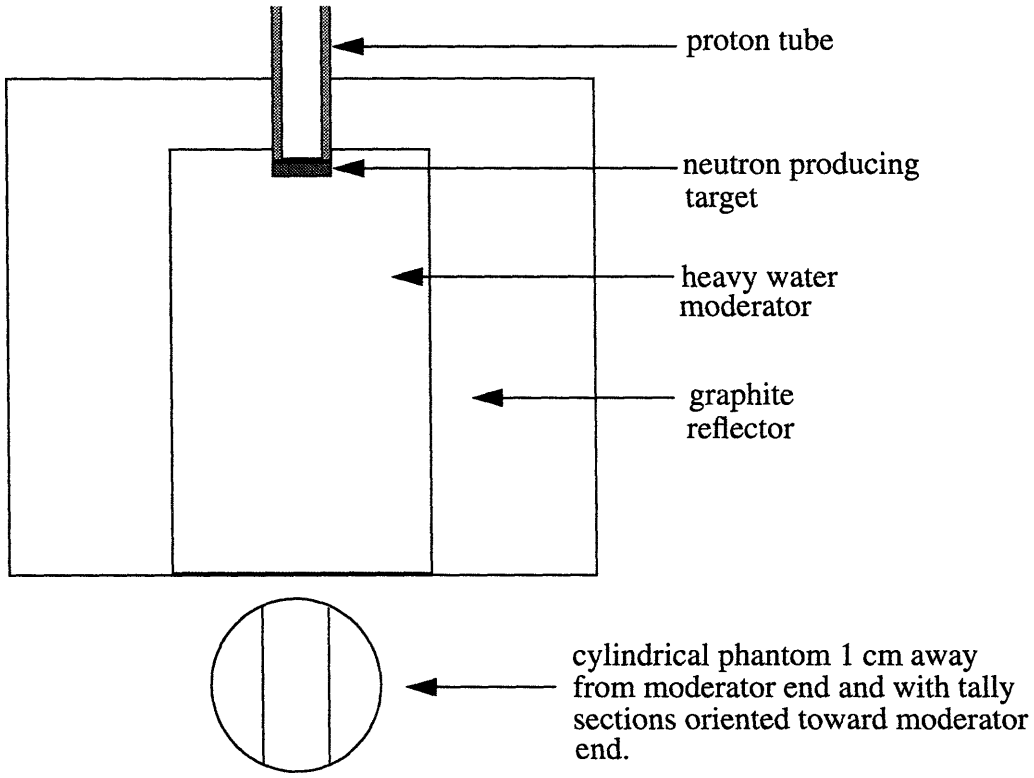

Figure 5.21 Geometry for evaluation of figure of merit in a phantom.

The two moderator/reflector configurations evaluated with the Figure of Merit in Section 5.2.1 were run with the cylindrical joint phantom. The ratios of synovium dose to capsule dose and synovium dose to bone dose were determined in the same manner that they were determined for the ideal beam study. The results for the runs with the phantom are given in the following table, Table 5.7, for comparison with the values in Table 5.6.

Table 5.7: Evaluation using joint phantom

Configuration	Syn/Capsule Average	Syn/Capsule Range	Syn/Bone Average	Syn/Bone Range
M/R #1	23	21 - 24	33	29 - 41
M/R #2	61	59 - 64	67	57 - 73

As can be seen in Table 5.7, both the average ratios of synovium dose to capsule dose and of synovium dose to bone dose for the M/R #1 were grossly overestimated using any of the Figure of Merits presented in Table 5.6. The values were closer for the M/R #2, particularly for the value of the Syn/Capsule ratio, but were still not the same.

The average Syn/Capsule ratio for the M/R #1 calculated in the joint phantom is 23, about half of the value predicted by the Figure of Merit with the monodirectional beam study weighting, i.e. a value of 53. The isotropic beam study weighting for the figure of merit gave a somewhat lower value of 51. Thus, weighting by the isotropic ideal beams yielded a slightly closer result using the Syn/Capsule weighting ratio. The difference in results between the Figure of Merit and the phantom runs was more apparent with the Syn/Bone weighting. The monodirectional beam weighting gave a Figure of Merit of 73, more than twice the average of given by a run with a phantom, i.e. 33. The isotropic weighting gave a closer value at 53, less than half as much.

The figures of merit using the isotropic and monodirectional beam study weightings fared better in the ratios for M/R #2. They were nearer to the values obtained by the Figure of Merits, though still not the same. The average Syn/Capsule ratio given in Table 5.7 for the M/R #2 is 61 which is higher than the figure of merit using the isotropic weightings (56) and lower than that using the monodirectional beams (78). Neither figure of merit is within the range given by the run with the joint phantom. However, the value obtained for the Syn/Bone using the isotropic weighting, 69, is within the range of the Syn/Bone using a joint phantom, which ranges from 57 - 73.

Figure 5.22 shows the dose per depth profiles using both the M/R #1, Figure 5.22(a), and M/R #2, Figure 5.22(b). As expected, the dose rate for M/R #1 is higher than M/R #2. In fact, as seen in Figure 5.22, the dose rate is generally two orders of magnitude higher for all components except the nonthermal neutron dose. For the M/R #1, the nonthermal dose is greatest at the surface of the joint phantom until a depth of about 2 cm, at which point it is comparable to the gamma dose. As moderator length and diameter increased, M/R #2, the nonthermal neutron dose decreased such that it is an order of magnitude lower than the thermal and boron doses.

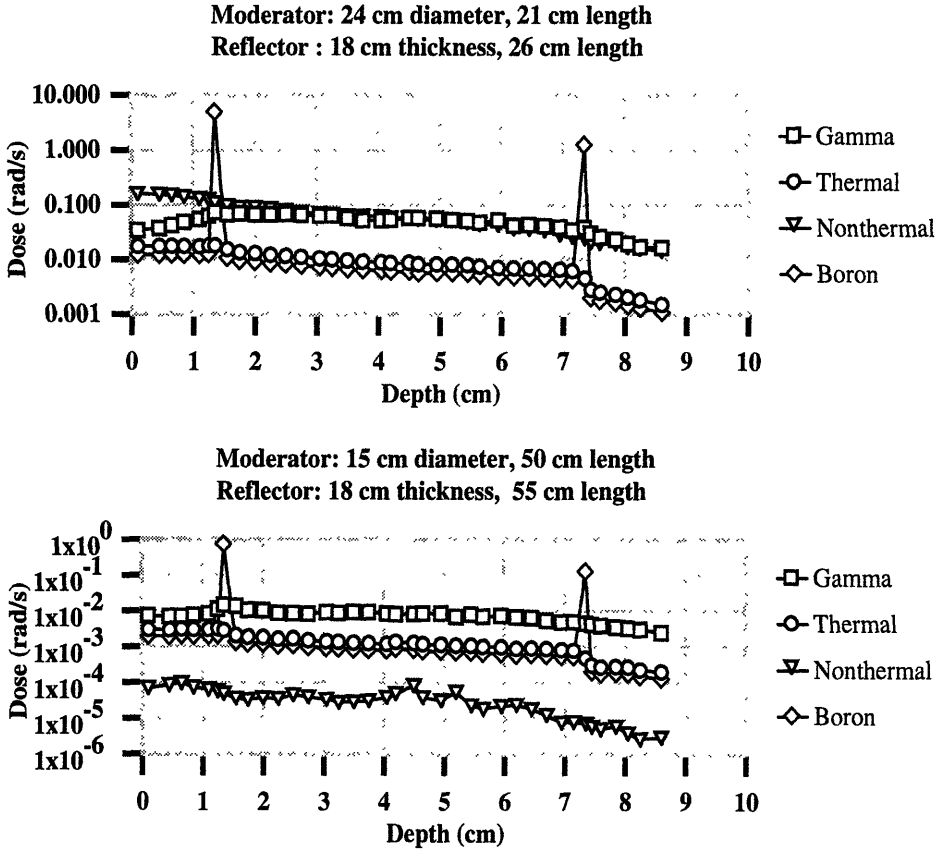

Figure 5.22 Plots showing the profiles of dose per depth in the joint phantom for (a) M/R #1, described both in the figure itself and the preceding paragraph and (b) M/R #2, also described in the figure and preceding paragraph.

The evaluation of the Figure of Merit in a phantom has shown that the results obtained using the Figure of Merit do not necessarily coincide with the actual synovium dose to

healthy tissue dose as calculated in a phantom. Therefore, in order to obtain accurate ratios of synovium dose to healthy tissue dose, it is recommended that the Figure of Merit not be used and the phantom be inserted in the moderator/reflector geometry.

5.3 Target Selection

Of the possible accelerator targets for the production of neutrons, the $^{7}Li(p,n)^{7}Be$ reaction has received considerable attention by BNCT investigators (e.g. Yanch et al 1992, Wu et al 1993). This has been the target of choice owing to its relatively low neutron energies and high neutron yields (Shefer, 1990). These characteristics are due to the presence of a large cross-section resonance, 580 mb, at 2.25 MeV which is just above the proton threshold energy of 1.88 MeV. The neutrons in this reaction are preferentially emitted in the forward direction. Also, the low threshold implies that the proton beam power is low for a given proton current and that the energy per proton to be dissipated is relatively small (Shefer, 1990). The total neutron yield for this reaction is 8.96×10^{11} n/s per mA.

However, some practical disadvantages to lithium targets. For example low melting point and low thermal conductivity, have prompted the investigation of beryllium as alternate target material, i.e. via the reaction $^{9}Be(p,n)^{9}Be$. Disadvantages to the use of this latter reaction included the lacuna of knowledge of the low energy end of the spectrum. This has recently been corrected by the work of Howard et al (Howard, 1996). In order for the beryllium target to be used, a higher proton energy, 4.0 MeV, must be applied to the target than with a lithium target. The total neutron yield for the beryllium reaction is slightly higher than the lithium reaction at 1.51×10^{12} n/s per mA.

In light of the results of the evaluation of the evaluation of the Figure of Merit in the joint phantom, the two target materials, lithium and beryllium, were evaluated using the joint phantom and several moderator/reflector configurations, which will be described below.

The moderator diameter was kept constant at 15 cm, the reflector thickness at 18 cm and the reflector length at 5 cm greater than the moderator length which was sequentially set at

20 cm, 35 cm and 50 cm. The proton energy on the lithium target was modelled as being 2.5 MeV and on the beryllium target as 4.0 MeV. For both targets, a 4 mA proton current which is achievable in the tandem electrostatic accelerator constructed at MIT LABA, was used for the determination of the total neutron yield for each reaction. Thus, for the lithium target the total neutron yield was calculated to be 3.6×10^{12} n/s, while for the beryllium target it was calculated to be 6.04×10^{12} n/s.

5.4 Moderator/Reflector Assembly

It must be noted that the data acquired did not fill a three dimensional space but rather a one dimensional space. A three dimensional investigation would require that, for example, for every change in diameter of the moderator, simulations be run for all different lengths modelled. In a one dimensional study, on the other hand, the diameter of the moderator was arbitrarily chosen and only the length varied. This was deemed acceptable on the assumption that the diameter dependence for other lengths should have a similar shape and characteristics with the exception of a scaling factor. One set of data was acquired to check this assumption.

5.4.1 Material Selection

This section will present the criteria and selection of materials for the components of the neutron beam design, i.e. moderator and reflector. Issues such as patient shielding were not considered in this investigation. The selection of materials presented here is based on the work of Yanch et al for the design of an epithermal accelerator based beam for BNCT (Yanch et al, 1992) but adapted for BNCS.

Several criteria exist for choosing an optimum moderator material. One is that the material have a large scattering cross section and a small mass number, to enable a great deal of energy loss in a small amount of space. Another requirement is that it have a greater probability of interaction with fast neutrons than thermal or epithermal neutrons, preventing the output neutron spectrum from being saddle-shaped and fast neutrons contaminating the beam. An optimal moderator also helps the beam maintain a forward direction. A light isotope is desirable because isotropic scattering in the center-of-mass system transforms to

a more forwardly biased scattering in the lab system. Finally, capture gamma production must be low so that gamma shielding does not have to be placed between the moderator and the patient.

A detailed investigation was made by Yanch et al (Yanch et al, 1992) on the following materials: alumina, beryllium oxide, titanium deuteride, light water and heavy water. Of these five materials, it was found that three of them, i.e. alumina, titanium deuteride and light water produced a significant number of energetic capture photons. They were thus excluded as potential moderator materials. The other two, heavy water and beryllium oxide, were somewhat similar in their moderating abilities. Heavy water was chosen as the moderating material for BNCT because it maintained a higher flux of epithermal neutrons, desirable for BNCT, and had the advantage of being much less toxic and less expensive to handle than beryllium oxide. The fact that heavy water maintains a higher epithermal flux of neutrons is not of interest for the design of a neutron source for BNCS because the desired flux of neutrons is primarily thermal. heavy water may be better for thermal neutrons as well since the Z is smaller. This, combined with the consideration that heavy water is less toxic than beryllium oxide, led to the choice of heavy water as the moderator for BNCS.

Generally, the purpose of placing a reflector around the moderator is to improve the yield of therapy neutrons at the patient position (Yanch et al, 1992). Energetic neutrons trying to leave the moderator in places other than the patient position can be scattered by the reflector back into the moderator and thus can become therapy neutrons again. In order for a material to be a good reflector, it should be a heavy isotope because it will avoid excessive neutron energy losses in the process described above (in which case the neutrons may be so thermalized that they will not make it to the moderator end). Also, the heavy isotopes stop gammas thus effectively improving the purity of the beam with respect to gamma contamination and reducing the background dose.

The reflectivity of several materials, namely lead, bismuth, graphite and alumina, was investigated in previous work (Yanch et al, 1992) and the relevant results are summarized

below. Lead, graphite and alumina all had similar reflectivity whereas bismuth was less reflecting. In terms of gamma production, graphite was seen to be the cleanest while alumina the most contaminating. Lead and bismuth fell somewhere in between. For the epithermal beam design, Yanch et al chose lead because graphite was considered too moderating. However, for BNCS, increased moderation is desirable since, as will be shown in the results of the ideal beam studies in the following chapter, BNCS requires a thermal neutron beam.

5.4.2 Geometry

The proposed geometry for the moderator/reflector assembly, consisting of two cylinders, is shown in Figure 5.22. This time the tallies were taken across the surface of the end of the moderator cylinder (inside the reflector cylinder). The neutron spectrum was that of 2.5 MeV protons hitting a lithium target 5 cm in diameter and 1 cm in thickness.

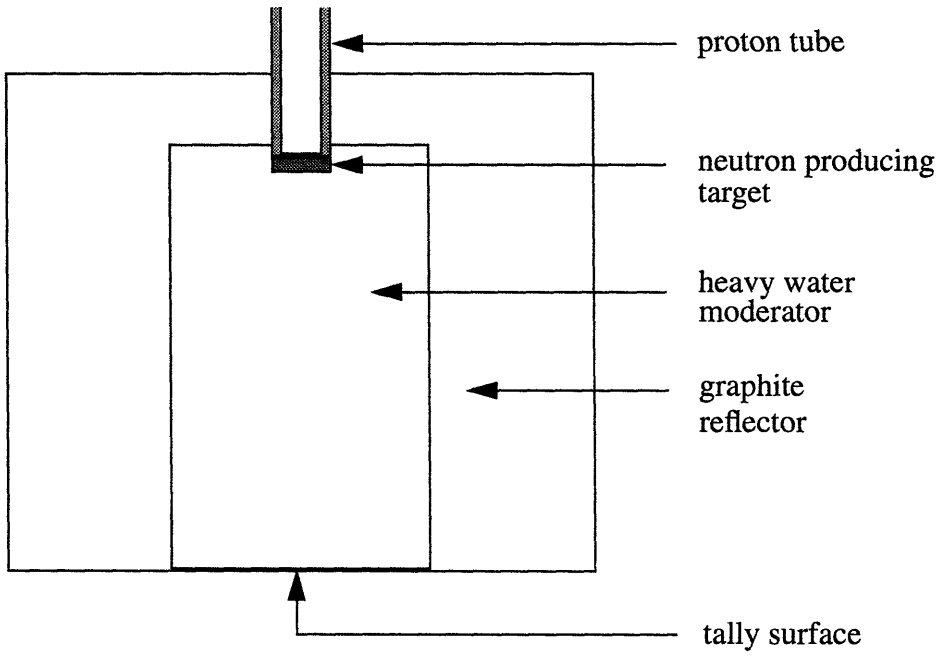

Figure 5.22 Moderator/reflector configuration of neutron beam for BNCS.

For all simulations, particle flux of all components, i.e. thermal neutrons (neutrons with a cutoff energy of 0.36 eV), nonthermal neutrons (neutrons with energies above 0.36 eV) and photons, was obtained across the surface of the moderator end. In order to obtain dose rates, both neutron and photon fluxes were modified with the fluence-to-kerma conversion

factors of Caswell et al (Caswell, 1982) and Zamenhof et al (Zamenhof, 1975).

The dependence of dose and flux of thermal neutrons, nonthermal neutrons and gammas on moderator length and diameter were examined sequentially. Keeping the moderator diameter fixed at 15 cm, the moderator length was varied from 20 to 60 cm in increments of 5 cm. Then, keeping the moderator length fixed at 45 cm, the diameter was varied from 10 to 24 cm, specifically from 10 cm to 15 cm in increments of 1 cm and then 18 cm and 24 cm. The percent contributions of the different components were examined in order to maximize the favorable and minimize the unfavorable components. Reflector thickness was kept at 15 cm and the length was fixed to be 5 cm longer than the moderator.

In a separate set of runs, the reflector thickness was varied from 5 cm to 24 cm while the moderator length was kept at 45 cm and the diameter at 15 cm. The reflector length was kept coupled with the moderator length. The effect of the added length of the reflector length was tested by keeping all other parameters constant and changing the added length from 5 cm to 15 cm.

6 Neutron Beam Design: Results

6.1 Target Selection

This section will present a comparison between beryllium and lithium neutron-producing targets using a geometry that includes the cylindrical joint phantom with several potential moderator/reflector configurations. The difference in the potential moderator/reflector configurations lies in the length of the moderator which is set at 20, 35 and 50 cm.

Before presenting the results, a brief review of the parameters used in this comparison is given. The moderator diameter was kept constant at 15 cm, the reflector thickness at 18 cm and the reflector length at 5 cm greater than the moderator length. The proton energy on the lithium target was modelled as being 2.5 MeV and on the beryllium target as 4.0 MeV. For both targets, a 4 mA proton current, achievable in the tandem cascade accelerator constructed at MIT LABA, was used for the determination of the total neutron yield for each reaction. Thus, for the lithium target the total neutron yield was calculated to be 3.58×10^{12} n/s and for the beryllium target it was calculated to be 6.04×10^{12} n/s.

Table 6.1:Comparison of Beryllium and Lithium Targets

Target: Mod. Length	Syn/Capsule Average	Syn/Capsule Range	Syn/Bone Average	Syn/Bone Range
Lithium: 20 cm	17	16 - 17	27	21 - 30
Beryllium: 20 cm	10	9 - 10	15	13 - 17
Lithium: 35 cm	59	55 - 66	55	50 - 61
Beryllium: 35 cm	46	42 - 50	50	45 - 78
Lithium: 50 cm	61	59 - 64	67	57 - 73
Beryllium: 50 cm	57	53 - 63	60	53 - 67

The dose profiles for these neutron beams are provided in Figures 6.1 through 6.3, divided by moderator length. The first dose profile shows the 20 cm moderator long moderator for both the lithium and beryllium targets. In addition to the Syn/Capsule ratio and Syn/Bone ratio, it is instructive to see the dose profiles.

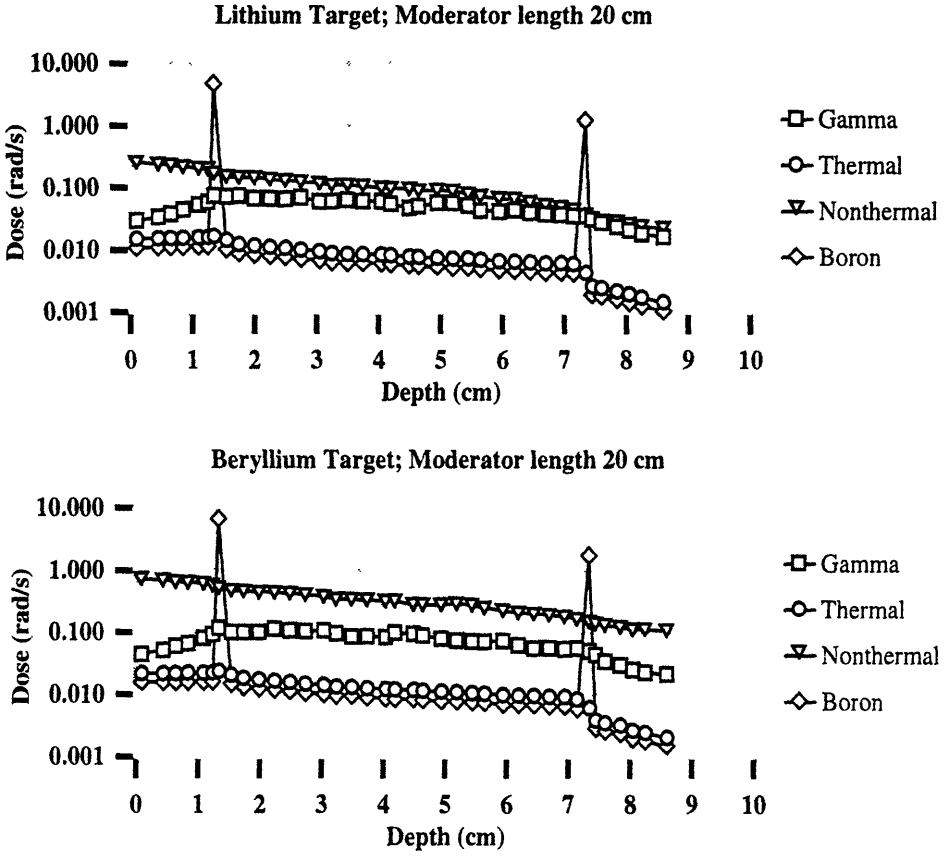

Figure 6.1 Figure showing the difference in dose profiles of a (a) lithium and (b) beryllium target using a heavy water moderator of length 20 cm, diameter 15 cm, and graphite reflector of length 25 cm and thickness 18 cm.

As Figure 6.1 shows, the dose rate due to nonthermal neutrons is lower in the lithium target rather than the beryllium target. Using the lithium target, the nonthermal dose would not be very much higher than the gamma dose whereas using the beryllium target would yield a nonthermal dose larger than the gamma dose which is similar using both targets. The thermal neutron and boron dose rates are comparable and show the same profile using both targets.

The next figure, Figure 6.2, shows the differences between lithium and beryllium targets using a 35 cm long moderator. The other parameters of the moderator/reflector configuration are the same as previously.

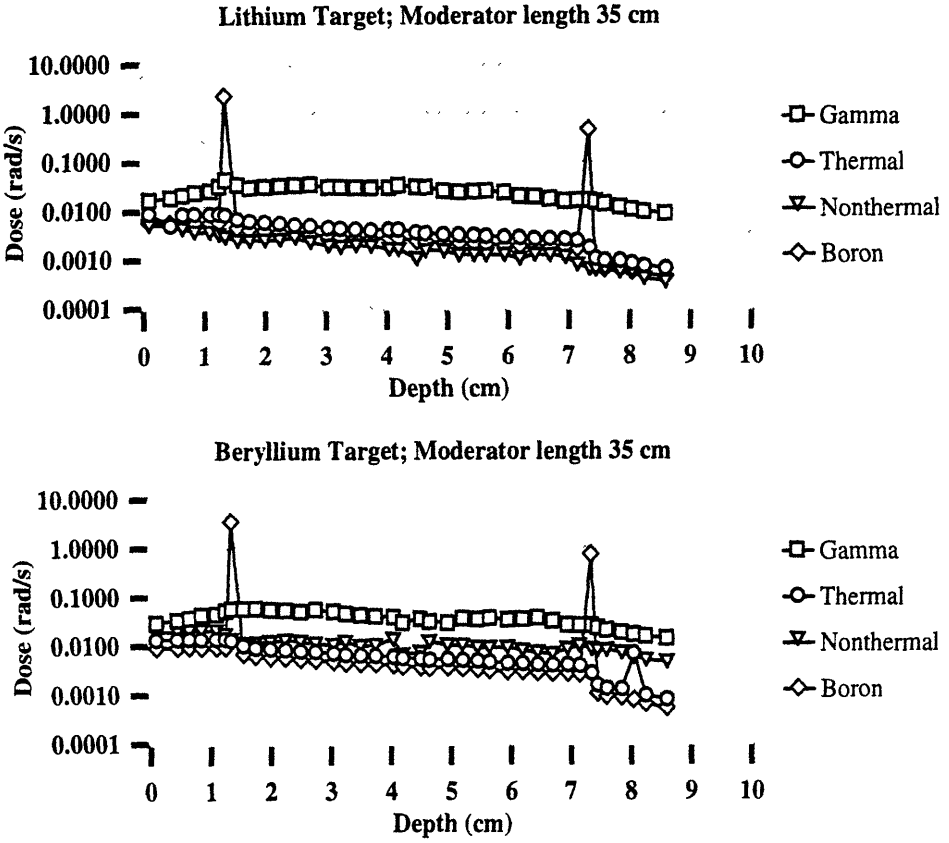

Figure 6.2 Figure showing the difference in dose profiles of a (a) lithium and (b) beryllium target using a heavy water moderator of length 35 cm, diameter 15 cm, and graphite reflector of length 25 cm and thickness 18 cm.

Although the gamma dose is similar, the thermal and nonthermal neutron and boron dose rates are higher for the beryllium target rather than the lithium target. With the lithium the thermal neutron, nonthermal neutron boron dose components remain below 0.01 rad/s while with beryllium they are all hovering around 0.02 rad/s. Through the phantom, the nonthermal neutron dose is almost an order of magnitude higher with the beryllium target rather than the lithium target. However, it must be noted that at this particular length, the nonthermal is always smaller than the gamma dose rate which is not as easy to reduce in that it includes the gamma dose due to induced photons.

The next set of plots, Figure 6.3, shows the difference in dose profiles of a lithium and beryllium target but this time using a moderator with a length of 50 cm.

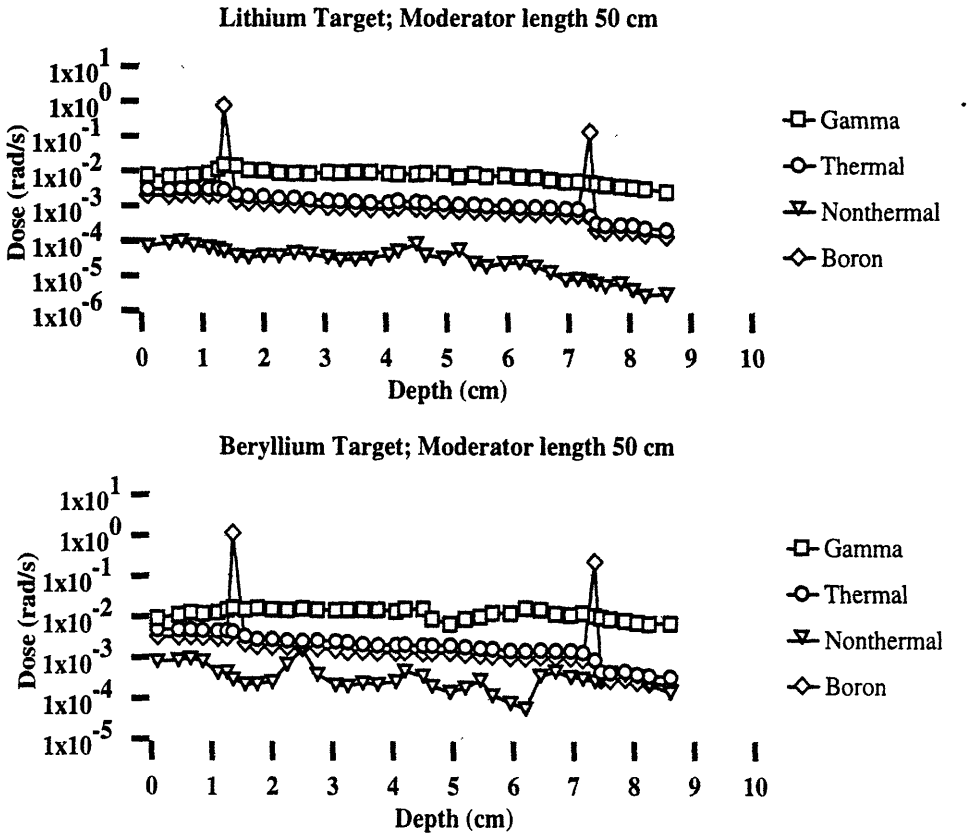

Figure 6.3 Figure showing the difference in dose profiles of a (a) lithium and (b) beryllium target using a heavy water moderator of length 50 cm, diameter 15 cm, and graphite reflector of length 25 cm and thickness 18 cm.

The interesting thing that emerges from Figure 6.3 is that the gamma, thermal neutron and boron doses are essentially the same with both lithium and beryllium targets. However, the nonthermal neutron dose is an order of magnitude higher using the beryllium target rather than lithium. The fluctuations in the nonthermal neutron dose using the beryllium target are due to statistical noise.

6.2 Moderator/Reflector Assembly

As a first step the moderator length was varied from 20 to 60 cm in increments of 5 cm. During this set of runs the moderator diameter was kept constant at 15 cm, the reflector

thickness was also 15 cm and the reflector length was always kept 5 cm larger than the moderator length. The source spectrum was that from 2.5 MeV protons hitting a lithium target which was 5 cm in diameter and 1 cm thick. For the dose calculation, a total neutron yield of 3.584×10^{12} n/s was used. Figure 6.4 shows the change in the flux and dose with moderator length and other parameters as described above.

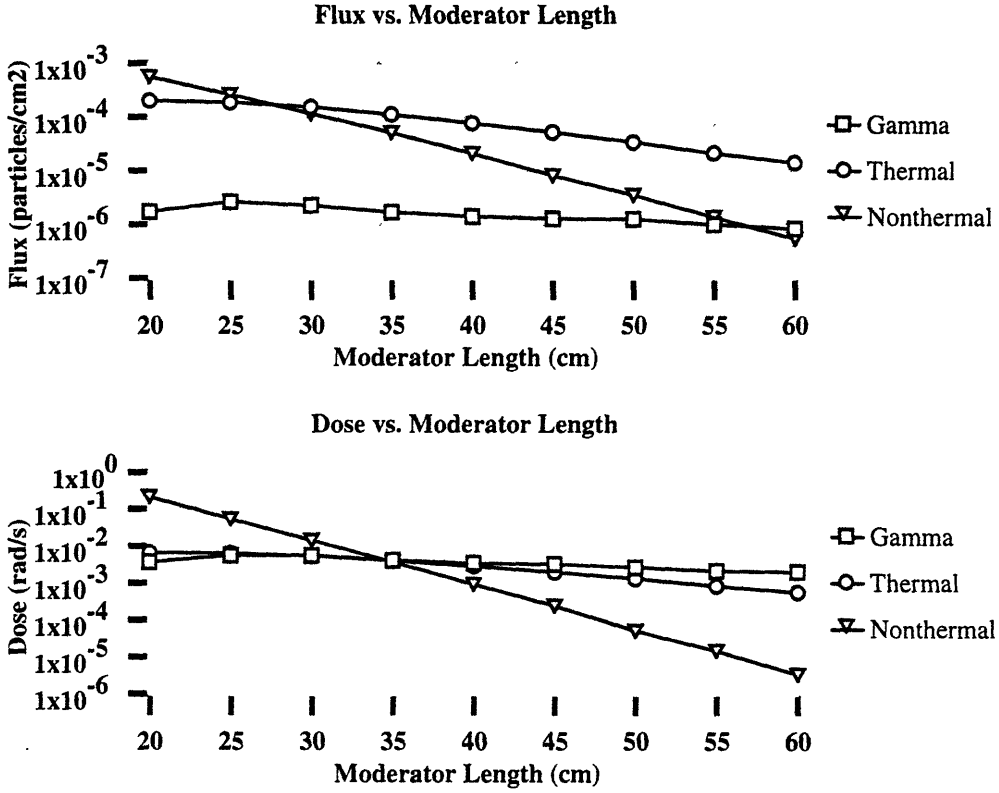

Figure 6.4 Plots showing the effects of changing moderator length on (a) flux and (b) dose. The other parameters were as follows: moderator diameter 15 cm, reflector thickness 15 cm with the length always 5 cm greater than moderator.

As seen in Figure 6.4, the change in moderator length had a significant effect on the non-thermal neutron flux and dose, as well as an effect on the thermal neutron flux. Around 30 cm, the thermal and nonthermal neutron fluxes were the same, after which the nonthermal neutron flux decreased much more quickly than the thermal neutron flux. The gamma flux remained roughly constant and at 55 cm it was equal to the nonthermal neutron dose. The dose components were all equal at 35 cm, after which the gamma and thermal neutron dose components remained relatively constant while the nonthermal neutron dose component decreased rapidly.

Since the moderator length had such a pronounced effect on the dose components, the percent contributions were plotted versus moderator length in Figure 6.5, in order to see them more clearly. In fact from Figure 6.5(b), there appears to be a peak in thermal neutron dose at 40 cm, something which was not clear from Figure 6.4(b).

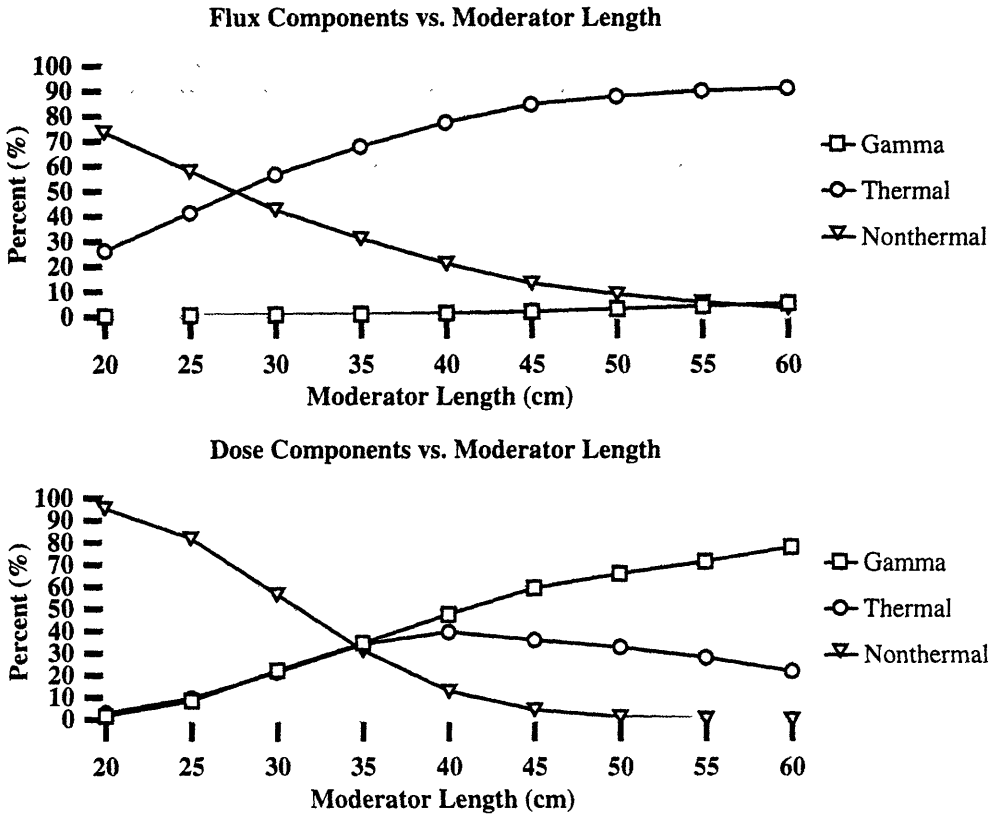

Figure 6.5 Plots showing the effects of changing moderator length on the components of (a) flux and (b) dose. The other parameters were as follows: moderator diameter 15 cm, reflector thickness 15 cm with the length always 5 cm greater than moderator.

The next parameter varied was the moderator diameter. It was varied from 10 cm to 24 cm, with increments of 1 cm between 10 cm and 15 cm and then an increment of 3 cm (total of 18 cm) and one increment of 6 cm (total 24 cm). The moderator length was fixed at 45 cm. The reflector length and thickness were kept at 15 cm and 50 cm respectively. The effects on flux and dose are shown in Figure 6.6.

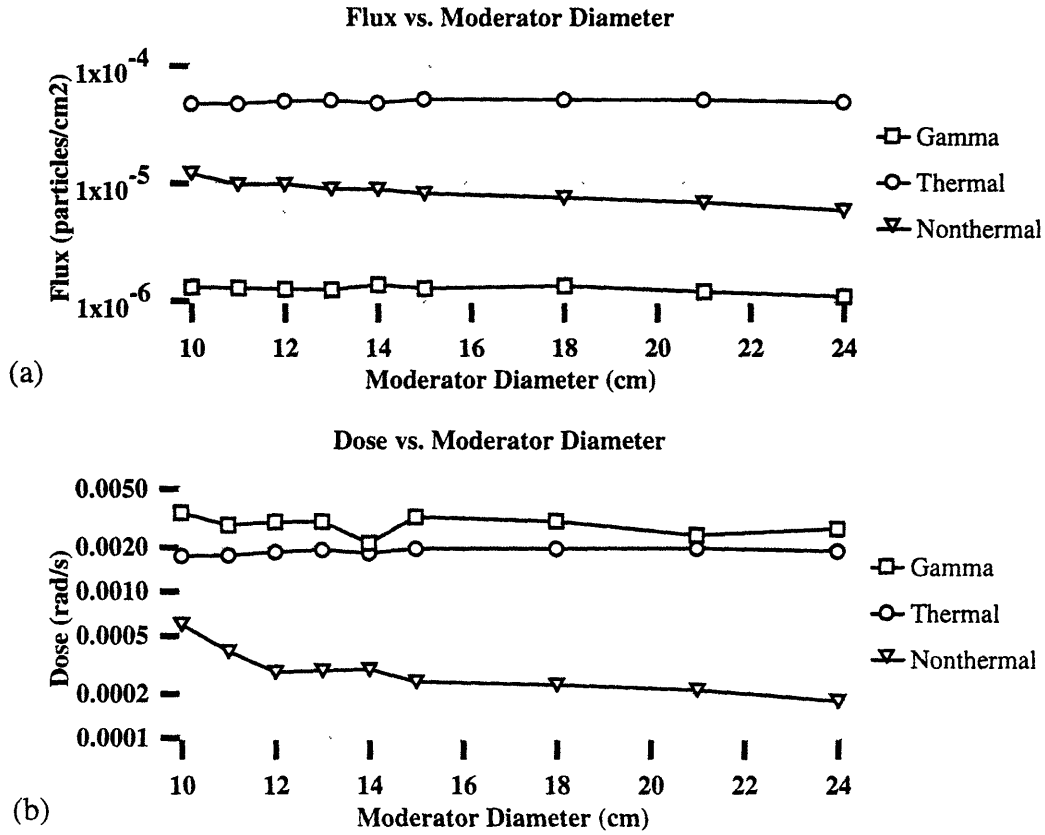

Figure 6.6 Plots showing the effects of changing moderator diameter on the components of (a) flux and (b) dose. The other parameters were as follows: moderator length 45 cm, reflector thickness 15 cm and length 50 cm.

As can be seen from Figure 6.6, changing the moderator diameter did not have significant effects on dose and flux as changing the moderator length. The gamma flux remained constant at 2% while thermal neutron flux increased about 80% to 90% and the nonthermal neutron flux decreased accordingly. The dose contribution of the gamma rays oscillated between 50% and 60% while the thermal neutron contribution oscillated between 30% and 40%. The contribution of the nonthermal neutrons decreased smoothly from about 10% to 4%. There were no changes greater than 10% by varying the moderator diameter at this length.

These two degrees of freedom in the moderator dimensions, i.e. diameter and length, were also examined conjunctively, thus an acquisition of three dimensional data. Table 6.2 lists the fluxes obtained for four moderator diameters at two moderator lengths while Table 6.3

lists the dose rates for the same.

Table 6.2: Effect of Increasing Moderator Length and Diameter on Flux

Length:flux*	diam:15 cm	diam:18 cm	diam:21	diam:24cm
40:gamma	1.39e-06	1.78e-06	1.34e-06	1.06e-05
40:thermal	7.65e-05	7.67e-05	7.62e-05	7.23e-05
40:nonthermal	2.09e-05	1.87e-05	1.67e-05	1.45e-05
45:gamma	1.27e-06	1.34e-06	1.19e-06	1.08e-06
45:thermal	5.18e-05	5.12e-05	5.08e-05	4.86e-05
45:nonthermal	1.87e-05	7.51e-06	6.81e-06	5.83e-06
* units are (cm): (particles/cm^2)				

Table 6.3: Effect of Increasing Moderator Length and Diameter on Dose

Length:dose*	diam:15 cm	diam:18 cm	diam:21	diam:24cm
40:gamma	3.42e-03	3.55e-03	2.87e-03	2.38e-03
40:thermal	2.85e-03	2.90e-03	2.90e-03	2.77e-03
40:nonthermal	9.28e-04	8.63e-04	6.34e-04	6.46e-04
45:gamma	3.23e-03	3.01e-03	2.41e-03	2.68e-03
45:thermal	1.95e-03	1.95e-03	1.95e-03	1.88e-03
45:nonthermal	2.43e-04	2.30e-03	2.13e-04	1.78e-04
*units are (cm):(rad/s)				

There are several trends to be noticed. One is the effect of changing the diameter on the different components. For example, looking at the gamma contributions to both flux and dose across the diameters, first at 40 cm and then at 45 cm, it can be seen that the gamma flux and dose decrease with increasing diameter for both the 40 and 45 cm cases, while the thermal flux dose and flux at both 40 and 45 cm remains the same.

Then choosing a moderator diameter of 15 cm and length of 35 cm, the dimensions of the reflector were varied. First, the reflector thickness was varied from 5 cm to 24 cm, in increments of 5 cm between 5 cm and 15 cm and then in increments of 3 cm until 24 cm.

The reflector length was kept at 50 cm, i.e. 15 cm greater than the moderator length. The results are shown below in Figure 6.7.

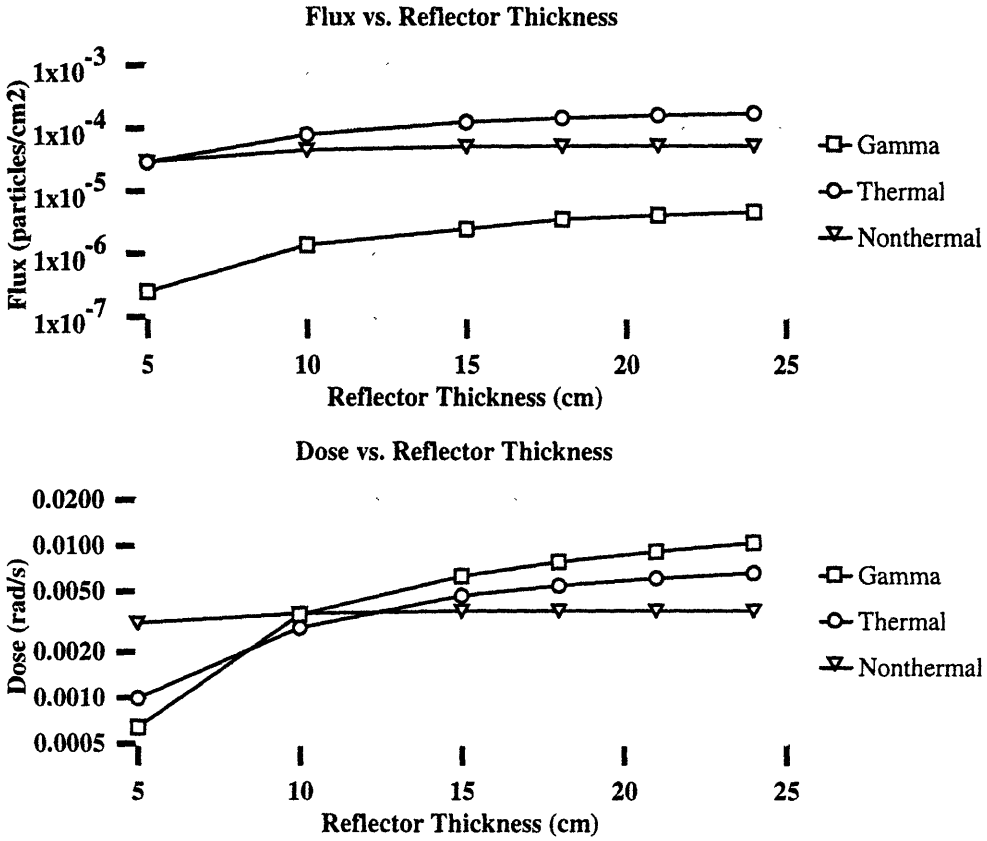

Figure 6.7 Plots showing the effects of changing reflector thickness on the (a) flux and (b) dose. The other parameters were as follows: moderator diameter 15 cm and length 35 cm; reflector length 50 cm.

The flux of the various components increases until 18 cm, after which each plateaus at its own value; approximately $1.6x10^{-4}$, $5.3x10^{-5}$ and 4.510^{-6} particles/cm^2 for the gamma rays, thermal and nonthermal neutrons respectively. The change in flux for all components is less than 2% after the 18 cm mark. The shapes of the gamma and thermal doses follow those of the flux while the shape of the nonthermal neutron dose differs greatly; it is a curve with a very small slope, making its percent contribution range from 65% to 18%. The gamma dose increases by 4% and the thermal dose by 1%.

Since the reflector length was usually coupled with the moderator length, a comparison was made between an increment of 5 cm or 15 cm. In other words, two configurations

were tried where in one the reflector length was 5 cm more than the moderator and in the other the reflector length was 15 cm more than the moderator length. The reflector thickness was kept constant at 15 cm. The moderator diameter and length were fixed at 15 cm and 35 cm, respectively. The results are summarized in the Table 6.4 below.

Table 6.4: Effect of Reflector Length on Flux and Dose

Quantity	Component	Increment of 5 cm particles/cm^2	Increment of 15 cm particles/cm^2
Flux	Gamma	1.68e-06	2.46e-06
	Thermal	1.11e-04	1.28e-04
	Nonthermal	5.09e-05	5.17e-05
Dose	Gamma	4.08e-03	6.30e-03
	Thermal	4.03e-03	4.68e-03
	Nonthermal	3.70e-03	4.02e-03

As can be seen in Table 6.4, the addition of 15 cm to the moderator length increased the overall total flux and dose coming out of the moderator end, as well as shifting the relative contributions. The gamma flux was increased by about 30% while both the thermal and nonthermal neutron fluxes increased by about 15%. There were comparable increases in the dose, i.e. the gamma dose increased by about 30%, while the thermal dose increased by about 15% and the nonthermal by 10%.

7 Conclusion

This thesis had two major aims. The first was to analyze in vitro uptake of ^{10}B by samples of Rheumatoid Arthritic synovium and Rheumatoid Arthritic and Osteoarthritic cartilage in order to gain an estimate of the ^{10}B levels potentially attained in vivo. The second was to design an accelerator-based neutron beam for Boron Neutron Capture Synovectomy. Conclusions and recommendations for future work relating to these two major aims will be drawn sequentially in this chapter.

The in vitro analysis included three different parts. The first, and most extensive, was quantification of bulk tissue uptake via Prompt Gamma Neutron Activation Analysis. The second was an attempt to verify cell kill following thermal neutron irradiation of boron-loaded tissue sample. The third was an attempt to spatially localize boron using Neutron Induced Alpha Track Autoradiography.

The compound used, $K_2B_{12}H_{12}$, represented an attempt at finding an optimal compound for BNCS which is non-toxic, remains sufficiently long in the joint space and delivers large amounts of ^{10}B to the synovium. It must be emphasized again that this boron compound contained natural boron which is 80% of ^{11}B and 20% of ^{10}B which implies that all the concentrations reported in this thesis connected with the use of this compound could be increased by a factor of five by using a compound 100% enriched in ^{10}B.

Quantification of bulk ^{10}B uptake in the form of $K_2B_{12}H_{12}$ by RA synovium revealed that at an incubation time of 1 hour and nominal incubation concentrations of 100 ppm, 500 ppm and 1000 ppm, the average bulk tissue uptake was 33 ppm (range: 19 ppm to 42 ppm), 189 ppm (range: 79 ppm to 332 ppm), and 330 ppm (range: 190 ppm to 497 ppm), respectively. Some discrepancies existed in these results, particularly in Table 4.4, where the uptake of synovium when incubated at a nominal incubation concentration of 1000 ppm for 24 hours was lower than expected (supposing that concentration always increases with incubation time).

Results of the quantification of bulk tissue uptake corroborated preliminary investigations of Johnson et al which found very high synovium uptake following incubation in boron particulate and nominal concentrations of boric acid solution (Johnson et al, 1994). Prompt Gamma Neutron Activation Analysis was a reliable and accurate means of boron quantification.

As seen in Figure 4.1, there seemed to be an inverse relationship between uptake of some compounds and the size of the sample. This could be due to limited diffusion distance of the compound into the tissue. The limited diffusion distance into tissue would affect the measurement of concentration in that the measurement is dependent on the B/H ratio where the H is proportional to the size of the sample. If the sample were larger and limited diffusion existed, then the H would increase while the B would remain constant making the B/H ratio and consequently the concentration smaller. Differences in tissue type could also result in different diffusion rates.

Results presented in Table 4.6 revealed encouraging results of RA cartilage uptake. The average uptake of RA cartilage in this experiment was approximately a factor of ten lower than the uptake in RA synovium (averaging 4 ppm for an incubation time of 1 hour and nominal concentration of 100 pm and 42 ppm at an incubation time of 1 hour and nominal concentration of 1000 ppm). Two other experiments, whose results are shown in Tables 4.4 and 4.5, were performed using the boron compound in varying concentrations. These resulted in either unobtainable results (i.e. those results yielding negative concentrations) or comparatively large uptake. This could be due size of the sample in relation to the vial. Every vial is slightly different in size and when the background measurement is done, only one vial is used as a representative of the set. This does not affect the B/H ratio when the sample size is considerably bigger than the vial size. However, when the sample size is so small compared to the vial, subtraction of background results in negative value which in turn results in negative concentrations. It must be noted that the experiment providing the encouraging results (Table 4.6) was performed with newly bought, homogeneous teflon vials.

The aforementioned hypothesis relating sample size and uptake was also tested in bovine cartilage which served as a substitute for OA and RA cartilage. As shown in Table 4.9, the average uptake by the bovine cartilage was 617 ppm at an incubation concentration of 1000 ppm. This is 100 times larger than the cartilage results presented above. According to the above hypothesis, the sample size should have been 100 times smaller. However, the average sample size was 100 larger and thus in direct contrast with the hypothesis relating sample uptake and sample size. However, it should be noted that differences could exist between RA or OA and bovine cartilage, although they were expected to behave similarly.

Unfortunately, the attempt to verify cell kill by the boron neutron capture reaction yielded equivocal results. A possible reason for the lack of difference between the boronated and the nonboronated irradiated samples was that no boron was present from the beginning. The lack of difference between the set of irradiated and non-irradiated samples could be a result of other dominating tissue processes, namely autolysis. Unfortunately, the complete lack of results in Neutron Induced Alpha Track Autoradiography (due to experimental problems) could not help address any of these issues.

Recommendations for future work include careful investigation of the toxicity of $K_2B_{12}H_{12}$ and of the length of its stay in the joint, although it must be noted that a double-blind study was conducted at the Royal Melbourne Hospital in Sydney, Australia suggesting that boron is therapeutic for RA (Travers et al, 1990). This has been supported by another study suggesting that a daily dose of boron is a safe and effective treatment for some forms of arthritis (Newnham, 1994).

Other boron compounds should be analyzed in vitro in order to ensure that the optimal compound form has been developed. After this, it is recommended to proceed to animal studies using an antigen induced arthritis (AIA) model which bears close resemblance to RA in humans and has been used extensively to assess potential radiation synovectomy agents (Zuckerman, 1989). Animal studies yield information which can not be completely simulated in vitro and thus are invaluable for determining the feasibility of BNCS.

The second aim of this thesis was to design an accelerator based neutron beam for BNCS. Neutron beam design for BNCS is quite different from that of BNCT due to the shallow depth of the synovium and the large concentrations readily achieved in the synovium as shown earlier.

The monoenergetic, photon-free "ideal" beam studies indicated that the therapeutically useful neutron energy range for BNCS is from 0.025 eV to 100 eV. This range represents the energies at which the fast neutron dose is below the gamma dose which is a result of interactions of neutrons with endogenous tissue.

After the therapeutically useful neutron energy range for BNCS was determined, attention was turned to the development of a moderator/reflector configuration to achieve this range from the energetic neutrons coming from an accelerator source.First, a Figure of Merit was developed using the results of the ideal beam studies to weight the spectrum coming out of the moderator end. If successful, the Figure of Merit would enable the determination of a therapeutically useful moderator/reflector configurations without the insertion of the cylindrical joint phantom in the geometry. However, it was not found not reliable when tested in a phantom.

The next step was to evaluate which of two neutron producing reactions, $^{7}Li(p,n)^{7}Be$ or $^{9}Be(p,n)^{9}Be$, would be most appropriate for BNCS. The material which when irradiated with protons produces neutrons, such as lithium and beryllium, is referred to as target material. The lithium target consistently showed lower nonthermal neutron doses (except at the moderator length of 35 cm where the lithium and beryllium nonthermal doses were comparable) and higher average Synovium/Bone and Synovium/Capsulė ratios. These two tissue spaces were chosen because the capsule or the skin is the first point of contact of the neutron beam. The bone was chosen in accordance with the identification of bone surface as a principal radiosensitive area which is necessary to protect in procedures involving bone irradiation (ICRP, 1977).

Materials for the moderator/reflector configuration were selected based on the findings of Yanch et al while designing their neutron beam (Yanch et al, 1992). The material chosen for the moderator was heavy water. For the reflector, graphite chosen because it had the least gamma contamination and was found to be very moderating. In the neutron beam design for BNCT, lead was used as the reflector material because graphite, although cleaner with gammas, was considered too moderating. In BNCS, heavy moderation is desired.

The dose and flux dependence on both the length and diameter of both the moderator and reflector was investigated. The moderator diameter did not cause very large changes in flux and dose between 10 cm and 24 cm. At 14 cm, there was a slightly lower gamma dose than at other diameters. Increasing moderator length served to decrease the fast neutron flux and dose while having almost no effect on the gamma dose and flux. In the range of 20 cm to 60 cm, the dose and flux components were equal at 35 cm, meaning that only moderator lengths greater than 35 cm can give an increase of thermal neutrons over fast neutrons. Interestingly, the peak percent contribution of thermal neutrons occurred at 40 cm. At this same moderator length, the gamma dose contribution was very close to the thermal neutron. These results suggest that a moderator 14 cm in diameter and 40 cm in length is optimal.

The increase in flux with increasing reflector thickness began to plateau after 18 cm, corroborating previous findings (Yanch et al, 1992). The dose due to fast neutrons remained the same at reflector thickness ranging from 5 cm to 25 cm. As seen in figure 6.7, dose contributions of all components were the same at 10 cm, indicating at reflector thickness greater than 10 cm is the absolute lowest threshold for reflector thickness. Since the increase between 18 cm and 20 cm was not significant and the thermal neutron flux and dose seemed to have reached a saturation point around 18 cm, it was decided that 18 cm represented an optimal reflector thickness. The reflector length was generally coupled with the moderator length. At a reflector thickness of 15 cm, the effect of the length of increasing reflector length did not produce large changes in the flux and dose.

In order to give more perspective to this design, it must be mentioned that the intended source of neutrons for BNCS is the 4.1 MeV, 4 mA tandem electrostatic linear accelerator constructed in the MIT Laboratory for Accelerator Beam Applications (Yanch et al, 1995). The advantages of this type of accelerator over other neutron producing sources include a continuously tunable beam energy and proton current, the delivery of continuous current to the target, the ability to operate at higher accelerating gradients for protons in the range of 2-4 MeV, thus leading to a more compact system, high electrical power efficiency and modest cooling requirements (Shefer et al, 1994). Its compact size would enable an easy installation in a research or clinical environment (Yanch et al, 1993).

Future work will include the optimization of the moderator/reflector configuration and the addition of shielding considerations (which have been ignored in this thesis). Other issues will include consideration of therapy times (in order to deliver 10,000 rad to the synovium as is done in radiation synovectomy) and the consideration of a multi-directional gantry system. Ultimately, the moderator/reflector configuration for the MIT LABA accelerator will need to be constructed for use in the animal studies.

Overall, results of this thesis indicate that BNCS has potential of becoming a new therapy modality. High concentrations of ^{10}B can be achieved in the synovium and a neutron beam from an accelerator source of neutrons can provide the therapeutically useful neutron spectrum.

References

Abe M, Amano K, Kitamura K, Tateishi J and Hatanaka H. Boron distribution analysis by alpha-autoradiography. *J Nucl Med* **27**:677-684 (1986).

Amano K and Sweet WH. Alpha-autoradiography of ^{10}B compound distribution in tissue by use of superimposition. *Nippon Acta Radiol*, **33**:267-272 (1973).

Barth RF, Soloway AH, Fairchild RG, Brugger RM. Boron Neutron Capture for Cancer. *Cancer* **70**:2995-3008 (1992)

Briesmeister JF. MCNP-A General Monte Carlo Code for Neutron and Photon Transport. Los Alamos National Laboratory LA. 7396-M Rev.2 (1986)

Calabro JJ. Rheumatoid arthritis: diagnosis and management. *Clin Symp* **38**:1-32 (1986).

Caswell RS, Coyne JJ and Randolph ML. Kerma factors for elements and compounds for neutron energies below 30 MeV. *Int J Appl Radiat Isot* **33**:1227-1262 (1982).

Chabeuf JMN. A prompt gamma activation analysis facility based on a diffracted neutron beam and improvement of the on-line beam monitor system for the medical beam at the MITR-II. Master of Science Thesis, Department of Nuclear Engineering Department, Massachusetts Institute of Technology (1993).

Cotton FA and Wilkinson G, Basic Inorganic Chemistry. John Wiley & Sons, Ann Arbor (1985).

Deutsch E, Brodack JW and Deutsch KF. Radiation synovectomy revisited. *Eur J Nucl Med* **20**:1113-1127 (1993).

Durani SA and Bull RK. Solid State Nuclear Track Detection: Principles, Methods and Applications. Plenum, New York (1987).

Fairchild RG, Gabel D, Hillman M and Watts K in the Proceedings of the First International Symposium on Neutron Capture Therapy ed. RG Fairchild and GL Brownell. Brookhaven National Laboratory, New York (1983).

Fleming A, Benn RT, Corbett M and Wood PH. Early rheumatoid disease: patterns of joint involvement. *Ann Rheum Dis* **35**:361-364 (1976).

Harris ED Jr. Rheumatoid arthritis: pathophysiology and implications for therapy. *N. Engl. J. Med* **322**:1277-1289 (1993).

Harling OK, Chabeuf JMN, Lambert F and Yasuda G. A prompt gamma neutron activation analysis facility using a diffracted beam. *Nucl Instr Meth Phys Res* **B 83**:557-562 (1993).

Howard WH et al. Manuscript in preparation (1996).

International Commission on Radiation Protection. ICRP-26: Recommendations of the ICRP (1977).

Johnson LS, Yanch JC, Shortkroff S and Sledge CB. Temporal and Spatial Distribution of Boron Uptake in Excised Human Synovium. The Sixth International Symposium on Neutron Capture Therapy for Cancer, Kobe, Japan (1994).

Knoll GF, Radiation Detection and Measurement. John Wiley &Sons: Ann Arbor (1989).

Larin CA, Desmarchias J, Daziano L et al. Long-term results of synovectomy of the knee in a rheumatoid patient *J. Bone Joint Surgery* **56(A)**: 521-531 (1974).

Lipsky PE. Rheumatoid Arthritis. In Harrison's Principles of Internal Medicine, 12th Ed., ed JD Wilson et al, p. 1437-1443. McGraw-Hill, New York (1991).

Lui CH. Determination of spatial resolution of sumperimposed neutron-induced Boron-10 alpha-autoradiography technique. Combined Bachelor of Science and Master of Science Thesis, Department of Nuclear Engineering Department, Massachusetts Institute of Technology (1989).

Mori M. A review of knee joint synovectomy in rheumatoid arthritis with theoretical and technical considerations. *Ann Chir Gynaecol*, **74**: 40-47 (1985).

Newnham RE. Essentiality of Boron for Healthy Bones and Joints. *Env Health Perspec* **102**(Suppl 7):83-85 (1994).

Shefer RE, Klinkowstein RE, Yanch JC and Howard WB. Tandem electrostatic accelerators for BNCT. In the Proceedings of the First International Workshop on Accelerator-Based Neutron Sources for Boron Neutron Capture Therapy. Idaho National Engineering Laboratory (1994).

Shefer RE, Klinkowstein RE, Yanch JC and Brownell GL. A versatile new accelerator design for Boron Neutron Capture Therapy: accelerator design and neutron energy considerations. In Neutron Beam Design, Development and Performance for Neutron Capture Therapy, ed OK Harling et al. Plenum Press, New York (1990).

Shortkroff S, Jones AG, Sledge CB. Radiation Synovectomy. In Advances in Metals in Medicine vol 1, pp 155-186. JAI Press (1993).

Solares GR. High resolution alpha track autoradiography and biological studies of Boron Neutron Capture Therapy. Ph.D. Thesis, Department of Nuclear Engineering, Massachusetts Institute of Technology (1991).

Solares GR, personal communication (1995).

Thellier M, Laurent-Pettersson M, Martini F and Ripoll C.Biological applications of neutron capture radiography. *Neutron News* **2**:26-30 (1991).

Travers RL, Rennie GC and Newnham RE. Boron and arthritis: the results of a double-blind pilot study. *J Nutr Med* **1**:127-132 (1990).

Wu TH, Brugger RM and Kunze JF. Low energy accelerator-based neutron sources for neutron capture therapy. In Advances in Neutron Capture Therapy, ed AH Soloway et al. Plenum Press, New York (1993).

Yanch JC, Shefer RE, Klinkowstein RE and Howard WH. A High-Current Tandem Cascade Accelerator Facility for Medical Applications Research. American Association of Physicists in Medicine Annual Meeting, Boston (1995).

Yanch JC, Zhou XL and Brownell GL. A Monte Carlo investigation of the dosimetric properties of monoenergetic neutron beams for neutron capture therapy. *Rad. Res* **126**:1-20 (1991).

Yanch JC, Zhou XL, Shefer RE and Klinkowstein RE. Accelerator-based epithermal neutron beam design for neutron capture therapy. *Med Phys* **19(3)**: 709-721 (1992).

Yanch JC, Shefer RE, Hughey BJ, Klinkowstein RE. Accelerator-based epithermal neutron beams for neutron capture therapy. In Advances in Neutron Capture Therapy, ed AH Soloway et al. Plenum Press, New York (1993).

Zamenhof RG, Clement SD, Harling OK, Brenner JF, Wazer DE, Madoc-Jones H and Yanch JC. Monte Carlo based dosimetry and treatment planning for neutron capture therapy of brain tumors. In Neutron Beam Design, Development, and Performance for Neutron Capture Therapy, ed OK Harling. Plenum Press, New York (1990).

Zamenhof RG, Murray BE, Brownell GL, Wellum GR, Tolpin EI. Boron Neutron Capture Therapy for the treatment of cerebral gliomas. I. Theoretical evaluation of the efficacy of various neutron beams. *Med. Phys.* **2**: 47-60 (1975).

Zuckerman JD and Sledge CB. Total joint replacement: latest developments for the geriatric patient. *Geriatrics* **40(3)**: 71-73 (1985).